

# Azidation Technology: From Photoaffinity Labeling to Molecular Tattooing

PhD Thesis

by **Miklós Képiró**

**Supervisor: András Málnási-Csizmadia, DSc**

Associate Professor

Structural Biochemistry Doctoral Program

Doctoral School in Biology

**Program Leader: Prof. Nyitrai László, DSc**

**Head of the School: Prof. Erdei Anna, DSc**



Eötvös Loránd University, Faculty of Science  
Institute of Biology, Department of Biochemistry

**Budapest, 2014**

# Content

I. Summary .....	3
II. Összefoglaló (Summary in Hungarian).....	4
III. Introduction .....	5
Drug discovery in a nutshell .....	5
Target deconvolution .....	8
Photoaffinity labeling .....	10
Myosin research.....	14
Fluorescent microscopy.....	22
Optopharmacology .....	26
IV. Aims .....	28
V. Results.....	30
Part 1: Target deconvolution.....	32
Part 2: Para-nitroblebbistatin, a novel tool in myosin research .....	39
Part 3: Molecular tattooing .....	52
VI. Discussion and Conclusions .....	66
VII. Materials and Methods.....	75
IX. Acknowledgements .....	91
VIII. Appendix.....	93
IX. Abbreviations .....	97
X. List of Figures and Tables .....	99
XI. Publications Concerning this Thesis.....	101
XII. References .....	103

## I. Summary

The lack of general target deconvolution techniques suitable for interactome mapping of small molecules is a serious obstacle in the pharmacological field. To address this problem we have investigated new aspects of photoaffinity labeling of azido-modified bioactive compounds in target deconvolution, determining strong and weak binding partners as well as their apparent binding affinity ( $EC_{50}$ ) to their targets. After the synthesis of a series of azidated ligands we chosen azidoblebbistatin for further characterization, the photoinducible derivative of blebbistatin, the most widely used myosin II inhibitor. After we confirmed that azidoblebbistatin has identical myosin II inhibitory properties to that of blebbistatin and azidoblebbistatin can be photocrosslinked to myosin, we showed that the most specific target of blebbistatin in *Dd* cells is myosin II ( $EC_{50} \approx 5 \mu\text{M}$ ) although at higher inhibitor concentrations we also identified several weak binding partners ( $EC_{50} > 30 \mu\text{M}$ ). During the characterization of azidoblebbistatin, we found that unlike blebbistatin, it is not phototoxic. This observation inspired us to synthesize para-nitroblebbistatin, where the azido group was replaced by a non-photoreactive nitro group, which has similar electron withdrawing characteristics. We proved by *in vitro* and *in vivo* experiments that para-nitroblebbistatin lacks all of the adverse effect of blebbistatin (photoinstability, fluorescence, cyto- and phototoxicity) while its myosin II inhibitory properties are unaffected, providing an unrestricted alternative of blebbistatin both *in vitro* and *in vivo*. We demonstrated that myosin II can be covalently saturated by azidoblebbistatin even at low concentrations by using multiple photo-crosslinking cycles (cycles of azidoblebbistatin addition + UV irradiation). This recognition and the discovery that azidated compounds can be activated by two-photon irradiation led us to the design of molecular tattooing, a novel drug-targeting technology. Molecular tattooing delivers and covalently attaches a photoreactive bioactive compound to its specific target by two-photon irradiation. The biological effect of the compound can be confined to even subfemtoliter volumes with no systemic effects outside the targeted area. Using single cell and live animal experiments we demonstrated how molecular tattooing can be applied to localize the effect of bioactive compounds even into subcellular regions. Furthermore, we illustrated the extreme usefulness of molecular tattooing in the exploration of local molecular mechanisms as well as its power to distinguish local and global effects of specific target enzymes.

## II. Összefoglaló (Summary in Hungarian)

Egy adott hatóanyagok teljes célfehérje hálózatának (interaktom) kísérletes meghatározása - erős, gyenge kölcsönhatások és az egyes komplexek kötési állandói ( $EC_{50}$ ) - jelenleg nem lehetséges. Kísérleteink során, első ízben arra kerestük a választ, hogy a szerkezeti biokémiában széleskörűen használt fotokémiai reakció, a fotoaffinitás jelölés (PAL, Photoaffinity labeling) alkalmas-e azidált hatóanyagok teljes célfehérje spektrumának meghatározására. Miután szerves kémiai szintézissel számos azidált hatóanyagot állítottunk elő, a blebbistatin (miozin II inhibitor) azido származékát, az azidoblebbistatint választottuk ki további karakterizálásra, és interaktomikai vizsgálatokra. Megállapítottuk, hogy az azido szubsztitúció nincs hatással az azidoblebbistatin miozin inhibíciójára, illetve, hogy az azidoblebbistatin miozin komplex UV besugárzással kovalensen keresztköthető. Interaktomikai vizsgálataink alapján, a blebbistatin legspecifikusabb kölcsönható fehérjepartnerre *Dd* sejtekben a miozin II ( $EC_{50} \approx 5 \mu M$ ), azonban nagy inhibitor koncentrációknál ( $>30 \mu M$ ) a blebbistatin számos egyéb kölcsönható fehérjepartnerrel rendelkezik. Az azidoblebbistatinnal folytatott kísérleteink során észrevettük, hogy ellentétben a blebbistatinnal, az azidoblebbistatin nem fototoxikus. Ez a felismerés vezetett a para-nitroblebbistatin szintéziséhez, ahol a C15 pozícióban lévő azido csoportot egy hasonlóan elektronszívó karakterisztikájú, de nem fotoreaktív nitro csoportra cseréltük. *In vitro* illetve *in vivo* kísérletekkel igazoltuk, hogy a C15 nitro-szubsztituált blebbistatin származék - para-nitroblebbistatin - miozin inhibíciós tulajdonságai megegyeznek a blebbistatinéval, azonban az új származék fotostabil, nem fluoreszcens, nem fototoxikus és nem citotoxikus.

Kimutattuk, hogy fényindukált keresztkötési ciklusok alkalmazásával (azidoblebbistatin kezelés és UV besugárzás ciklusos alkalmazása) a miozin azidoblebbistatinnal kovalensen telíthető, még akkor is, ha az egyes ciklusokban alkalmazott azidoblebbistatin jóval a telítési koncentráció alatt van. Kimutattuk továbbá, hogy a miozin-azidoblebbistatin komplex két-foton gerjesztés hatására kovalensen kapcsolható. E két megfigyelés alapján kifejlesztettünk egy új optofarmakológiai technikát (Molekuláris Tetoválás), mely azidált hatóanyagok hatásának akár szubfemtoliteres térfogatokra való, hosszan tartó lokalizációját teszi lehetővé. A technológia alkalmazhatóságát zebra hal embriókkal illetve humán melanoma sejtekkel végzett *in vivo* kísérletekkel demonstráltuk.

### III. Introduction

#### Drug discovery in a nutshell

The use of small molecule therapeutic agents - i.e. drugs – originates from the very early period of human history. The oldest pharmacological text coming from the ancient Mesopotamia 2600 BC, reports approximately 1000 plants and plant derived substances with healing properties such as the oils of Cedrus species (cedar) or the juice of poppy seed [1].

By the 18<sup>th</sup> century, advances in analytical chemistry enabled to purify individual bioactive ingredients from natural sources. One such example is the potent analgesic morphine isolated from opium extracts by Sertürner in 1815 [2].

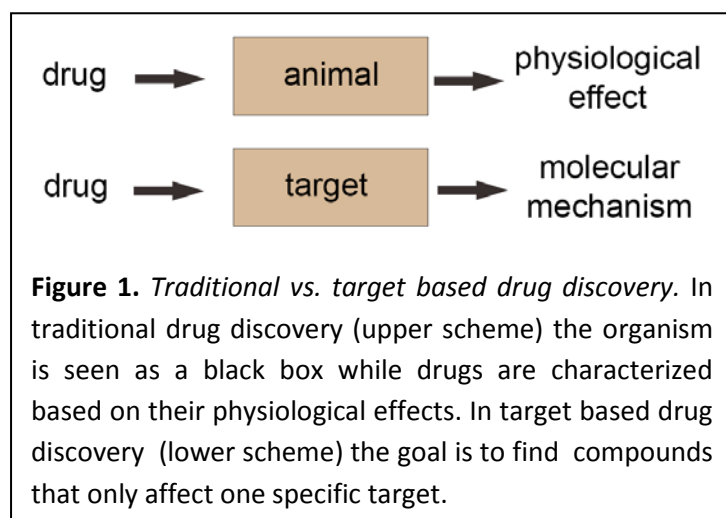
In 1865 Kekulé published his pioneering theory about the structure of aromatic molecules, which gave a huge impulse to the research of coal-tar derivatives, especially dyes [3]. Coal-tar is also one of the main byproduct of coke production, extremely rich in aromatic and aliphatic compounds. The selective affinity of dyes for biological tissues was the particular observation which led Paul Ehrlich to postulate the existence of “chemoreceptors” at the end of the 19<sup>th</sup> century [2]. In 1905, Langley formulated a more functional concept, where the receptor could accept signals that generate responses which results in biological or pharmacological effects [4]. Later, Ehrlich proposed that certain receptors on parasites, microorganisms and cancer cells can be different from analogous structure in host tissue, which could be employed therapeutically [2]. According to Ehrlich’s view, successful drugs are “magic bullets” with the ability to hit specifically their pharmacological target without effecting host tissues. This concept had a profound effect on medical sciences and guided drug discovery through the whole 20<sup>th</sup> century.

As more and more biologically active molecules were determined and synthesized, the toolkit of medical chemistry expanded. By the combinations of the identified structural elements and the application of derivation techniques it became possible to develop various drugs with different therapeutic effects. Later, it was realized that the desired activity could be further refined by adding or removing side chains or functional groups in the process called chemical optimization.

Along with technical advancements the structural determination of biologically active compounds became faster and easier. Advanced spectrometers (NMR and MS) and powerful separation techniques (HPLC) appeared, while small molecules were screened in panels of assays for various types of desired activities.

#### *Traditional vs. target based drug discovery*

Around the beginning of the 20<sup>th</sup> century, the foundations of reliable biological screening and evaluation procedures were laid, which permitted to test compounds in a scientific way.



That was the beginning of a new era, called traditional or physiology-based drug discovery [5]. Drugs were characterized based on their physiological effects in complex disease-relevant models, such as animals or isolated organs. The assays were developed based on the clinically effective drugs, basic biological or disease-

related knowledge. The testing procedures did not require the understanding of the biology of the disease or the mechanism of action of the drug. Instead, the organism was seen as a black box. This approach enabled many major drugs to be developed, but it was slow and could not be easily scaled up (Figure 1).

Advent of recombinant DNA techniques, DNA sequencing, cell-based assays, x-ray crystallography, combinatorial chemistry, molecular modeling tools and automated high-throughput screening resulted in another revolution in the pharmacological industry by the end of the 20<sup>th</sup> century. It has led to a conceptual change utilizing the magical power of large numbers. Targets were incorporated into *in vitro* or cell-based assays and exposed to chemical libraries, enormous numbers of compounds representing numerous variations of a few chemical theme or, more recently fewer variations on a great number of chemical themes. As a result, at beginning of the 1990<sup>th</sup>, a new concept emerged called target-based drug discovery [2]. Here, the organism has been seen as a series of genes and pathways, and the goal was to develop compounds that affect only one molecular mechanism (the target),

in order to selectively treat the disease without producing side effects. The approach consists of five steps: 1. target identification - the exact target is identified 2. target validation - the therapeutic value of the target is determined, 3. assay development - the target is expressed in an HTS assay system, 4. lead identification - compound libraries are screened against the target and 5. lead optimization - the target was further modified in order to achieve better affinity and selectivity [5]. The main disadvantage of the approach is that drugs can be optimized only against a small number of targets.

### *The problems of target-based drug discovery*

When it came to the scene, target-based drug discovery was expected to revolutionize drug discovery. However, the outcomes of the last years are in contrast with this expectation. In spite of the increasing levels of investments in the pharmaceutical industry, there has been a steady decline in the number of new drugs entering to clinical development and reaching the market [5-7]. Moreover, as a striking fact, the start of decline in productivity largely coincides with the introduction of target-based drug discovery. Only 10 molecules of every 80.000 compounds tested on animals reach clinical phase, from where an additional 9 fail. The major cause of withdrawal is toxicity.

The complexity of an organism is way beyond our level of understanding. Compounds exerting beneficial pharmacological properties on isolated proteins will not behave necessary in the desired manner *in vivo*. When a compound enters into the human body it encounters an enormous diversity of proteins: next to binding to its target, there is a very good chance that it will bind to other off-target proteins as well, although with different binding constants. As a consequence, next to desired effect, drug molecules also have side-effects.

As we know more and more about the molecular mechanisms of drug molecules we realize that they are generally promiscuous, so they hit multiple targets to achieve their therapeutic effects [8]. Moreover, recent data implicates that drug molecules have 6 targets on average [9], therefore the “one drug – one target” hypothesis, thought being the cornerstone of target-based methods, is clearly not correct.

Further difficulties may arise from the compound libraries applied in HTS. According to certain views, the switch from natural products to combinatorial libraries might have been

one of the main reasons which led to the current paucity in drug development [1]. The chemical space is enormous and these libraries simply do not cover it.

## **Target deconvolution**

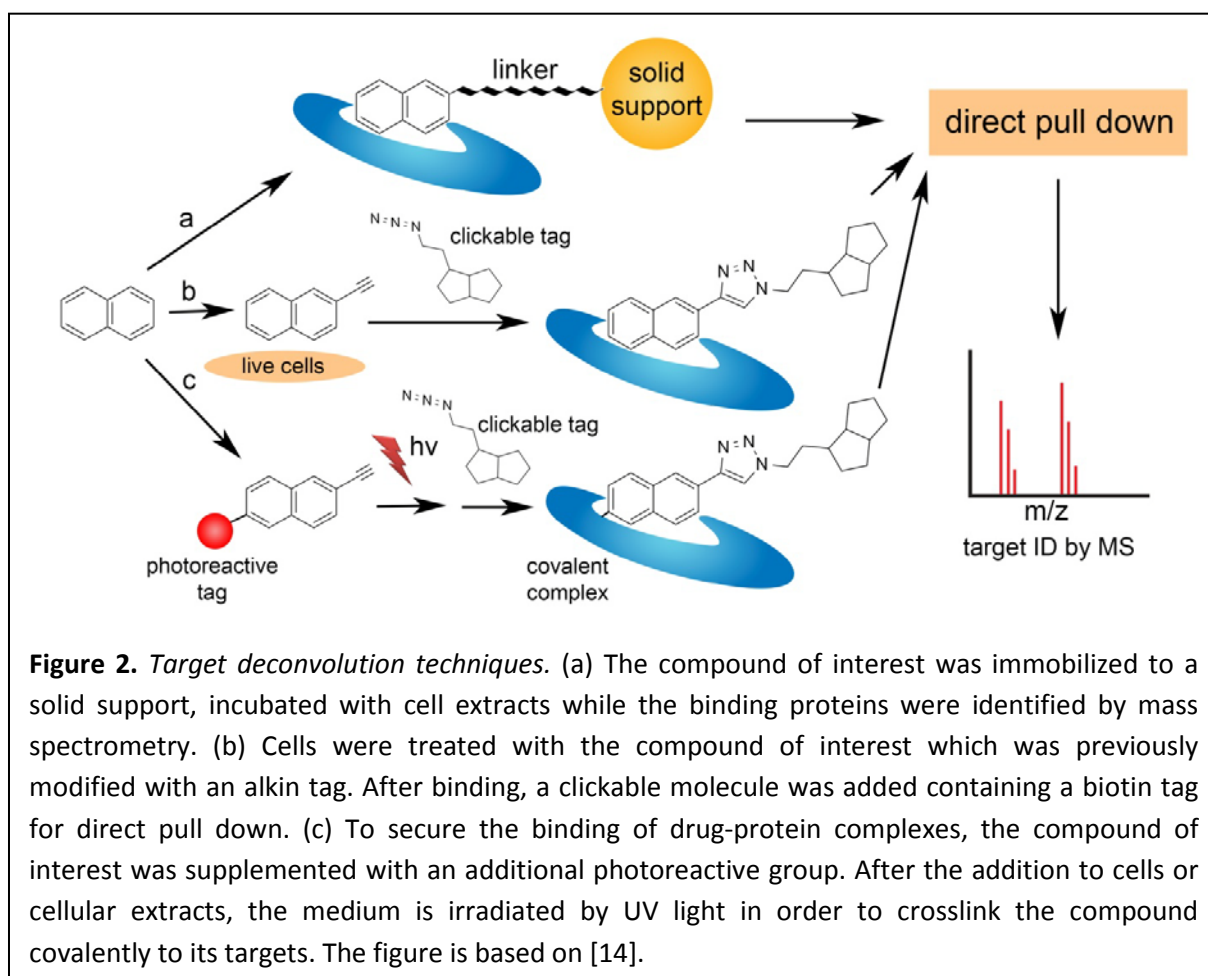
Hitting multiple targets simultaneously is probably the way how a successful compound works [10], what we should consider in the drug discovery process. Despite the fact that the target spectrum of approved or developing-phase drugs is only partially known, there is a pressing need in the pharmaceutical industry for discovering new druggable targets. Currently, approximately 500 targets are exploited in the development process, nevertheless the human body consists of tens of thousands of different proteins not to mention splice forms, post-translational modifications, and mutants. This leads to an estimated 3.000-10.000 potential druggable targets [11].

There is an urgent need in the pharmaceutical field to develop target identification techniques. Considering that the process is expected to generate a whole spectrum of targets (interactome), the term “target deconvolution” was chosen to describe the method more accurately. Consequently, interactomic investigation of the approved drug molecules is crucial: it generates new druggable targets, helps to explore the mechanism of actions and may reveal new effects of drugs (repositioning). Although significant investments have been allocated into the development of target deconvolution techniques, right now there is no generally applicable methodology.

### *Affinity chromatography-based approaches*

Affinity purification is the most widely used approach to isolate specific target proteins from a complex mixture. The compound of interest is conjugated to a derivatized biotin agent or immobilized directly on a resin, for example to agarose beads which are available with different spacer lengths and coupling chemistries. If the compound of interest does not contain a suitable functional group for the coupling, chemical synthesis is necessary to introduce one. The analog is incubated with cell extracts where it binds to its targets. Non-binders are disposed by extensive washing steps followed by specific methods in order to elute the specific binding proteins. These proteins can be separated by gel electrophoresis and identified by mass spectrometry or can be directly analyzed by ‘shotgun’ type

sequencing methods with multidimensional liquid chromatography [12]. One of the main difficulties with this approach is the immobilization of the drug. Any modification of the compound can dramatically affect its binding affinities and often requires significant chemical efforts to identify a site for the attachment of the affinity tag or the solid support. Moreover, addition of any kind of bulky tag to a small molecule usually affects its binding affinities. In order to overcome these problems, a relatively small azide or an alkyne tag has been widely used to minimize structural perturbation and to conjugate the affinity tag via 'click chemistry' [13] (Figure 2).



Further difficulty may arise from the fact that drugs usually bind weakly to their targets, which interactions can be destroyed by the extensive washing steps used in affinity chromatography. In order to secure the drug-protein interactions, they may be crosslinked covalently by photoreactive groups such as benzophenone, diazirine or arylazide. For the isolation of the complexes, small molecules also require a reporter group [14] (Figure 2).

### *Label-free techniques*

Label-free approaches have the advantage that they do not require the chemical modification of the active compound. This new type of technique relies on the changes in thermodynamic stability, as a result of the protein-drug interaction.

One such example is DARTS (drug affinity responsive target stability) which is based on the concept that a protein has conformational flexibility in solution, making it more susceptible to proteolysis. However, once it binds to a small molecule, the overall complex will be more resistant to proteolytic enzymes [15]. Another technique termed SPROX (stability of proteins from rates of oxidation) utilizes the same principle but instead of proteolysis, it uses an oxidizing agent ( $H_2O_2$ ) in the presence of increasing concentrations of a chemical denaturant to oxidize methionine residues in the proteins. After quenching of the reaction, the amount of non-oxidized and oxidized methionine containing peptides in each sample are quantified and plotted against the concentration of the denaturant. Ligand-bound proteins show bigger shifts towards high-concentrations of denaturant compared to non-binders [16].

### **Photoaffinity labeling**

Photoaffinity labeling (PAL) was introduced more than 40 years ago [17], but still, it is a commonly used technique in structural biology to investigate interactions between ligands and macromolecules. The ligand - which is usually a small bioactive molecule - is supplemented with a photoreactive group (label, photophore), then introduced into the system under study and subjected to irradiation. Photolysis of the label results in a highly reactive intermediate capable to form covalent bond with the nearest fragment of the actual binding partner of the ligand. For the detection of the crosslinked product, and the site(s) of modification, the probe has to contain a reporter tag [18]. In many cases, where high resolution structural analysis - i.e. x-ray crystallography or NMR - is extremely difficult or impossible, PAL is practically the only way to obtain structural information about the given ligand-macromolecule interaction. The combination of PAL with modern proteomic approaches and computer aided modeling enables to design models about receptor-ligand complexes [19].

The optimal photoaffinity probes need to fit the following requirements [18]:

- the probe must be chemically inert in the absence of light
- the photophore must be activated under mild condition and its activation must not damage the biological system and its components
- the lifetime of the excited state of the label has to be shorter than the lifetime of the ligand-receptor complex in study
- the activated probe has to non-specifically react with a neighboring group, with the production of a tight covalent bond
- the photophore introduction into the original substance molecule must not considerably alter its bioactivity
- the probe has to contain a reporter e.g. a radionuclide with a sufficiently high specific activity or an additional label attached through an elongated linker

Of course there is no "ideal" photoaffinity probe fitting all of these requirements, so some compromise has to be applied. The major types of photoreactive groups commonly used in PAL experiments are arylazides, diazirines and benzophenones.

### Arylazides

In PAL experiments, arylazides are used the most often. The main reasons are the relative simplicity of their chemical synthesis, the small size of the azido group, their biological inertness and chemical stability in the absence of irradiation. Aryl azides can be prepared by several synthetic strategies. One of them is to attach an arylazide group to the ligand

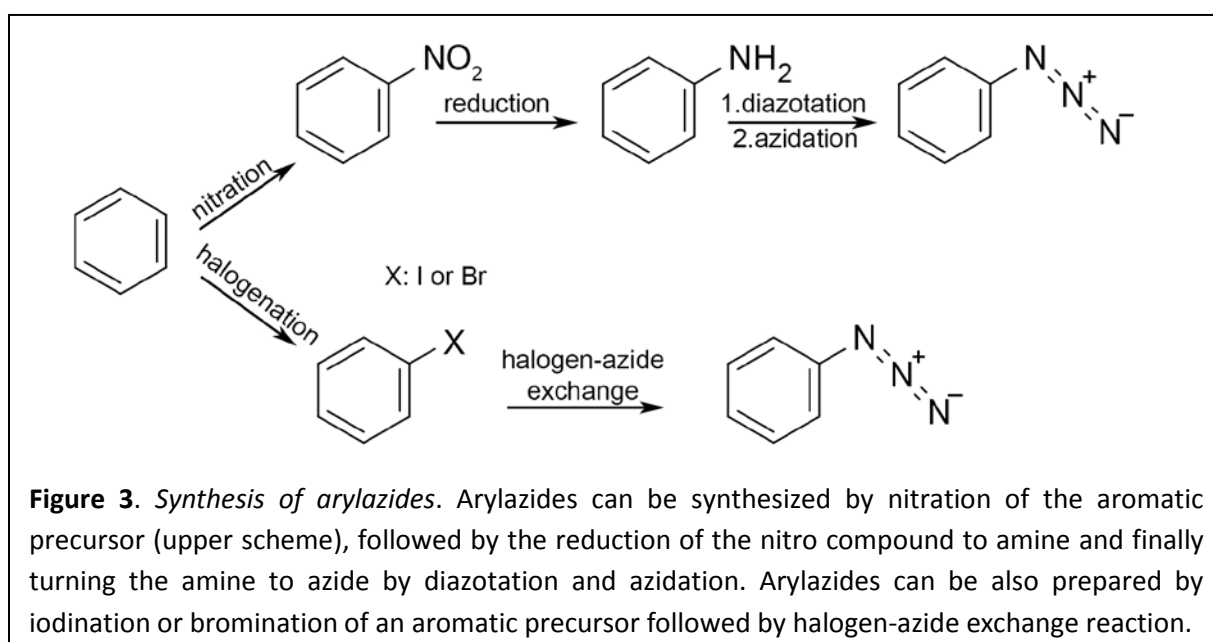
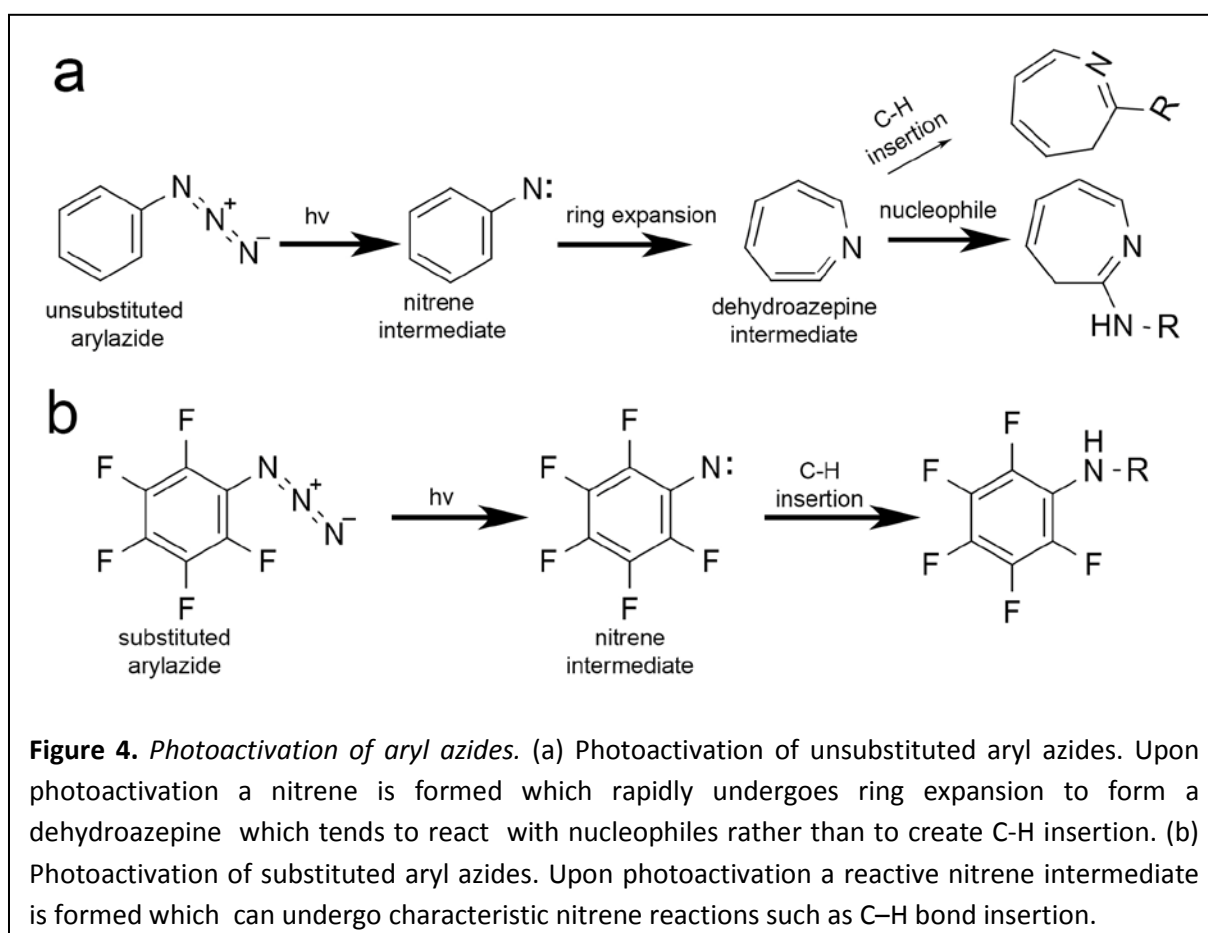


**Figure 3.** *Synthesis of arylazides.* Arylazides can be synthesized by nitration of the aromatic precursor (upper scheme), followed by the reduction of the nitro compound to amine and finally turning the amine to azide by diazotation and azidation. Arylazides can be also prepared by iodination or bromination of an aromatic precursor followed by halogen-azide exchange reaction.

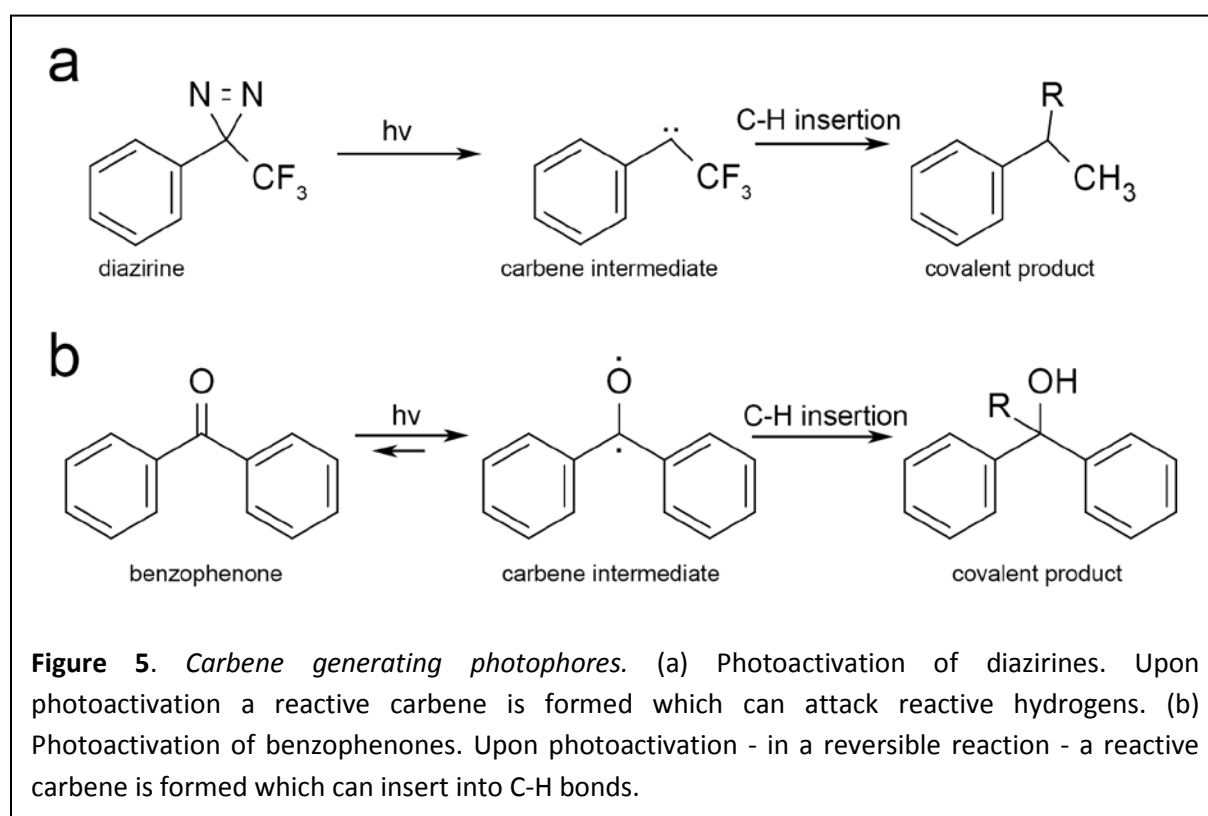
of interest by a conventional coupling reaction such as esterification [20]. In case of aromatic ligands, the azido group can be introduced to the existing aromatic ring thereby, minimizing structural perturbation. However, the azido group cannot be placed directly into the aromatic ring, it has to contain a proper substituent which can be converted into azide, like a primary amino, bromo or iodo group. Applying nitrites, primary aromatic amines can be converted to diazonium salts which can be further reacted with sodium azide resulting the corresponding arylazide [21]. The required amino precursor can be synthesized by aromatic nitration followed by the reduction of the nitro compound to amine (Figure 3a). Using halogen-azide exchange reactions aromatic iodo or bromo compounds can also be azidated [22] (Figure 3b). The corresponding aryl halide precursors can be prepared efficiently by using for example N-halosuccinimides and superacid catalyst [23].



Absorption of photons by arylazides applying proper wavelengths cause the transition of the molecules into an excited state, which results in the detachment of a  $N_2$  molecule and the production of an uncharged nitrene (excited state of N) intermediate. If the arylazide is unsubstituted (Figure 4a), this nitrene rapidly goes through a ring expansion to form a

dehydroazepine, a relatively long-lived reactive intermediate which tend to react with nucleophiles rather than forming C–H insertion products [24]. This is a disadvantage in PAL experiments, since in this case the covalent bond is formed with the nearest nucleophile group rather than the exact binding site. On the other hand, if the aryl azide is substituted, for example perfluorinated, the nitrene does not go through ring expansion and tend to undergo characteristic nitrene reactions such as C–H bond insertion with high efficiency (Figure 4b) [25], being favorable for PAL experiments. The absorption of arylazides is characterized by  $\lambda_{\max} < 280$  nm, so they can be efficiently photolyzed around that wavelength range.

### Carbene generating photophores



Next to nitrene generating photophores, PAL also uses carbene (excited state of C) generating photophores like diazirines and benzophenones. Carbenes are more reactive than nitrenes, so they react rapidly with the production of stable adducts with the majority of functional groups (OH, Ar, -C=C-, and even inactive C-H bonds of alkanes) [26].

Diazirines are a class of organic molecules consisting of a carbon bound to two nitrogen atoms, which are double-bonded to each other, forming a cyclopropene-like ring. The

diazirine label (Figure 5a) is small and can be photoactivated around 360 nm, which provides much milder irradiation conditions than the photolysis of arylazides [27]. Since diazirines generate carbene, they are very reactive and importantly they are not prone to side reactions. Although diazirines are usually described as the most superior PAL labels, it is important to mention that their superior advantages are usually true to those probes which contain the 3-(trifluoromethyl)-3-phenyldiazirine label. However, the introduction of this specific moiety into small molecules without affecting their binding properties is extremely difficult. About diazirines, the following shortcomings should be noted: complicated scheme of synthesis, possible loss of the labeled substrate upon the introduction into the NH-bond, and the instability of some PAL products under conditions of proteolysis during peptide mapping [18].

The other carbene generating photophores, benzophenones are diarylketones which can be photoactivated around 350 nm (Figure 5b). As distinguished from photolysis of arylazides and diazirines, generation of the reactive intermediate is reversible, which increases the labeling efficiency due to multiple excitation-relaxation cycles [18]. However, benzophenones are quite large, which is their biggest disadvantages: coupling a benzophenone to a small molecule can significantly affect its original binding properties.

## **Myosin research**

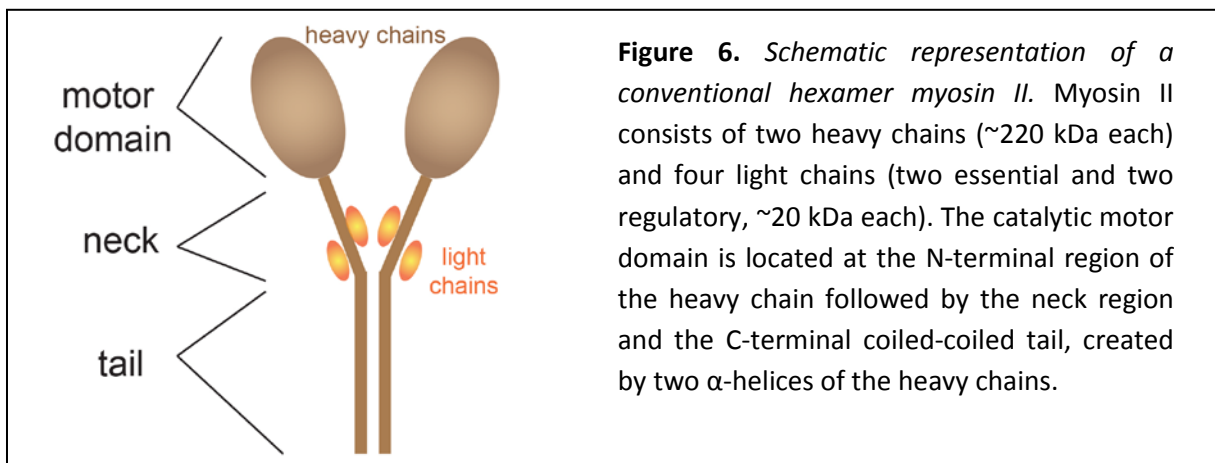
As our experiments are mostly carried out by photoreactive ligands that bind to myosin molecules, the next section is a brief introduction into the world of myosins.

Myosin research has an influential role in life sciences, particularly in biochemistry and biophysics. Many conceptual and experimental innovations are originated from the field of “myosinology” like kinetic [28], spectroscopic [29] or nanobiotechnological methods [30-32]. Classical advantages of myosin research may include the abundance of proteins, the high level of spatial organization and directly measurable macroscopic contractility.

Life, in the form as we know it – is inseparable from motility, the capability of a living system to perform active movement and associated work. Motility is driven by special enzymes called molecular motors, which have the ability to convert chemical energy into mechanical energy.

Myosins are actin-based, ATP driven molecular motors that can be divided into more than twenty classes, based on phylogenetic analyses [33]. In mammalian cells, there are twelve classes of myosins expressed [34]. The most abundant of them is the myosin II subfamily including skeletal, cardiac, smooth as well as non-muscle myosins. In vertebrates, there are over 15 different myosin II isoforms, containing different myosin II heavy chains (MHC).

Myosin II molecules, also known as "conventional myosins", are hexamers consisting of MHC dimers and two sets of two kinds of myosin light chains (Figure 6). The MHC has a three-part domain structure containing an N-terminal motor domain incorporating the actin binding regions and the magnesium adenosine triphosphatase site, a central neck or lever-arm region binding the modulatory light chains and a C-terminal tail domain responsible for cargo binding, self-assembly or intracellular targeting [35].



Despite the functional similarities, there are fundamental differences in the regulation within vertebrate myosin IIs. While the primary regulation of skeletal and cardiac muscle is through actin-associated proteins - i.e. troponin and tropomyosin -, the regulation of vertebrate smooth and non-muscle myosin IIs is through the phosphorylation of the regulatory light chains. This type of regulation enables non-muscle and developing muscle cells to respond to various signals originating both outside and inside the cell [36].

The remaining group of myosins is called 'unconventional myosins'. They are functioning in a wide variety of processes such as intracellular transport, tethering, cell division, cytoskeletal organization and signaling [37].

### *Nonmuscle myosin IIs*

Nonmuscle myosin IIs, similarly to other conventional myosins, have a bipartite structure containing an N-terminal head domain, responsible for the ATPase activity and a coiled-coil C-terminal tail, which is involved in filament formation. In mammalian cells, three different genes (MYH9, MYH10 and MYH14) encode three different NMHC (non-muscle myosin heavy chain) proteins, commonly referred to as NMHC IIA, NMHC IIB and NMHC IIC. The whole myosin II molecule (heavy chains and light chains) is usually referred to as NM II. The different NM IIs - called NM IIA, NM IIB and NM IIC - are determined by the three different NMHC isoforms [38].

The functions attributed to NMII appear to increase almost daily [36]. NM IIs have fundamental roles in the regulation of the actin cytoskeleton as well as in processes that require cellular reshaping and movement such as adhesion, cell division and cell migration. Due to the tail region of NM II, it can form filaments, which allows several myosin heads to maintain tension for a longer period of time. Furthermore, NMIIIs can provide the molecular basis of generating cell polarity by the ability to redistribute inside the cell. In addition, NMII might also function as a scaffold molecule, anchoring signaling molecules, such as kinases and Rho GTPase guanine nucleotide exchange factors [36].

Extensive studies have been performed on *Dictyostelium discoideum* (*Dd*) myosin II, since this myosin was among the first myosins which could be readily expressed from plasmids. *Dd* is a species of soil-living amoeba, commonly referred to as slime mold. Several *Dd* genes are homologous to human, making *Dd* a valuable model organism to study genetic, cellular, and biochemical processes. *Dd* cells express 12 different myosins, but only one conventional two-headed myosin II [39].

### *The role of myosin IIs in cytokinesis*

In animal cells, cytokinesis is the final stage of cell division during which the cell splits itself into half, mediated by the contractile ring [40]. Cytokinesis begins with the ingression of the cleavage furrow, a contractile ring containing actin and myosin IIs (Figure 7). As furrowing progresses, the spindle midzone transforms into an intracellular bridge or midbody, connecting the two dividing cells. The midbody contains antiparallel microtubules that meet

at the Flemming body, which provides an anchor for the ingressed cleavage furrow. The midbody is then cut during abscission, the final step of cytokinesis [41].

The analogies of the contractile ring to the muscle sarcomere have led to the long-held view that myosin's role in the constriction is to provide force by translocating actin in an ATP-dependent manner within a static actin assembly [42, 43]. Although, the molecular mechanism of constriction is studied excessively, basic questions like the structural mechanism of the constriction by actomyosin remains unclear. Emerging evidences indicate that the ability of myosin II to translocate actin is not required for cytokinesis. Its major roles are to bind and crosslink actin filaments as well as to exert tension on actin during contractile ring constriction [44]. Moreover, research show that myosin, either through light chain phosphorylation or through its ATPase activity, also plays an important role in both the assembly and disassembly of the actin contractile ring [45, 46].

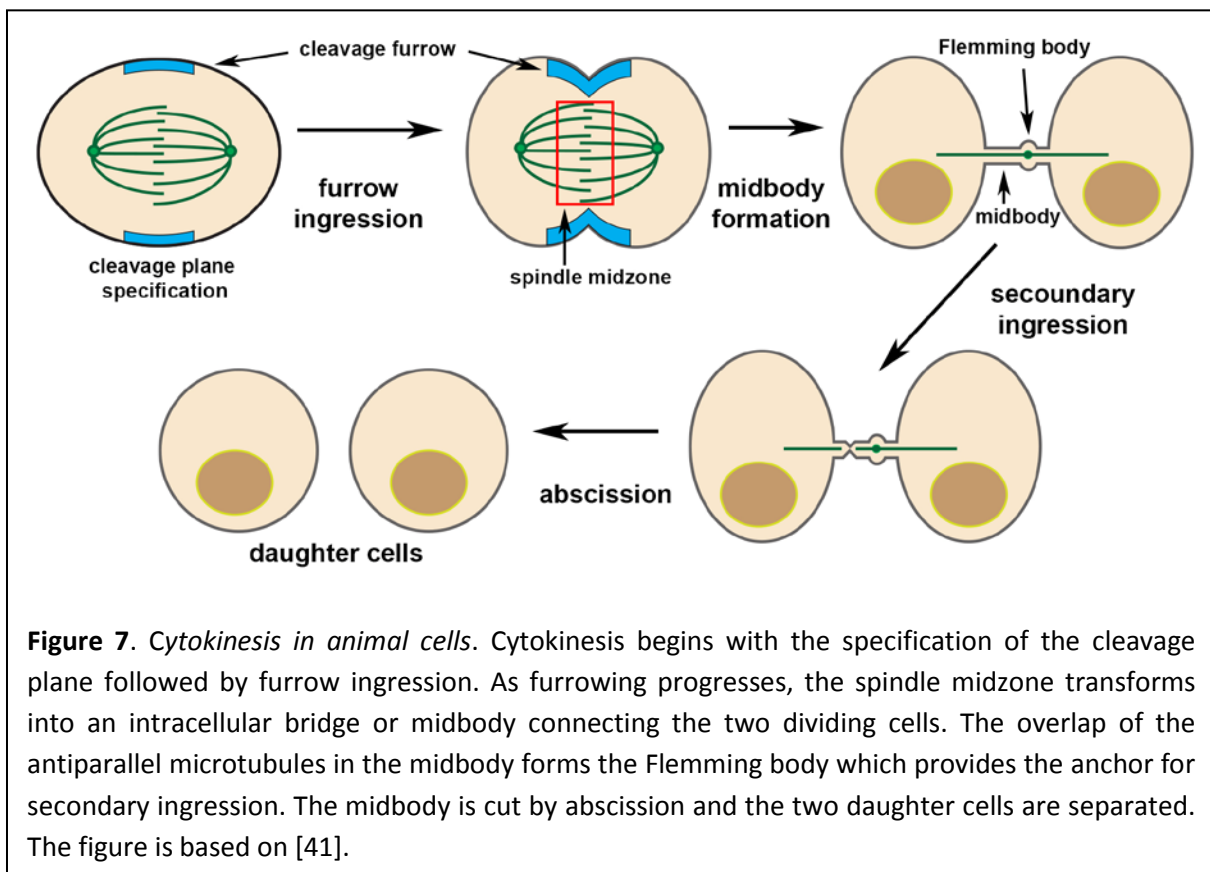


**Figure 7.** *Cytokinesis in animal cells.* Cytokinesis begins with the specification of the cleavage plane followed by furrow ingression. As furrowing progresses, the spindle midzone transforms into an intracellular bridge or midbody connecting the two dividing cells. The overlap of the antiparallel microtubules in the midbody forms the Flemming body which provides the anchor for secondary ingression. The midbody is cut by abscission and the two daughter cells are separated. The figure is based on [41].

How the secondary ingression forms and how abscission occurs is also a subject of debate in the field. Now, it is widely accepted that the final membrane fission required for abscission is mediated by ESCRT-III, the Endosomal Sorting Complex Required for Transport III, which brings opposing membranes together until scission can occur [41].

### *The role of myosin IIs in cellular blebbing*

Another phenomena driven by NMII and occur during cytokinesis, apoptosis or cell motility, is blebbing. In eukaryotic cells, the plasma membrane is tightly bound to the cellular cortex, a layer of actin, myosin and associated proteins. Myosin II molecules maintain the cortex under tension, thereby exerting constant hydrostatic pressure to the cytoplasm. Sometimes, the plasma membrane separates from the cortex and as a result of cytoplasmic pressure, the membrane grows into spherical shaped protrusions called blebs [47]. Thus, in contrast to other, actin polymerization driven cellular protrusions such as lamellipodia or filopodia, the growth of blebs are pressure driven.

Blebbing can be observed commonly in the execution phase of apoptosis, during cytokinesis and cell spreading although its exact mechanism, specific physiological and pathological role is a subject to debate [47]. Increasing number of recent studies highlight blebbing motility as an important alternative of lamellipodia-driven migration in three-dimensional environments. Many cell types such as embryonic or mammalian tumor cells can use blebs for motility [48], moreover, it can be also used by metastatic cells to escape anti-tumor treatments [49].

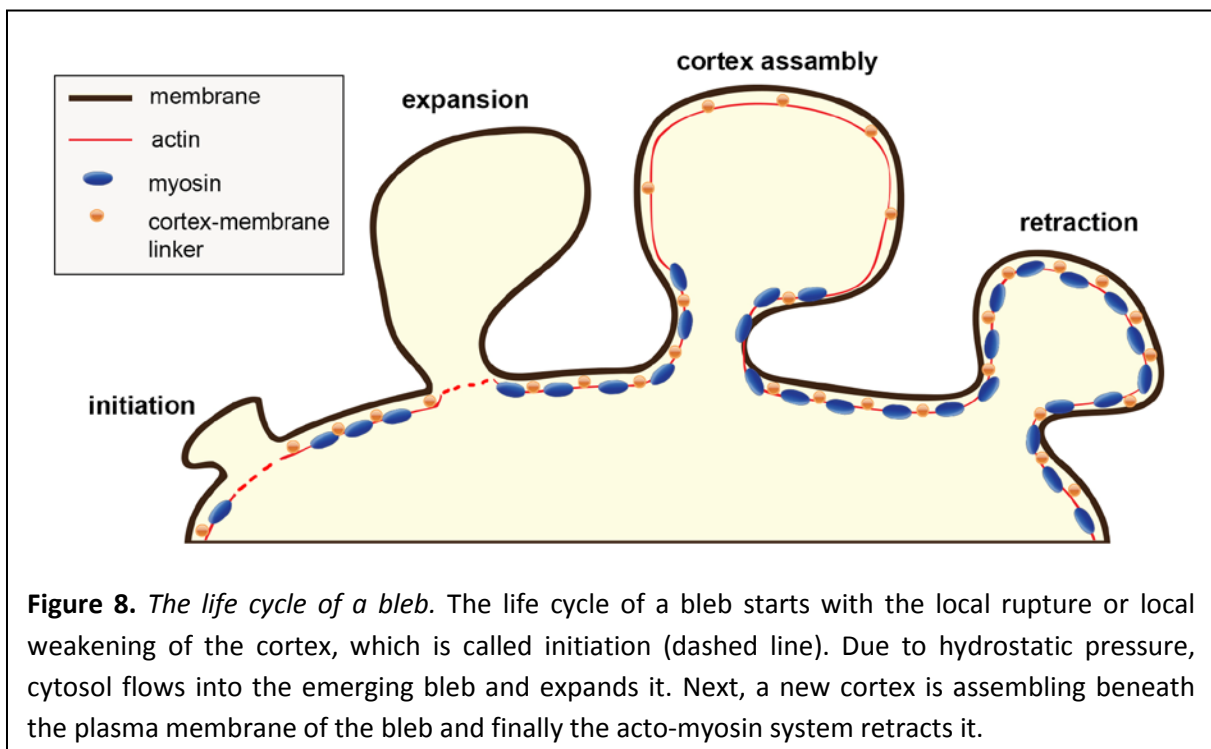


**Figure 8.** *The life cycle of a bleb.* The life cycle of a bleb starts with the local rupture or local weakening of the cortex, which is called initiation (dashed line). Due to hydrostatic pressure, cytosol flows into the emerging bleb and expands it. Next, a new cortex is assembling beneath the plasma membrane of the bleb and finally the acto-myosin system retracts it.

In non motile cells, the life cycle of blebs can be subdivided into three phases such as initiation, expansion and retraction (Figure 8). In migrating cells, retraction does not always

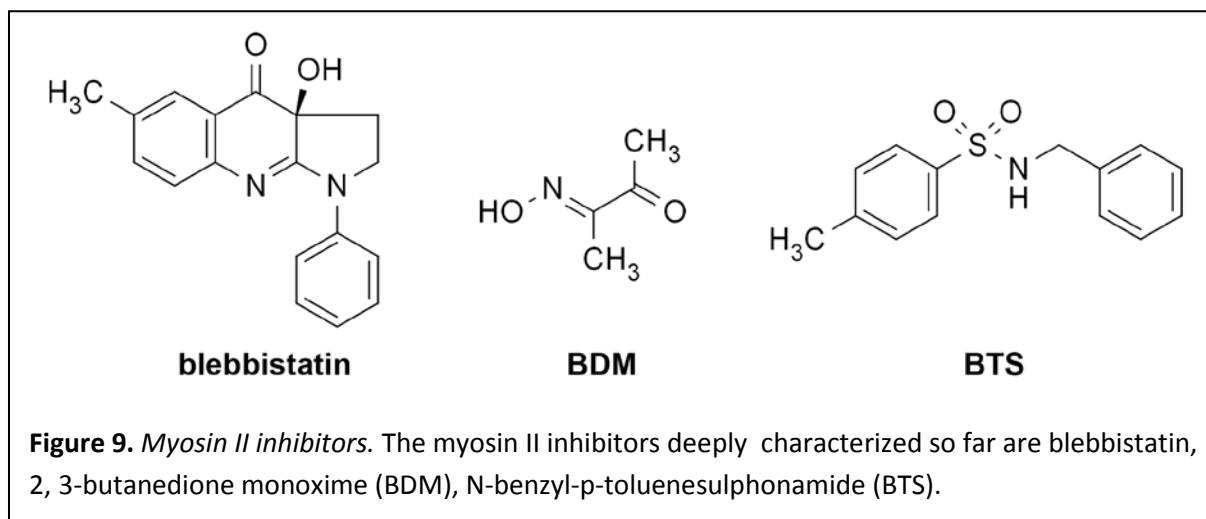
occur [50]. Two distinct mechanisms of bleb initiation have been observed so far: a local dissociation of the membrane from the cortex and a local rupture of the cortex [47]. Both observed types of initiation can occur as a consequence of localized myosin contraction, loss of membrane-cortex adhesion or intra/extracellularly-induced local cortex weakening. In the next phase, in bleb expansion, cytosol flows into the bleb and expands it as a result of the hydrostatic pressure. According to current studies, the pressure which drives the expansion can be either local or global. If the cytoplasm is tightly packed (ribosomes, mitochondria, vesicles, cytoskeleton) like in M2 cells, the pressure equilibration over the whole cell is slower than the timescale of bleb growth. In this case, active myosin molecules need to be localized close to the leading edge, where the pressure increase will lead to bleb formation, so blebs are driven by the generation of local pressure [51]. However, if the macromolecules are dilute, the pressure equilibrates much more rapidly than the lifecycle of blebs and the driven hydrostatic pressure is generated globally [52]. In the last stage, called retraction, a new cortex forms underneath the bleb membrane and by the contraction of the acto-myosin cortex it retracts [47]. The repolymerization of the actin cortex probably begins as the expansion slows, but the exact mechanism that regulates actin nucleation in blebs remains unclear.

### *Myosin II inhibitors*

The identification and characterization of cell permeable small molecular compounds that inhibit specifically the activity of different myosin isoforms has been the subject of many scientific researches. The selective inhibition of different myosins in the cellular environment is not only required for the understanding of their physiological functions, but it also serves as a resource for developing treatments for diseases involving myosin dysfunction or over-activity [53]. Moreover, stabilizing myosin in different structural states by the inhibitors provide a valuable tool to dissect and understand the certain steps of the myosin enzymatic cycle.

Until now, three myosin II inhibitors have been described and deeply characterized: 2,3-butanedione monoxime (BDM) [54, 55], N-benzyl-p-toluenesulphonamide (BTS) [56] and blebbistatin (Figure 9) [57-59]. As BDM has turned out to have a broad effect on many other proteins [60] and the inhibitory effect of BTS is limited to fast skeletal muscle myosin, until

now blebbistatin has been the only potent tool for the specific inhibition of myosin II-dependent processes in various species and cell types.



Inhibitors for unconventional myosins have also been characterized, such as pentachloropseudilin (myosin I) [61], pentabromopseudilin (myosin V)[62], MyoVin-I (myosin V)[63] and 2,4,6-Triiodophenol (myosin VI)[64].

### *Blebbistatin*

Blebbistatin, a derivative of 1-phenyl-2-pyrrolidinone was originally identified in a comprehensive high-throughput screening project employing commercially available chemical libraries, aiming to find inhibitors for non-muscle myosin IIA ATPase activity. [56]. After its discovery, blebbistatin rapidly became the compound of choice to inhibit myosin II-dependent processes in different species and cell types. Thus, blebbistatin has developed into a very popular research tool in wide varieties of experiments including cancer research, developmental biology and the field of cell motility [65-68].

In *in vitro* experiments blebbistatin inhibits myosin IIs from striated muscle, vertebrate non-muscle cells, and *Dictyostelium* by 95%, with an IC<sub>50</sub> of 0.5–5 μM (Table 1). Smooth muscle and *Acanthamoeba* myosin IIs are only inhibited incompletely by blebbistatin at concentrations as high as 160 μM [69]. Blebbistatin blocks myosin in an actin-detached/weak actin-binding state via binding with high affinity to the myosin-ADP-P<sub>i</sub> complex and slowing down phosphate release. This feature confers a crucial advantage in cellular studies exploring myosin function, since it prevents artifacts arising from the

formation of strongly-bound actomyosin complexes. Blebbistatin does not interfere with neither the binding of myosin to actin nor the ATP-induced actomyosin dissociation [58].

Myosin	Class	IC <sub>50</sub> (μM)
<b>Rabbit skeletal muscle</b>	II	0.50
<b>Porcine β-cardiac muscle</b>	II	1.2
<b>Scallop striated muscle</b>	II	2.3
<b>Human non-muscle IIA</b>	II	5.1
<b>Chicken non-muscle IIB</b>	II	1.8
<b>Turkey smooth muscle</b>	II	79.6
<i>Dictyostelium</i>	II	4.9
<i>Acanthamoeba</i>	II	83
<b>Rat 1b</b>	I	>150
<i>Acanthamoeba 1C</i>	I	>150
<b>Mouse V</b>	V	>150
<b>Bovine myosin X</b>	X	>150

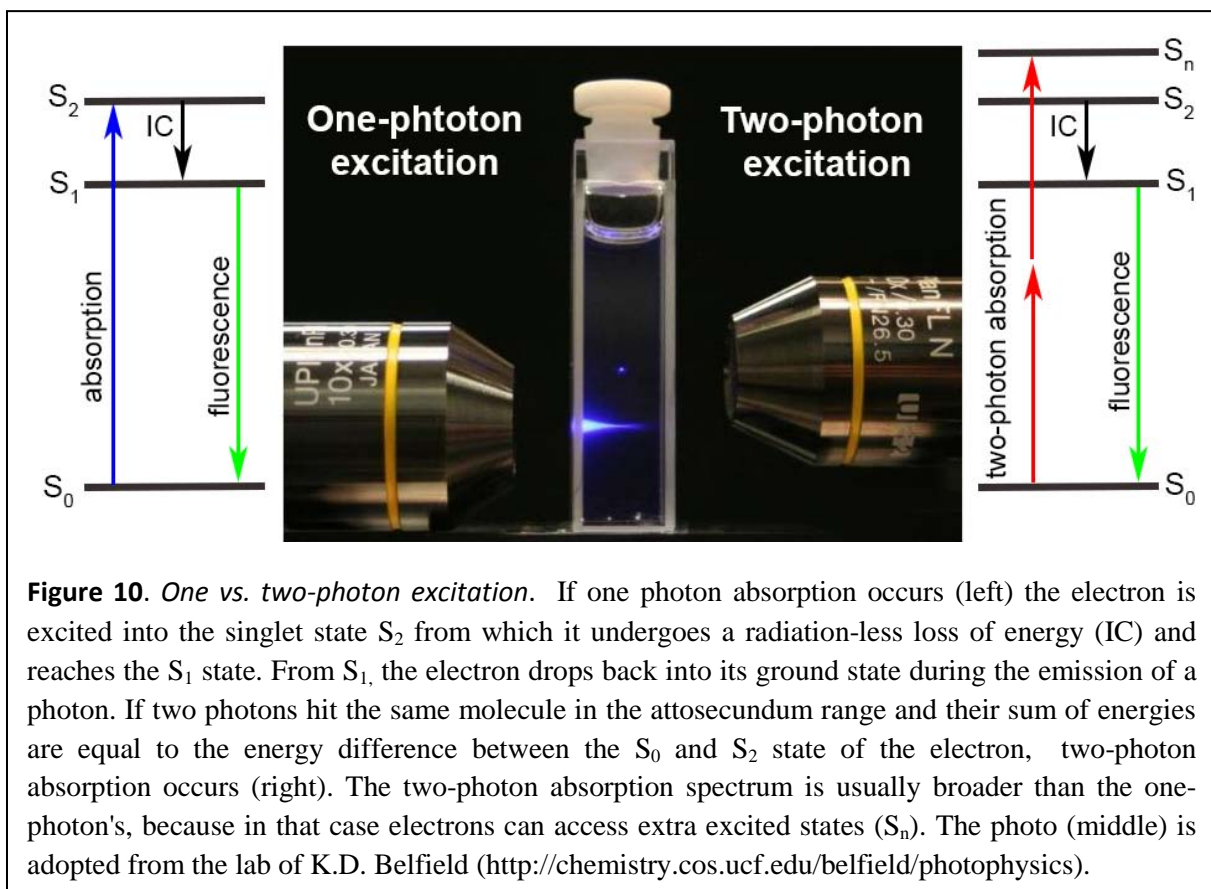
**Table 1.** Half maximal inhibitory concentrations (IC<sub>50</sub>) of blebbistatin for various myosins [69].

Despite the assumed specificity of blebbistatin for certain myosin isoforms, emerging evidences indicate that blebbistatin may interact with partners other than myosin II, as it also inhibits myosin II independent processes such as cell streaming and plaque expansion in myosin II-null *Dictyostelium* cells [70].

A well-known limitation of blebbistatin is its phototoxicity occurring upon illumination by blue light [71-73]. Irradiation at these wavelengths causes structural changes in the molecule, which is – according to current view – accompanied by the generation of reactive oxygen species responsible for the phototoxic effect [73]. Blue light susceptibility of blebbistatin greatly hinders its application in *in vivo* imaging techniques, since excitation wavelengths less than 500 nm seriously damage the sample [74-87]. Additionally, blebbistatin exerts a significant cytotoxic effect even without irradiation during long-time experiments [73], which is a serious problem in many *in vivo* systems. Further difficulties may arise from blebbistatin’s own fluorescence which can interfere with fluorescent signals such as GFP or with FRET-based experimental setups [88], troubling detection.

## Fluorescent microscopy

In the investigation of biological processes, visualization is crucial, for which the most extensively used phenomena is fluorescence. Fluorescence occurs when a photon is absorbed by a fluorophore, raising an electron to a higher, excited energy state from which it relaxes back to the ground state, emitting a longer wavelength photon. In order to achieve absorption, the energy of the incident photon has to match the energy difference between the excited state and the ground state. If absorption occurs, the molecule is excited into the singlet state  $S_2$  from which it undergoes a radiation-less loss of energy and reach the  $S_1$  state. From  $S_1$  most of the molecules return to the ground state while their energy is converted into heat. In some cases, after a delay of  $\sim 10^{-8}$ - $10^{-9}$  sec, the excited electron drops back into its ground state during the emission of a photon. Due to the  $S_2$ - $S_1$  conversion, the energy of this emitted fluorescent photon is lower (i.e. its wavelength is longer) than the photon originally absorbed, a phenomena known as the Stokes shift (Figure 10).



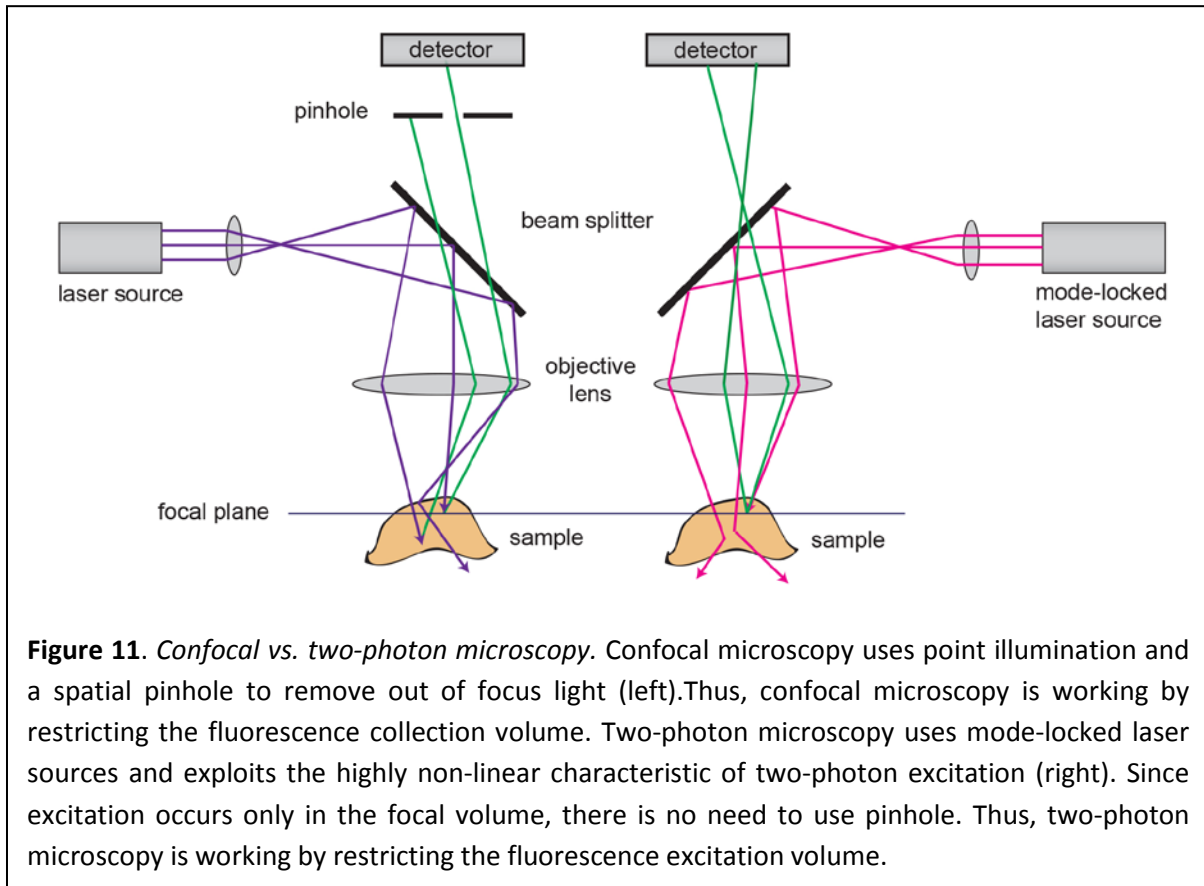
The absorption of an incident photon at room temperature is around the attosecond range ( $10^{-18}$  sec) [89]. If in this specified time window multiple photons hit the same molecule and

their sum of energies are equal to the energy difference between the  $S_0$  and  $S_2$  state of the molecule, multiphoton excitation occurs. Any combinations of the energies are sufficient, but for practical reasons, two photons with equal energies are usually used. There are no differences between the one- and two-photon fluorescence emission spectra of fluorophores but the two-photon absorption spectra can be substantially different from its one-photon counterparts. This is because in two-photon excitation the momenta of the two photons combine and give a higher degree of freedom than it can be found in single photon excitation. This allows electrons to access excited states like  $S_2$  and  $S_4$ , resulting in broader absorbance spectra of the molecules [89]. The quantitative measure of the probability of the two-photon absorption is called two-photon cross section ( $\sigma_{2p}$ ).  $\sigma_{2p}$  has units of  $\text{cm}^4 \text{s}$ , where  $10^{-50} \text{ cm}^4 \text{ s photon}^{-1}$  is called one Göppert-Mayer or 'GM' unit [90].

Multiphoton excitation requires extremely high photon flux compared to that of applied in common fluorescence microscopy techniques, typically  $10^{20}$ - $10^{30}$  photons/ $(\text{cm}^2\text{s})$ . To attain this high photon density - without burning both the equipments and the samples - instead of continuous illumination, pulsed light is applied. Nowadays only one type of commercially available light sources can be used for two-photon excitation and these are the Ti:sapphire lasers. These lasers generate  $\sim 100$  femtosecond pulses of high peak power at a low repetition rate ( $\approx 100$  MHz, i.e. 10 nanosecond between pulses) resulting in low average power (typically some 10 mW to 1-3 W). In order to get the required photon flux, the laser beam is focused to a subfemtoliter volume using a high numerical aperture (NA) objective. By concentrating the photons both temporally and spatially, the probability of two-photon absorption greatly increases. In case of one-photon excitation the amount of absorbed light is proportional to the intensity of the incident light. However, in case of two-photon excitation the absorption varies with the square of the excitation intensity, which decreases approximately with the square of the distance from the focus. As a result of this highly non-linear behavior (function of the  $\approx$  fourth power of intensity) only those molecules are excited which are very near of the focal point of the laser beam (Figure 10).

The use of fluorescence in microscopy was a real breakthrough in life sciences. In comparison with bright-field techniques (transmitted, reflected light) fluorescence microscopy has much better contrast, which derives from the specific labeling of subcellular structures of interest with fluorescent markers and the rejection of unwanted short

wavelength background by filtering the emitted, longer wavelength light [91]. However, in a conventional wide-field fluorescent microscope, not only photons arising from the focal plane are collected: photons from out-of-focus areas are also gathered, resulting in some blur in the region of interest.



To remove out-of-focus light, a new fluorescent microscopy technique emerged, called confocal microscopy. It uses point illumination and a spatial pinhole which is positioned precisely at the focus of the sample so they are "confocal". The pinhole enables the pass of light collected from confocal points in the sample and excludes the non-confocal, out-of-focus light (Figure 11). Although confocal microscopy enables the acquisition of high-resolution - and due to optical sectioning - three dimensional images in cell cultures and optically thin specimens, it has limited use in deep tissue imaging. This is mainly because of the vulnerability of the technique to light scattering. For example in brain tissue, the effective scattering length (the average distance that a photon travels between two scattering events) is approximately 50-100  $\mu\text{m}$  [89]. Moreover, the scattered excitation photons not only fail to contribute to the useful signal but they also excite diffuse

fluorescence and cause photobleaching. When focusing more than a few tens of micrometers deep into a tissue - as the consequence of those two effects - confocal images suffer a rapid loss in both contrast and intensity.

Light scattering of biological samples is a complex process but it can originate from basically two physical phenomena: Rayleigh and Mie scattering. Rayleigh scattering [92] occurs when light goes through such medium (e.g. transparent solids, liquids or gases) whose particles are much smaller than the wavelength of the incident light. This type of scattering is very sensitive for both the size of the particles (inversely proportional to the sixth power) and the wavelength of light (inversely proportional to its fourth power). The blue color of the sky is a wonderful example of this physical phenomena. However, the clouds on the sky are white, which is a consequence of another type of scattering called Mie scattering. Mie scattering refers to scattering by particles whose sizes are comparable to or larger than the wavelength of light [93]. Mie scattering is much less sensitive to the wavelength of light (although still inversely proportional), but it is more sensitive to the size of particles.

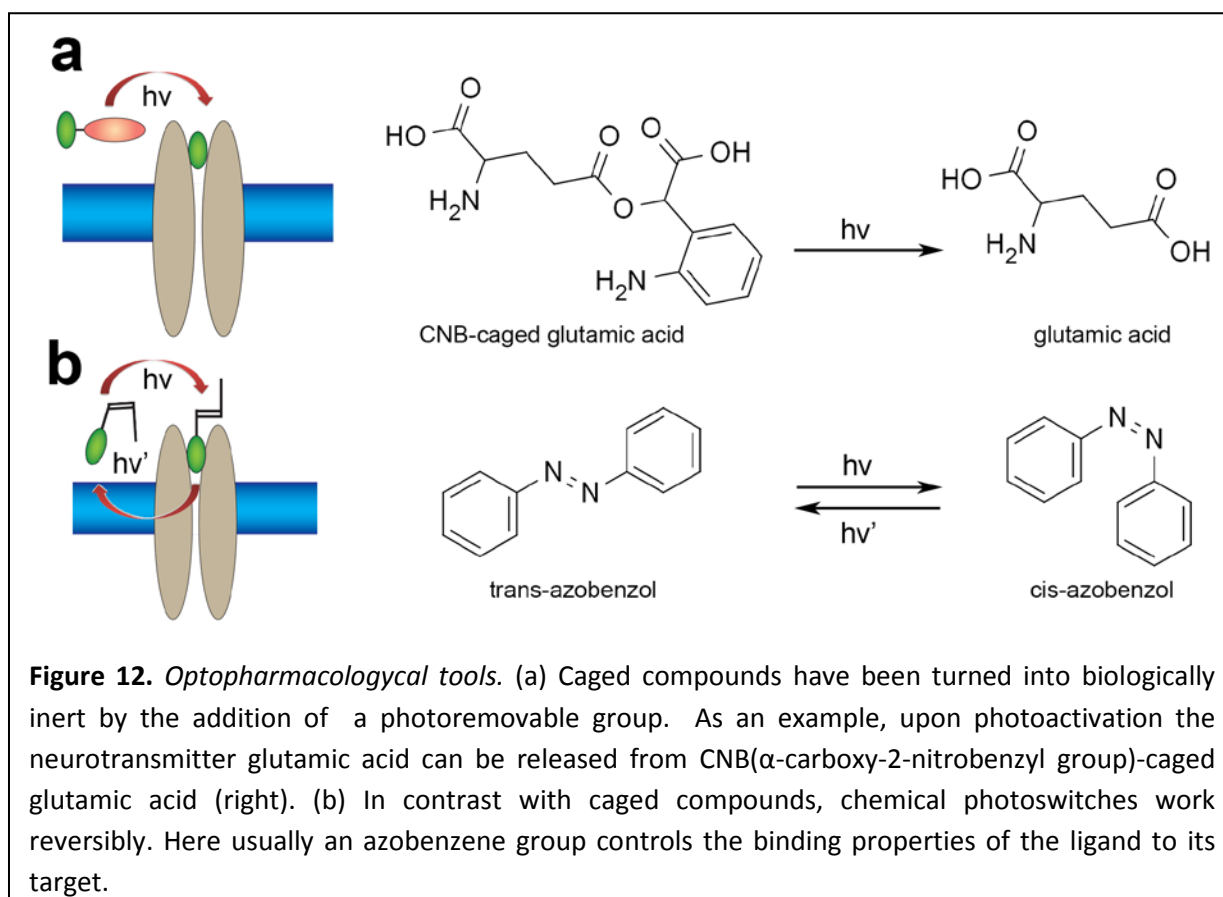
The recognition that light scattering is inversely proportional to the wavelength of light, the theory of two-photon absorption as well as the appearance of mode-locked infrared lasers in the 1990s led to the birth of a new kind of fluorescent microscopy, called two-photon microscopy [90]. Using tunable infrared lasers, two-photon microscopy provides much deeper penetration depth than confocal techniques, opening brand new perspectives in deep-tissue imaging. Another key advantage of two photon microscopy is the highly non-linear feature of two-photon absorption. As a consequence, the excitation occurs only where it is needed, in the focal spot, neither above nor under it. This unique characteristic not only provides unprecedented spatial control but significantly decreases the photodamage of the sample, allowing the development of improved live-imaging techniques. Furthermore, due to the capability of optical sectioning, three-dimensional reconstruction of structures is possible.

Knowing the dimensions of the two-photon focal volume is important, for instance to estimate the thickness of an optical section or to calculate the amount of caged compound released per laser pulse. It is defined by the illumination point spread function, IPSF ( $x, y, z$ ), which describes intensity everywhere in space near the focus. In two-photon microscopy,

IPSF<sup>2</sup> defines the true optical resolution which depends on the wavelength of the excitation laser and the numerical aperture of the objective (and not the magnification!). By approximating the IPSF<sup>2</sup> as a three-dimensional Gaussian volume, analytical integration over all space yields the two-photon excitation focal volume [90].

## Optopharmacology

Chemical reactions occur when a molecule is provided with the necessary "activation energy". As described in the previous section, if a molecule absorbs light, its electron structure changes and goes into the excited S<sub>1</sub> state from where it relaxes back to the ground state by giving off lower energy photon or heat. However, the absorbed energy can also serve as "activation energy" to promote chemical reactions. Chemical reactions occurring by the absorption of light are called photochemical reactions. The sub-discipline of chemistry which studies photochemical reactions is called photochemistry.



The idea of combining photochemistry with pharmacology has led to the rise of optopharmacology, where the effect of bioactive compounds are controlled by light,

providing precision as well as spatial and temporal control. Optopharmacological tools available today can be divided into two classes: caged compounds and chemical photoswitches [94]. Caged compounds are such derivatives of bioactive compounds which have been turned into biologically inert (caged) by the addition of a photoremovable protecting group, such as the  $\alpha$ -carboxy-2-nitrobenzyl group. Illumination of the desired area treated by the caged compound results in a concentration jump of the released biologically active molecule, affecting processes specific to the compound [95]. In contrast to caged compounds, chemical photoswitches (or photochromic ligands) work reversibly: in this case the ligand is attached to a photoisomerizable group - most frequently to azobenzene - which controls whether the ligand can fit into the binding site of the target protein or not [96].

## IV. Aims

The lack of experimental target deconvolution techniques suitable for the determination of both weak- and strong-binding interaction partners of pharmacological compounds is an unresolved problem. By mapping their interaction network, the exact mechanism of their action could be elucidated, adverse effects may be understood and predicted, novel druggable targets could be explored and importantly, new effects may be highlighted (i.e. repositioning).

The **first aim** of this study was to investigate new aspects of photoaffinity labeling of azido-modified bioactive compounds in target deconvolution such as the determination of both strong and weak binding partners as well as their apparent binding affinities (EC50) to their targets. Our goals in this project were:

- explore versatile synthetic methods to obtain aryl azido derivatives of bioactive compounds
- test the effect of the azido modification *in vitro* and *in vivo*
- photo-crosslink different concentrations of the azido derivative in a protein mixture, separate the crosslinked complexes, detect, quantify and identify them

Our experiments performed with azidoblebbistatin - a photo-crosslinkable derivative of the myosin II inhibitor, blebbistatin - has led to the following observations:

1. the C15 position of blebbistatin can be substituted without affecting its myosin II inhibitory properties
2. substituting an electron withdrawing group to this position alters the fluorescence and phototoxicity of blebbistatin
3. myosin can be covalently saturated by sequential crosslinking in the presence of azidoblebbistatin (cycles of azidated ligand addition + UV irradiation)

Based on the first two above mentioned observations, our **second aim** was to investigate the effect of the C15 substitution of blebbistatin by electron withdrawing substituents. Our goals in this project were:

- synthesize C15 chloro and nitro derivatives of blebbistatin

- measure their photostability and fluorescent properties
- measure their *in vitro* myosin II inhibition
- measure their *phototoxicity* on HeLa cells and zebrafish embryos
- characterize their *in vivo* myosin II inhibition on *Dd*, HeLa and M2 cells as well as on zebrafish embryos

The third observation and the discovery that azidated compounds can be two-photon activated initiated the **third aim** of this study, the development of a two-photon-microscopy-based drug targeting technology. Our goals in the project were:

- characterize the two-photon induced photoreaction of azidoblebbistatin
- measure the dimensions of the photoreaction using objectives with different numerical apertures
- Test the applicability of the new targeting technology by:
  - local inhibition of collective cell migration and organ development in zebrafish embryos
  - subcellular inhibition of myosin IIs in the continuously blebbing M2 human melanoma cell line

## V. Results

### Overview

The results section of the thesis is composed of three parts representing the three aims of the thesis.

Part 1. Target deconvolution by aryl azides.

In the course of the project, 10 azido modified bioactive compounds were synthesized, from which azidoblebbistatin, the first photoinducible myosin II inhibitor, was characterized deeply. We measured its photoreactivity, *in vitro* and *in vivo* *Dd* myosin II inhibition and photo-crosslinked to its cellular interaction partners. Its strong- and weak-binding interaction partners (along with the EC50 values of the complexes) were also identified.

Part 2. Para-nitroblebbistatin, an improved tool in myosin research.

The non-phototoxic behavior of azidoblebbistatin inspired us to replace its azido group with a nitro or a chloro group (which have similar electron-withdrawing characteristics to the azido group), to obtain a non-phototoxic derivative of blebbistatin. We synthesized para-nitroblebbistatin and para-chloroblebbistatin, then investigated their photostability, fluorescence, *in vitro* myosin inhibition, and phototoxicity. As para-chloroblebbistatin turned out to be even more phototoxic than blebbistatin, only para-nitroblebbistatin was subjected to further *in vivo* tests. Based on *in vivo* experiments performed with *Dd*, M2 and HeLa cells as well as with zebrafish embryos, para-nitroblebbistatin is not cytotoxic and has the same myosin II inhibition like blebbistatin.

Part 3. Molecular tattooing.

We have developed molecular tattooing, a two-photon microscopy based optopharmacological technology with the ability of confining the effect of bioactive compounds to well define regions within a live organism, even with subfemtoliter resolution. By *in vivo* tattooing of myosin II with azidoblebbistatin, yet inaccessible mechanisms of organ development of zebrafish and cellular blebbing of M2 cells have been revealed.

For the presentation of the results I use plural, to honor the colleagues who I worked with or who contributed to this work in any aspects. All presented experiments have been carried out or designed by myself unless otherwise stated.

## Part 1: Target deconvolution

The experimental determination of the interactom of a given drug molecule is an unresolved problem. According to the results accomplished so far, the chemical modification of the drug is inevitable in order to map its interaction network. Although, label-free techniques like SPROX and DARTS may seem very attractive at first glance, there is no evidence that these methods can be applied for whole interactom determination.

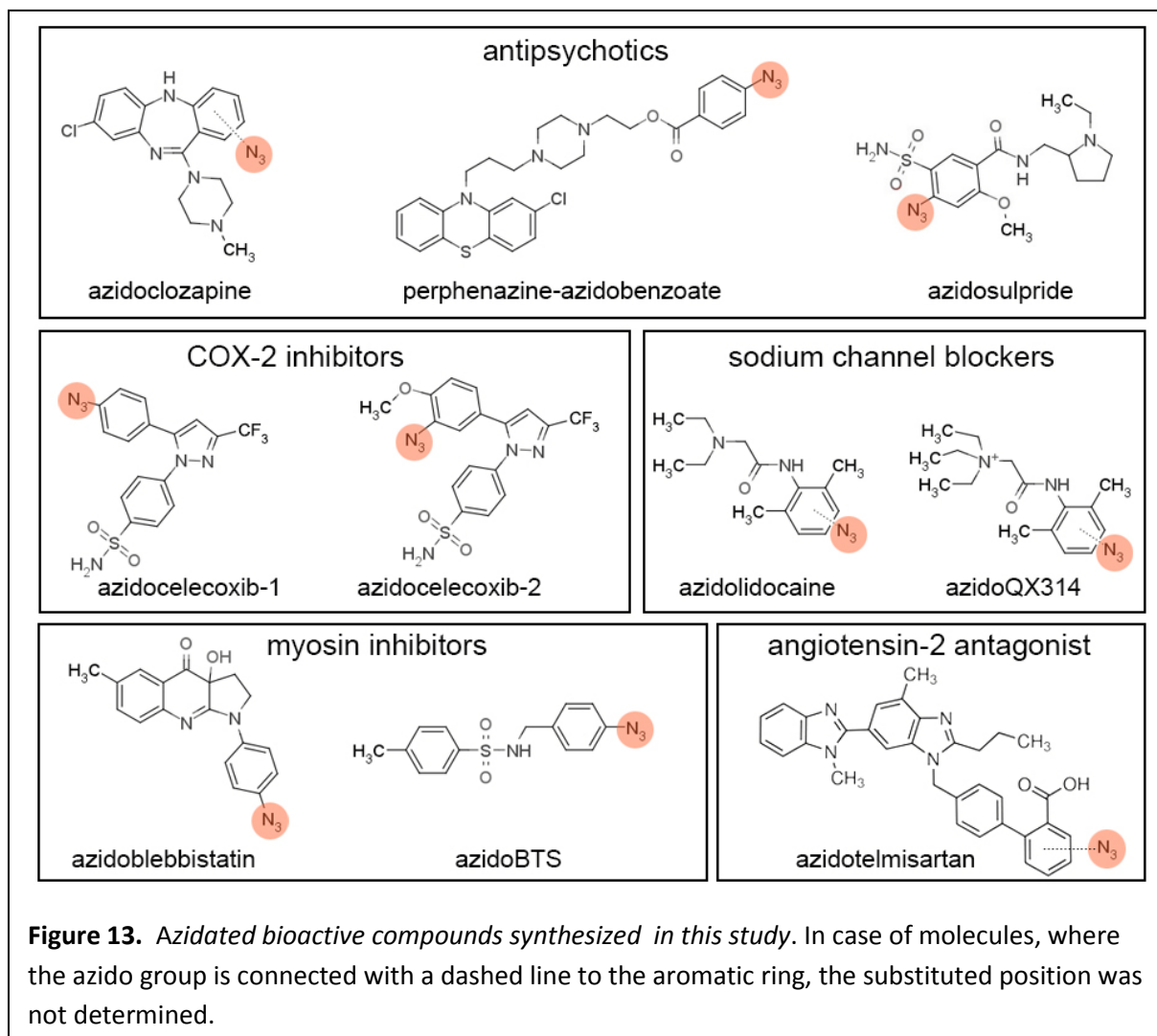
Chemical modification of the drug molecule is necessarily accompanied by structural perturbation, therefore the extent of perturbation is a key question. The goal in this sense is minimization, so applying as small change in the molecular structure as possible. The bulky tags utilized by affinity chromatography-based techniques clearly do not satisfy this requirement. Furthermore, affinity chromatography based approaches are not suitable for the identification of weak-binding partners. If the assay parameters are optimized for weak interactions, the selectivity is drastically reduced.

However, photolabelling of the aromatic group of the compound by azide may solve these obstacles. The azido group is small, biologically inert and stable in the absence of UV irradiation so there is a very good chance that this photoaffinity tag will not affect significantly the binding properties of the modified drugs. On the other hand, covalent crosslinking of the protein-drug complexes stabilizes the weak protein-drug interactions, even the weakly-bound complexes can be analyzed.

Turning drug molecules into photoaffinity agents and crosslinking them covalently to their target proteins in order to secure the weakly bound protein-drug complexes is not a new idea. If the drug is labeled (fluorescent tag, radioactive isotope), the isolation and subsequent identification of the complexes is possible with the help of proteomic methods, such as two-dimensional gel electrophoresis followed by mass spectrometry. Important to note, that photoaffinity labeling does not provide information about the binding affinity values between the drug and its target proteins.

In this part of my thesis I introduce an improved, photoaffinity labeling-based target deconvolution technique applicable for whole target identification as well as the

experimental determination of the apparent binding affinities of the protein-drug complexes.



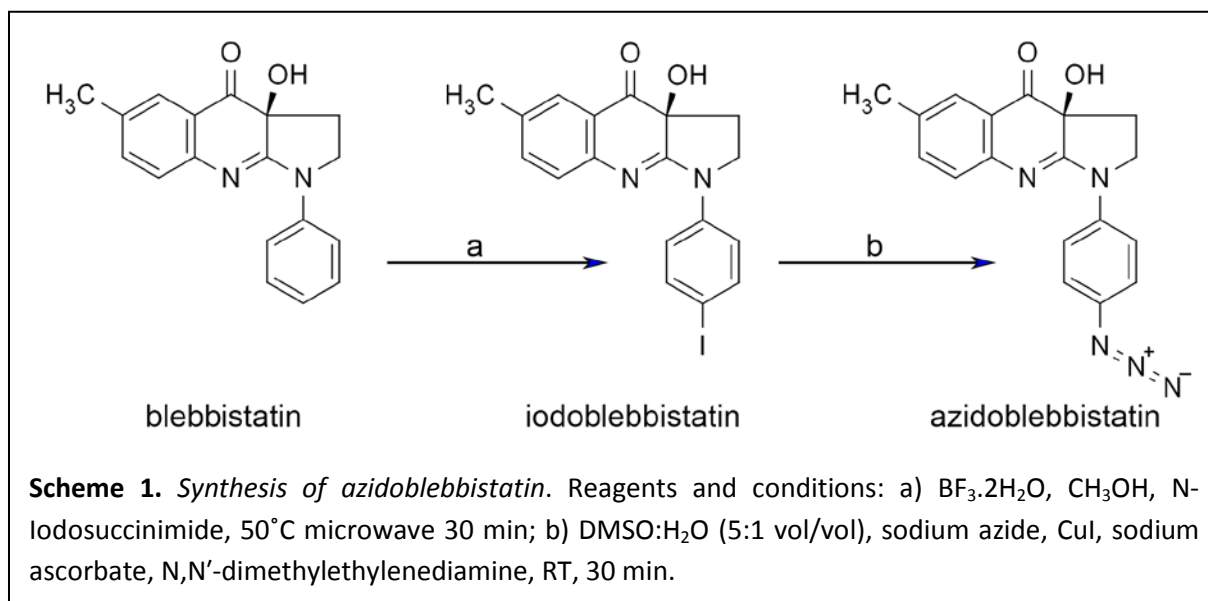
In the project 10 azido-modified bioactive compounds were synthesized including antipsychotics, COX inhibitors, sodium channel blockers, myosin inhibitors and an angiotensin 2 receptor antagonist (Figure 13.), using different synthetic strategies. Azidosulpride was obtained by converting its amino group to azide by diazotization. Azidoclozapine, azidolidocaine, azidoQX314, azidotelmisartan and azidoblebbistatin was synthesized by the iodination of the parent molecule followed by a halogen-azide exchange reaction (see Materials and Methods). Perphenazine-azidobenzoate was obtained by esterification of the hydroxyl group of perphenazine by azidobenzoate (see Materials and Methods). In case of azidoBTS [56] and the two celecoxib isomers [97, 98], their published

total synthesis were applied using iodinated building blocks (see Materials and Methods). Then, the iodo derivatives were converted to azides as the last step of the synthesis.

From the synthesized azido derivatives, azidoblebbistatin was chosen for further detailed characterization and interactomic investigation. The characterization of the other 9 compounds is in progress.

### Azido modification of blebbistatin

Blebbistatin is aromatic, therefore an azido substitution of its aromatic ring is sufficient for the aryl azide conversion. The traditional synthetic approach of aryl azides involves in the diazotation of primary aryl amines. The required amine precursors can be synthesized by aromatic nitration followed by the reduction of the nitro group to amine. However, nitration usually requires harsh reaction conditions, it has low yield and results in a variety of byproducts. In case of complex molecules – like bioactive compounds - it can also lead to the decomposition of the parent molecule.



Presumably, because of the above mentioned reasons our efforts to nitrate blebbistatin directly have failed. To overcome these problems, we used and improved strategy, based on aromatic iodination followed by a halogen azide exchange step [22, 23, 99-102]. The iodination was performed using N-Iodosuccinimide, while the reaction was catalyzed by the super acid boron trifluoride dihydrate, which was also the main solvent of the reaction. To improve the acid solubility of blebbistatin, methanol was added as co-solvent. According to

analytical HPLC, two products have been formed, from which the main peak was identified as iodoblebbistatin. The byproduct was not determined. After purification of iodoblebbistatin, the halogen azide exchange reaction was performed using sodium azide, copper (I) iodide catalyst, N,N'-dimethylethylenediamine and sodium ascorbate. In this reaction, only one product was formed, which was identified as azidoblebbistatin. NMR analyses confirmed that the azido group was substituted at para position of the phenyl ring of blebbistatin.

### UV-VIS spectra and photoreactivity

Photoactivation of aryl azides are accompanied by structural changes, which alter the absorption spectra of the molecules. Consistently, the first step of the characterization of azidoblebbistatin was to record its absorption spectrum before and after UV irradiation.

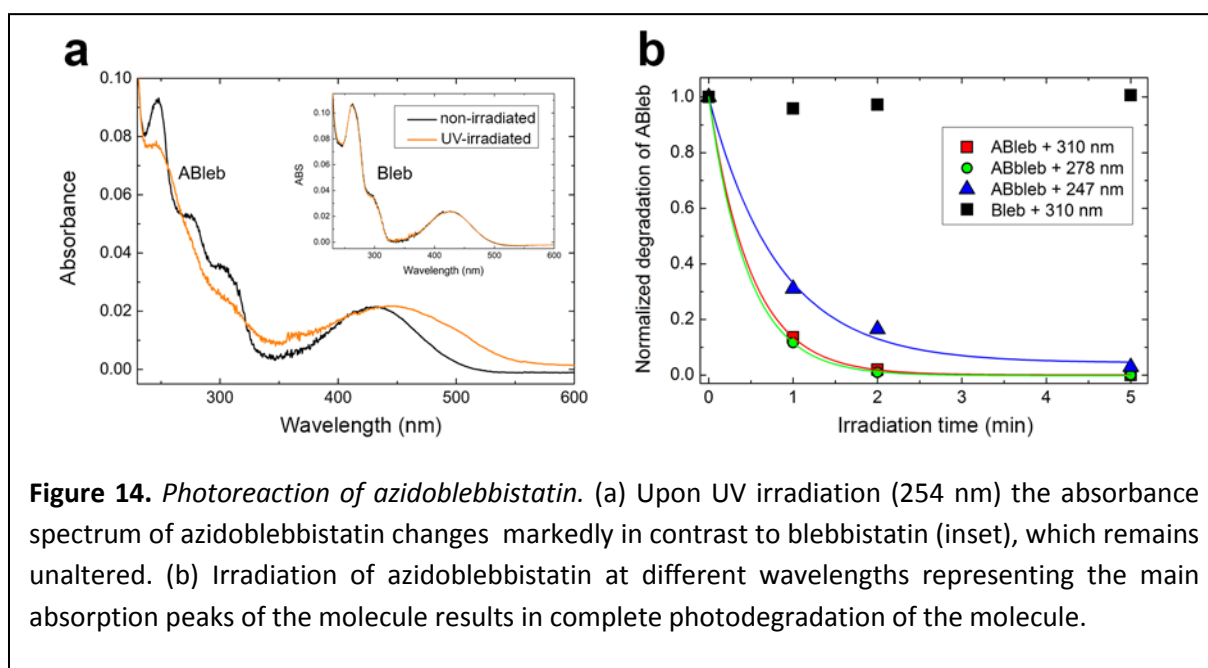
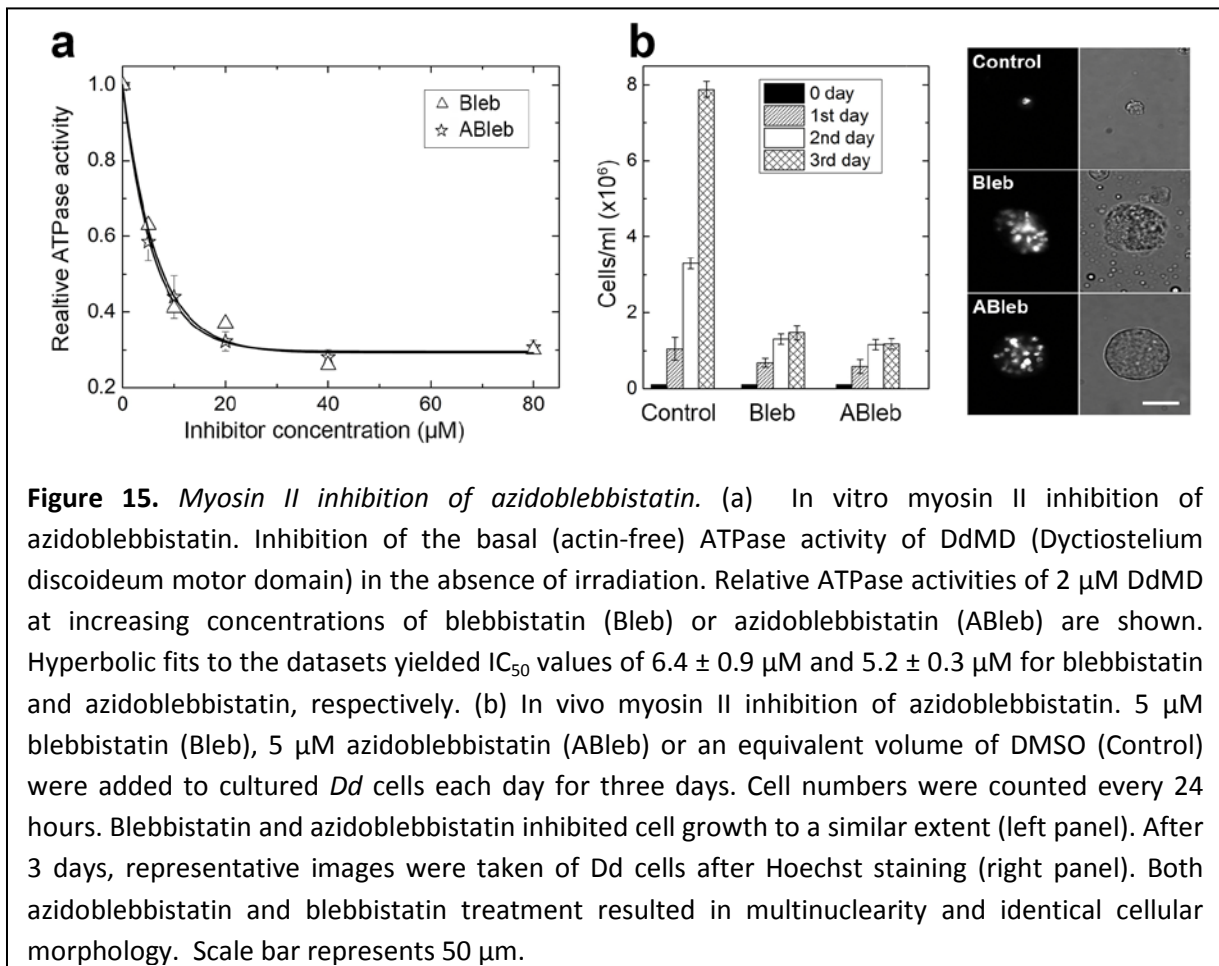


**Figure 14.** Photoreaction of azidoblebbistatin. (a) Upon UV irradiation (254 nm) the absorbance spectrum of azidoblebbistatin changes markedly in contrast to blebbistatin (inset), which remains unaltered. (b) Irradiation of azidoblebbistatin at different wavelengths representing the main absorption peaks of the molecule results in complete photodegradation of the molecule.

Figure 14a illustrates, that upon irradiation of azidoblebbistatin, its spectrum changes significantly, indicating successful aryl azide activation. In order to optimize the photoreaction, azidoblebbistatin was irradiated at three different wavelengths, which represent the main absorption peaks of the molecule. The irradiation was carried out in a fluorescence spectrometer, while LC-MS was applied to quantify the degradation of azidoblebbistatin (Figure 14b). Irradiation at 278 and 310 nm wavelengths resulted in rapid photodegradation, from which the 310 nm wavelength was chosen for further experiments, as it may be less phototoxic.

### ***In vitro* and *in vivo* myosin II inhibition of azidoblebbistatin**

Although azidation is a minimal perturbation of the molecular structure, its effect on the binding properties of the parent compound needs to be tested. Since blebbistatin is a myosin II inhibitor, we examined myosin II activity in order to test the effect of the modification both *in vitro* and *in vivo*.



First, we carried out a NADH/NAD-coupled assay to measure the *in vitro* inhibition of the basal ATPase activity of azidoblebbistatin on Dictyostelium discoideum myosin II motor domain (*DdMD*). In the experiment, *DdMD* was treated with increasing concentrations of blebbistatin or azidoblebbistatin and concentrations at half-maximal inhibition of the inhibitors were determined. Figure 15a shows that the IC<sub>50</sub> values of the molecules (5,2 μM and 6,4 μM respectively) are similar. The ATPase measurement was carried out by Boglárka Várkuti.

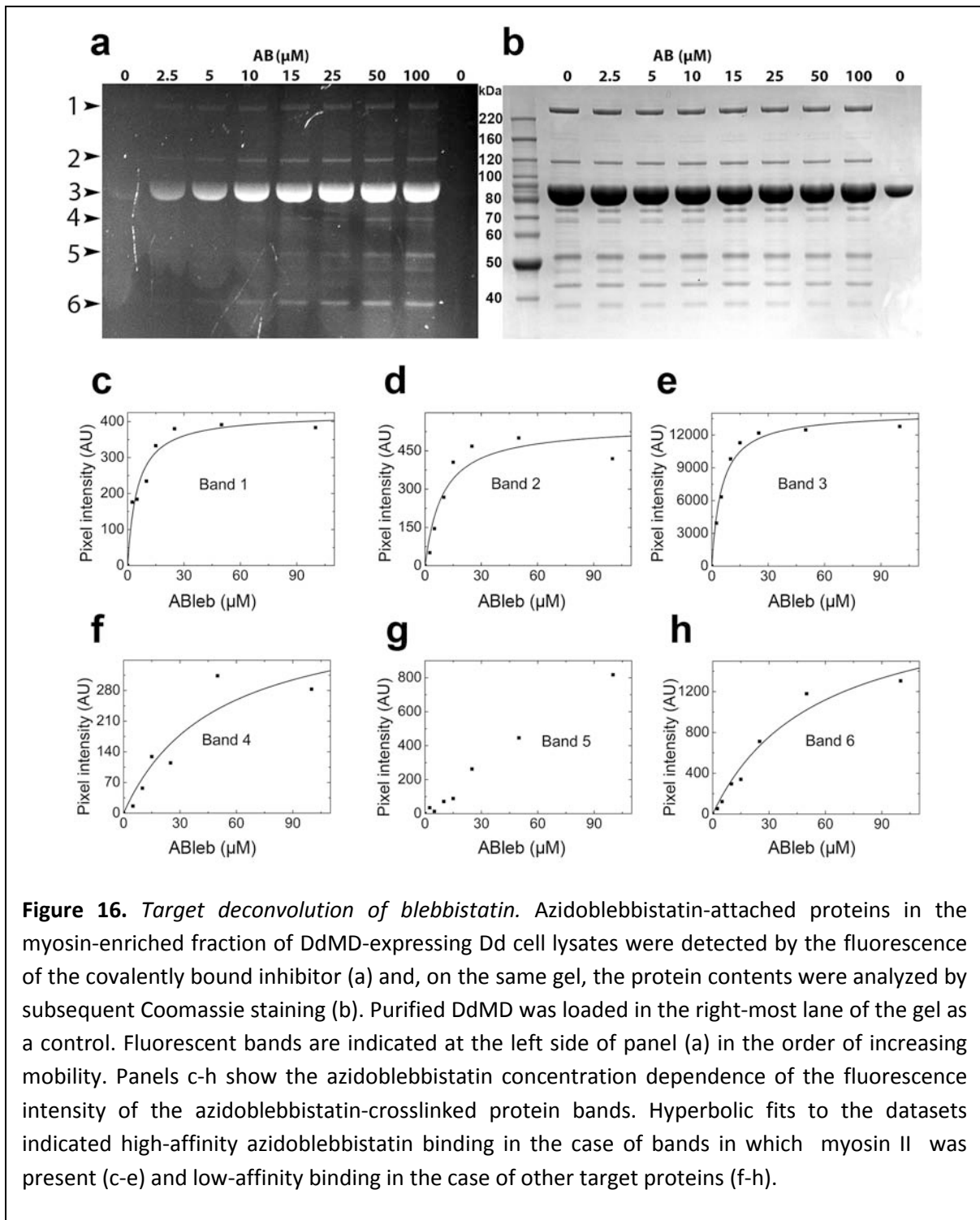
Growth of *Dd* cells in suspension culture is considered as a typical myosin II dependent process [103], so we chose it to evaluate the *in vivo* inhibitory properties of azidoblebbistatin and compared it to blebbistatin's. Cultured *Dd* cells were treated with azidoblebbistatin or blebbistatin - along with DMSO-treated control - every 24 hours for three days. During the experiment, changes in cell count were monitored and we observed no difference between cells treated by the two inhibitors (Figure 15b, left panel). Representative images taken at the third day indicate that treatment with both inhibitors resulted in the same cellular morphology (figure 15b, right panel).

### **Target deconvolution of blebbistatin**

Azidoblebbistatin is fluorescent, therefore it can be used for PAL experiments without any additional labeling. We speculated, that if we would crosslink azidoblebbistatin to its targets applying the inhibitor at increasing concentrations followed by SDS gel electrophoresis and subsequent densitometry of the fluorescent bands, the  $EC_{50}$  values of the azidoblebbistatin-protein complexes could be determined.

We prepared *Dd* whole cell lysates as well as myosin-enriched fractions of the lysates of a *Dd* cell line expressing recombinant *DdMd*, and subjected the samples to increasing concentrations of azidoblebbistatin and UV irradiation. Purified *DdMD* from irradiated samples and non-irradiated control as well were analyzed by SDS-PAGE utilizing the fluorescence of azidoblebbistatin. On the same gel, the protein content of the samples were detected by Coomassie staining (Figure 16, Figure A1). In the irradiated samples (myosin enriched fraction), six fluorescent bands were specifically observed, and analyzed by densitometry and mass spectrometry. As a result, we demonstrated that azidoblebbistatin binds the most specifically to myosin II heavy chain ( $EC_{50}=5.1\pm 1.4 \mu\text{M}$ ) or to its degradation product ( $EC_{50}=9.3\pm 3.7 \mu\text{M}$ ) and to recombinantly expressed *DdMD* ( $EC_{50}=5.2\pm 0.8 \mu\text{M}$ ). Furthermore, previously unknown low-affinity ( $EC_{50} \geq 50 \mu\text{M}$ ) interacting partners of azidoblebbistatin were also identified. These include vacuolar  $H^+$ -ATPase A subunit and RNA-binding region RNP-1 domain-containing protein (recovered from a single band,  $EC_{50} = 50 \pm 31 \mu\text{M}$ ), a protein termed "hypothetical protein DDB\_G0275045" (NCBI-NR database) and malate dehydrogenase (recovered from a single band,  $EC_{50} = 55 \pm 17 \mu\text{M}$ ), and elongation factor  $1\alpha$  ( $EC_{50} > 100 \mu\text{M}$ ). MS analysis was carried out by the Proteomics Research Group in Szeged,

Hungary. In the whole cell lysate we observed additional low-binding partners, which were not identified.



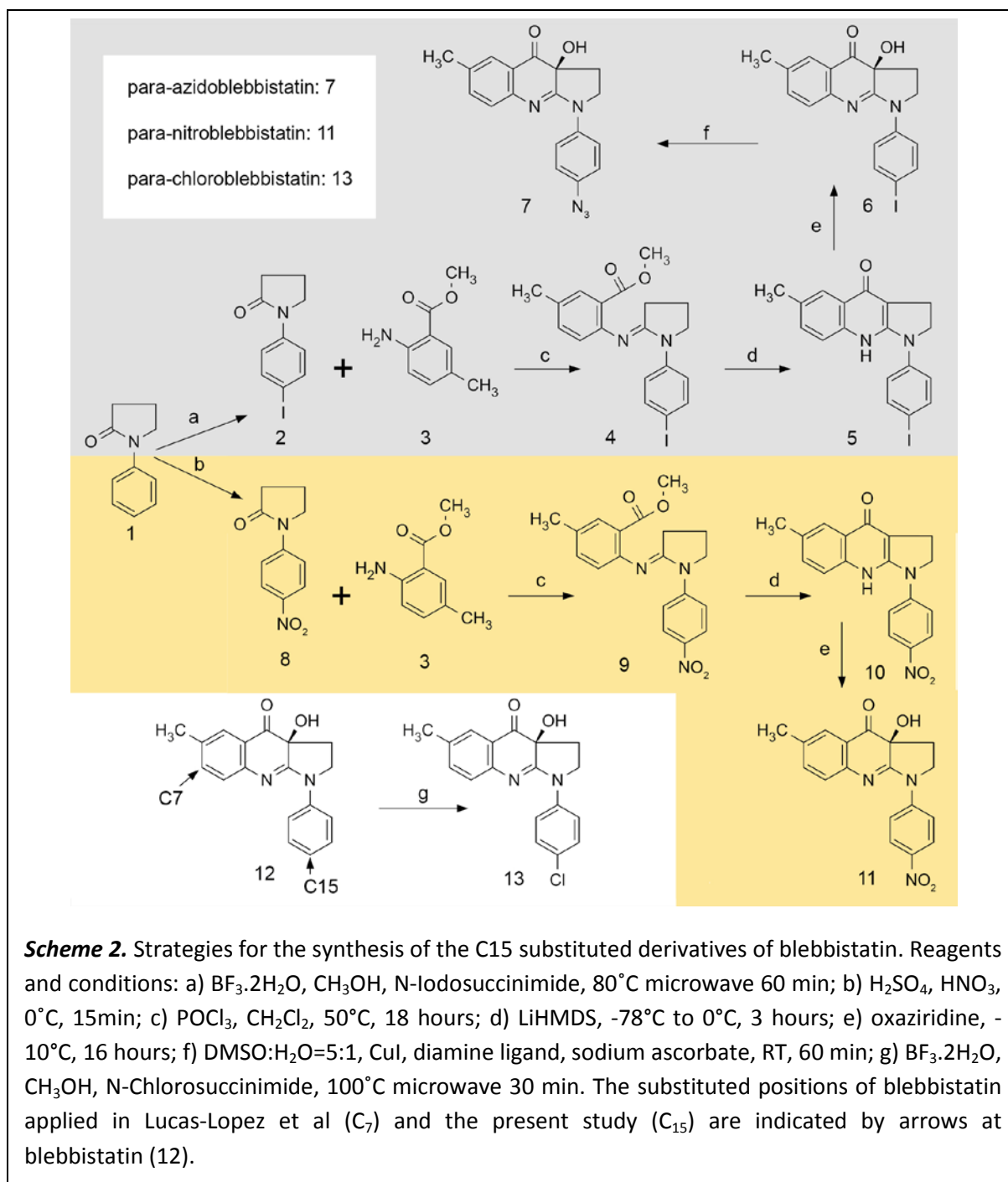
## Part 2: Para-nitroblebbistatin, a novel tool in myosin research

### Chemical modifications of blebbistatin at the C15 position

Despite the fact that blebbistatin is the most popular and the most widely used myosin II inhibitor, it has several limitations. It is phototoxic upon blue light irradiation, cytotoxic even in dark and fluorescent, which may hamper fluorescent imaging. Chemical optimization is a standard process in the development of pharmacological compounds: applying the tools of organic chemistry aiming to alter the physicochemical properties of blebbistatin has the potential to overcome its limitations, delivering the next generation of myosin II inhibitors. A significant enhancement has been reported by Lucas-Lopez *et al*, applying an electron-withdrawing nitro substituent at the C7 position of the tricyclic core of blebbistatin, resulting in reduced fluorescence and improved photostability [104]. However, the modification also decreased the myosin's affinity of the derivative by 5 fold ( $27.5 \pm 3\mu\text{M}$ ). Since the solubility of blebbistatin is below  $20\ \mu\text{M}$ , the usage of this blebbistatin derivative is very limited. Phototoxicity of the compound has not been characterized.

We recognized during the characterization of azidoblebbistatin, that unlike blebbistatin, the azido compound was not phototoxic upon blue light irradiation. Furthermore, by using para-azidoblebbistatin, even long-timescale fluorescent microscopic experiments could be conducted without phototoxicity. However, para-azidoblebbistatin is photoreactive, i.e. upon blue light irradiation it covalently attaches to myosin, which hinders its application as a reversible inhibitor. Considering the electrochemical properties of the azido group, and the results of Lucas-Lopez *et al.*, we presumed that a non-phototoxic blebbistatin derivative could be obtained if the azido group is replaced with a nitro group, a similar electron withdrawing substituent. Importantly, based on our experiments with azidoblebbistatin, we knew that the C15 position of blebbistatin tolerates substitution.

Para-nitroblebbistatin was synthesized by György Hegyi by applying the published synthetic route of blebbistatin [104], but using nitrated pyrrolidinone building block (Scheme 2).

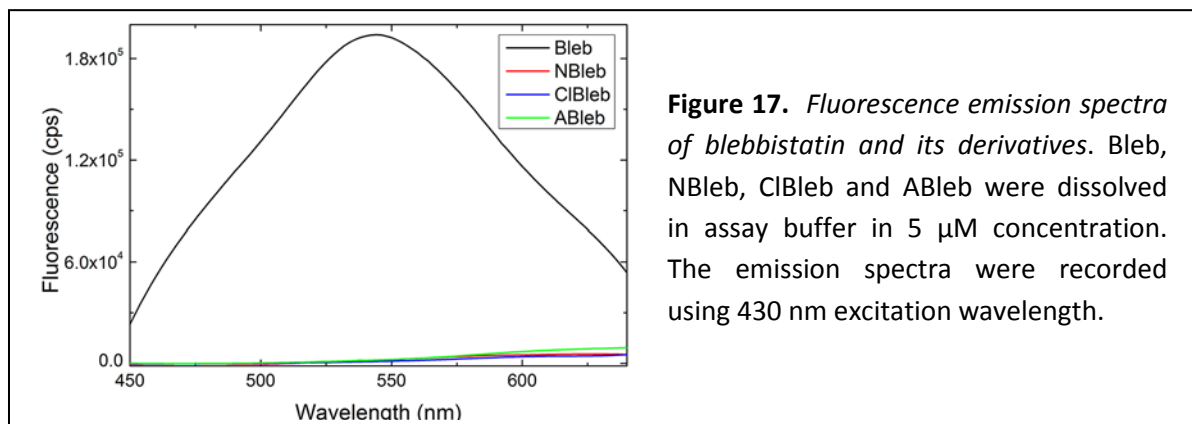


Using the same synthetic scheme, but utilizing iodinated pyrrolidinone we worked out the total synthesis of azidoblebbistatin enabling the preparation of the first photoinducible myosin II inhibitor at large scale (Scheme 2).

In addition, we synthesized para-chloroblebbistatin in order to investigate the effect of another electron-withdrawing substituent on photostability and phototoxicity at the  $\text{C}_{15}$

position. Para-chloroblebbistatin was obtained by direct chlorination of blebbistatin by N-Chlorosuccinimide (Scheme 2).

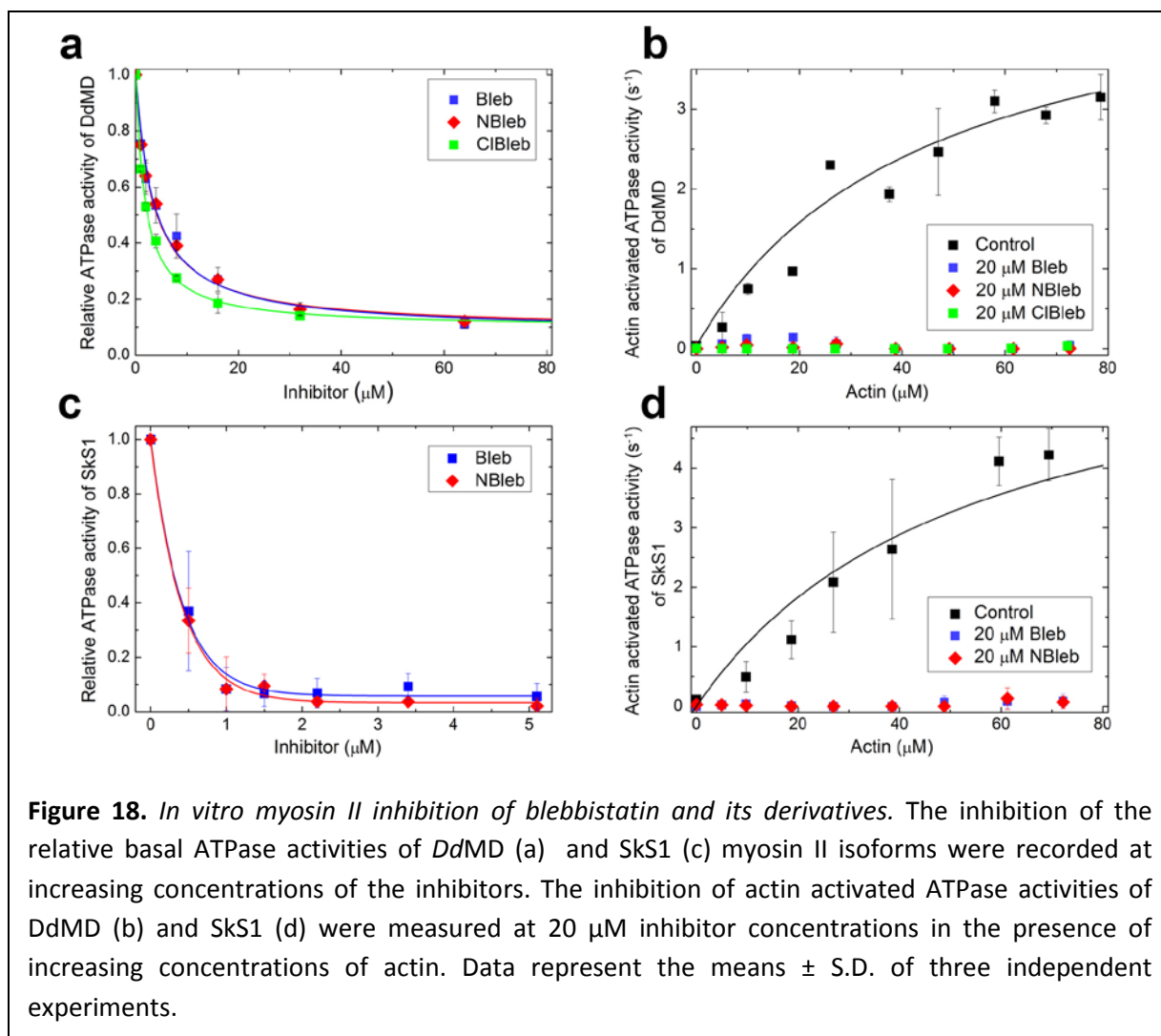
### The effect of the C15 substitution on the fluorescent properties of blebbistatin



The strong fluorescence of blebbistatin can be a serious limitation in fluorescence-based experimental setups. However, substitution of blebbistatin at the C15 position with an electron-withdrawing substituent such as nitro, chloro or azido group, significantly reduces the fluorescence of the derivative (Figure 17).

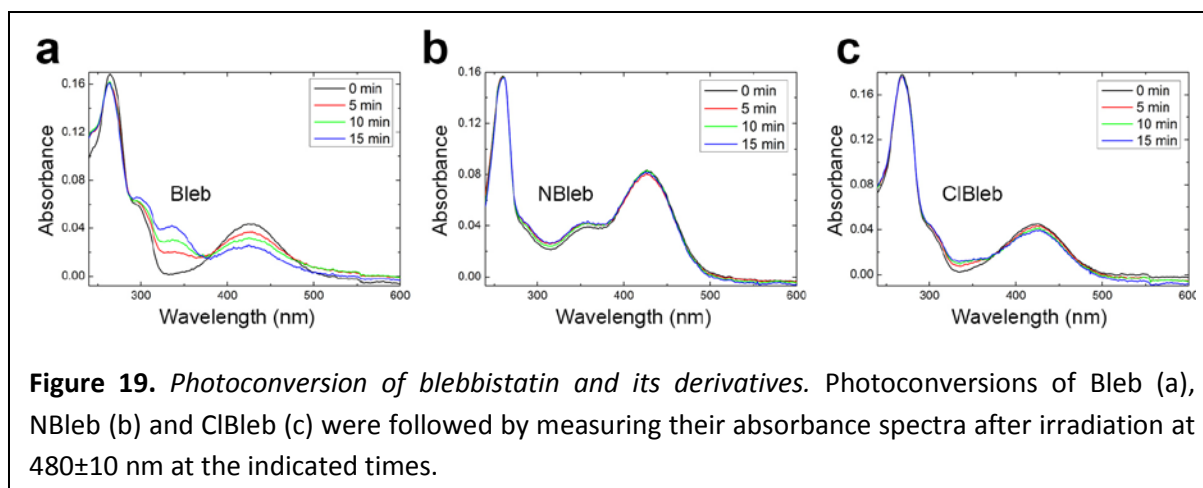
### Myosin II inhibition of para-nitroblebbistatin and para-chloroblebbistatin *in vitro*

We compared the inhibitory effect of para-nitroblebbistatin, para-chloroblebbistatin and blebbistatin on the steady-state basal as well as the actin activated ATPase activities on *DdMD* (Figure 18). Para-nitroblebbistatin and blebbistatin inhibit both the basal ATPase of *DdMD* to the same extent while para-chloroblebbistatin exerted a slightly stronger inhibition. The half-maximal inhibition values ( $IC_{50}$ ) were  $3.42 \pm 0.35 \mu$ M (para-nitroblebbistatin),  $3.56 \pm 0.49 \mu$ M (blebbistatin) and  $1.85 \pm 0.11 \mu$ M (para-chloroblebbistatin). Additionally, para-nitroblebbistatin and blebbistatin were also compared by the inhibition of rabbit skeletal muscle myosin S1 (SkS1), where the  $IC_{50}$  values were  $0.24 \pm 0.03 \mu$ M and  $0.49 \pm 0.04 \mu$ M, respectively. All of the inhibitors completely suppressed actin activation of the myosin ATPase activity even at high concentrations of actin (80  $\mu$ M). Since all three derivatives have very similar myosin II inhibitory properties, these results prove that C15 substitution of blebbistatin does not substantially alter its inhibitory characteristics. The ATPase measurements were carried out by Boglárka Várkuti and László Végner.

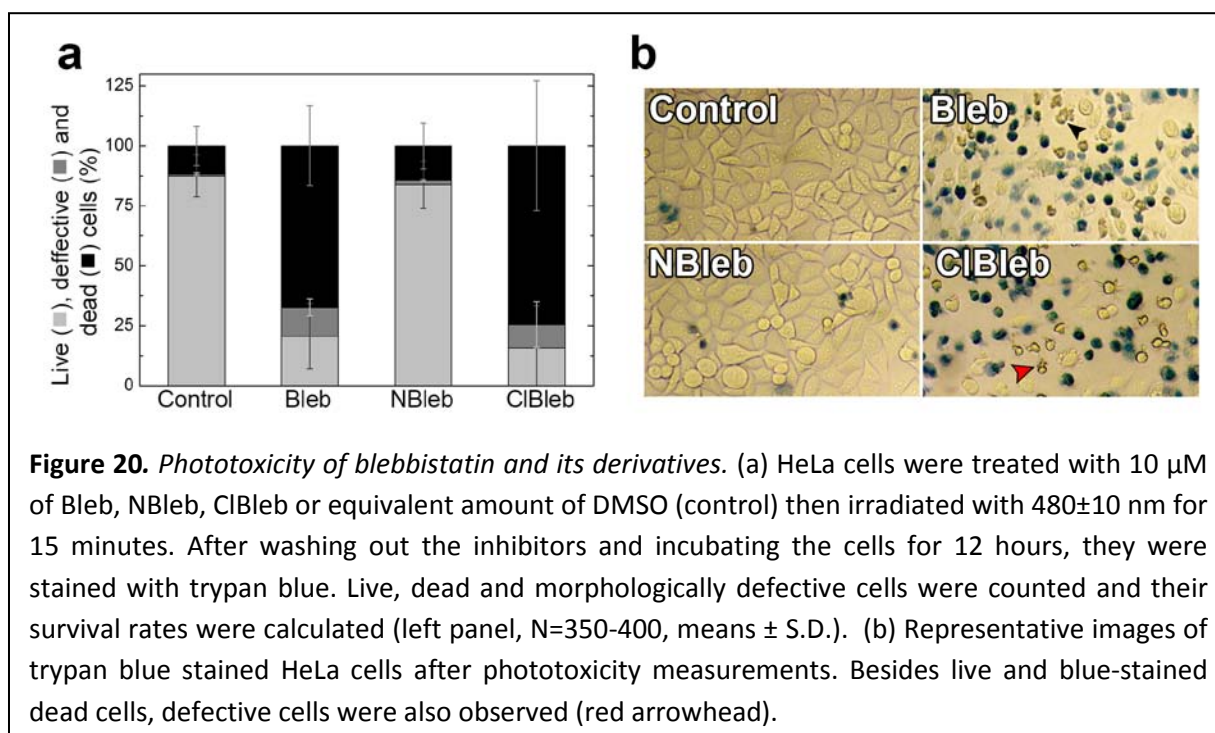


### Relationship between photostability and phototoxicity of the blebbistatin derivatives

To characterize the photostability of para-nitroblebbistatin, para-chloroblebbistatin and blebbistatin, the effect of blue light irradiation on their absorption spectra were compared (Figure 19), since blebbistatin is frequently used in confocal microscopic live cell imaging e.g. following GFP signals with 480 nm excitation wavelength.



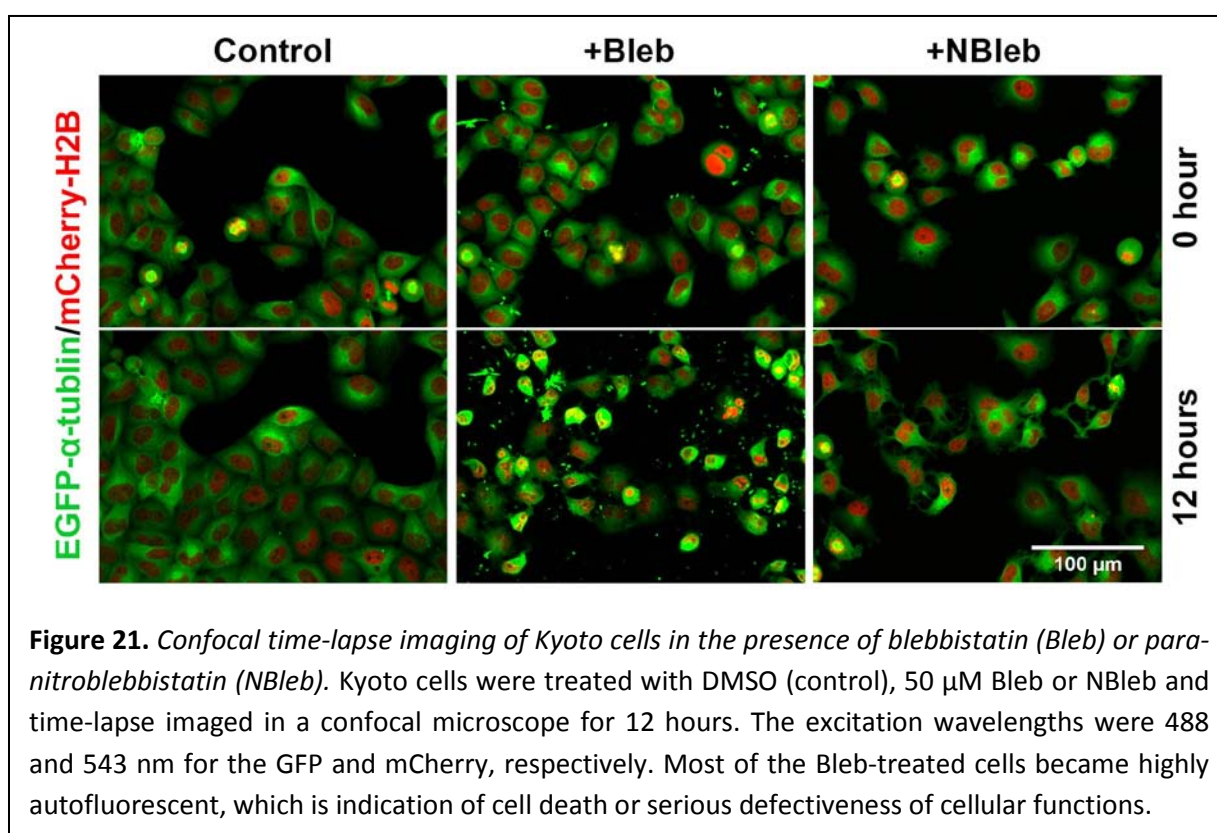
Upon irradiation, the absorption spectrum of blebbistatin changed markedly, consistently with previously published studies [72, 73, 105], indicating photo-induced changes in the molecular structure. The absorption spectra of the C15 chloro and nitro substituted derivatives remained essentially unchanged upon blue light irradiation which proves that the photostability of the derivatives have greatly increased.



We presumed that the improved photostability may be accompanied by a reduced phototoxic effect of the inhibitors. To test our hypothesis, we measured the blue-light induced phototoxicity of the compounds on HeLa cells. HeLa cells were treated with blebbistatin, para-nitroblebbistatin or para-chloroblebbistatin then irradiated with blue light.

The irradiation wavelength was  $480\pm 10$  nm, which is the most commonly used excitation range in fluorescence microscopy for GFP detection. The energy density was  $3.3\cdot 10^{-3}$  mJ/ $\mu\text{m}^2$ , which is an average input energy in confocal microscopy applications ( $0.001 - 1.4$  mJ/ $\mu\text{m}^2$ ) [71]. Following irradiation, the inhibitors were washed out immediately and after 18 hours of incubation the mortality rates were determined by trypan blue staining and subsequent counting of the cells. We observed no difference in mortality and cell morphology between the non-treated control and para-nitroblebbistatin treated cells, while blebbistatin treatment caused extensive cell death and led to a number of morphologically defective cells unstained by trypan blue (Figure 20). Para-chloroblebbistatin treatment resulted in similar or even more pronounced cell death than blebbistatin. This result indicates that improved photostability is not necessarily accompanied with reduced phototoxicity. Since para-chloroblebbistatin proved to be phototoxic, we excluded this derivative from further experiments.

To test the applicability of para-nitroblebbistatin in live-cell imaging, we performed a series of confocal microscopy-based experiments employing blue light excitation.



EGFP-alpha-tubulin H2B-mCherry labeled Kyoto cells were time-lapse imaged for 12 hours in a confocal microscope applying 3 z-sections in every 10 minutes in the presence of 50  $\mu\text{M}$  of blebbistatin or para-nitroblebbistatin, which is a commonly applied concentration of blebbistatin in several published studies. After receiving blebbistatin treatment, cells became defective as neither of them entered into mitosis and most of them died or became morphologically seriously defective by the end of the experiment (Figure 21). Cells, which were already in the mitotic phase did not exceed cytokinesis and resulted in multinuclear cells upon blebbistatin treatment, as a consequence of myosin II inhibition [70]. Additionally, the microscopic images were highly disturbed by the fluorescent precipitates of blebbistatin. Cells treated with para-nitroblebbistatin did not show any sign of phototoxic damage and none of them died by the end of the experiment. The same ratio of the para-nitroblebbistatin treated cells entered into the mitotic phase as in the control experiment. Due to the myosin II inhibitory effect of para-nitroblebbistatin, all of the mitotic cells failed to perform cytokinesis, thus they became multinuclear. Since para-nitroblebbistatin is not fluorescent, fluorescent aggregates did not perturb microscopic imaging.

Beside HeLa cells, phototoxicity of blebbistatin and para-nitroblebbistatin was also compared on *Danio rerio* (zebrafish) embryos as a vertebrate model.

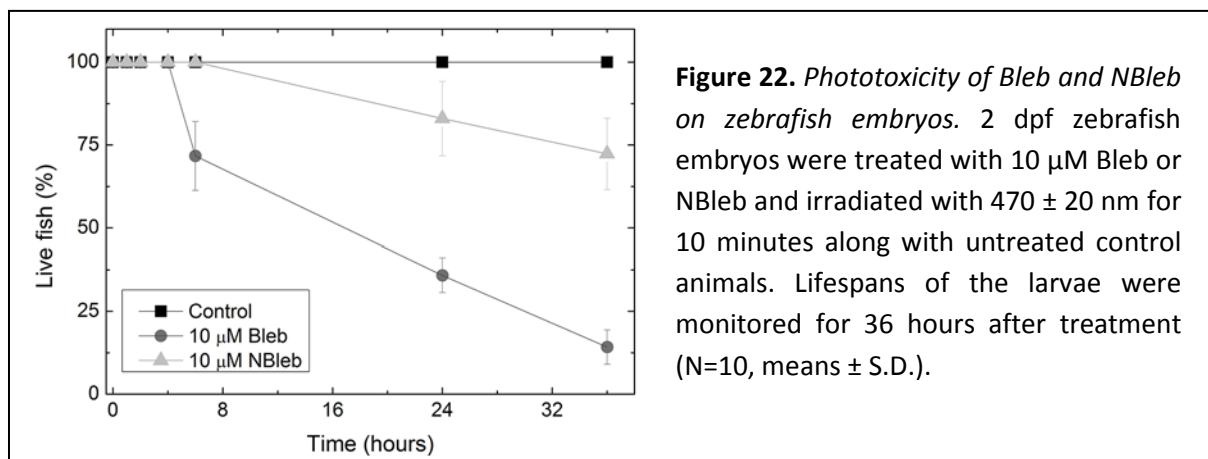


**Figure 22.** Phototoxicity of Bleb and NBleb on zebrafish embryos. 2 dpf zebrafish embryos were treated with 10  $\mu\text{M}$  Bleb or NBleb and irradiated with  $470 \pm 20$  nm for 10 minutes along with untreated control animals. Lifespans of the larvae were monitored for 36 hours after treatment (N=10, means  $\pm$  S.D.).

3 dpf (days post-fertilization) old embryos were treated with the inhibitors at 10  $\mu\text{M}$  concentrations and irradiated with blue light (wavelength:  $470 \pm 20$  nm, energy density:  $0.4 \cdot 10^{-3} \text{ mJ}/\mu\text{m}^2$ ). The mortality rates of the embryos were monitored for the following 36 hours (Figure 22). After 36 hours, the majority of the larvae receiving blebbistatin treatment

died ( $86 \pm 5$  %) while the mortality in para-nitroblebbistatin-treated samples was significantly lower ( $18 \pm 10$  %).

### Myosin II inhibition of para-nitroblebbistatin *in vivo*

To evaluate the myosin II inhibition of para-nitroblebbistatin *in vivo*, we performed a series of experiments on different human cell cultures (HeLa, M2), *Dd* cells and zebrafish embryos. First we compared the effect of para-nitroblebbistatin and blebbistatin on the cytokinesis of HeLa cells. Cells were treated with the inhibitors at  $20 \mu\text{M}$  concentrations while the change in cell number, viability and the ratio of multinuclearity were monitored for 3 days (Figure 23).

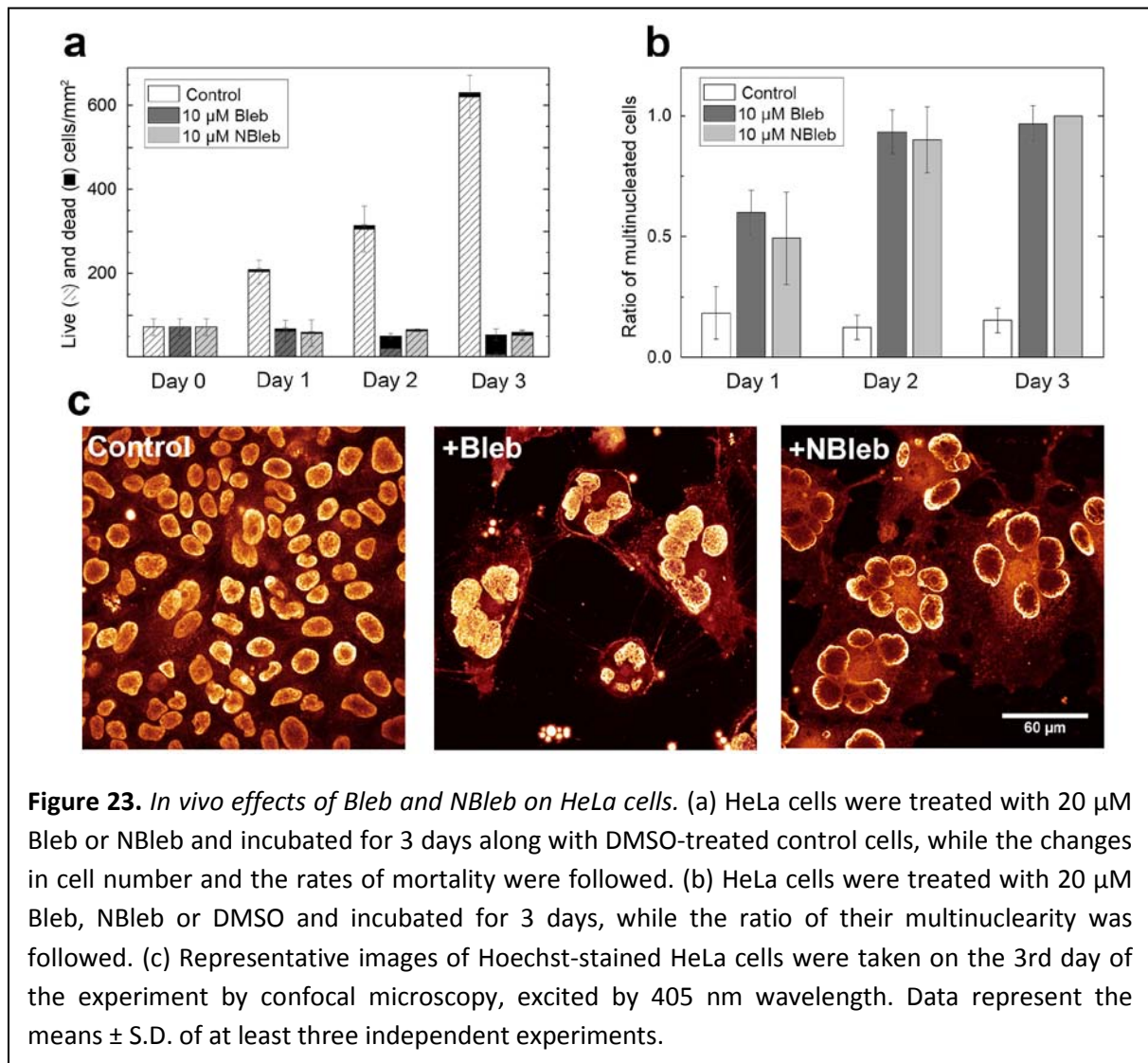
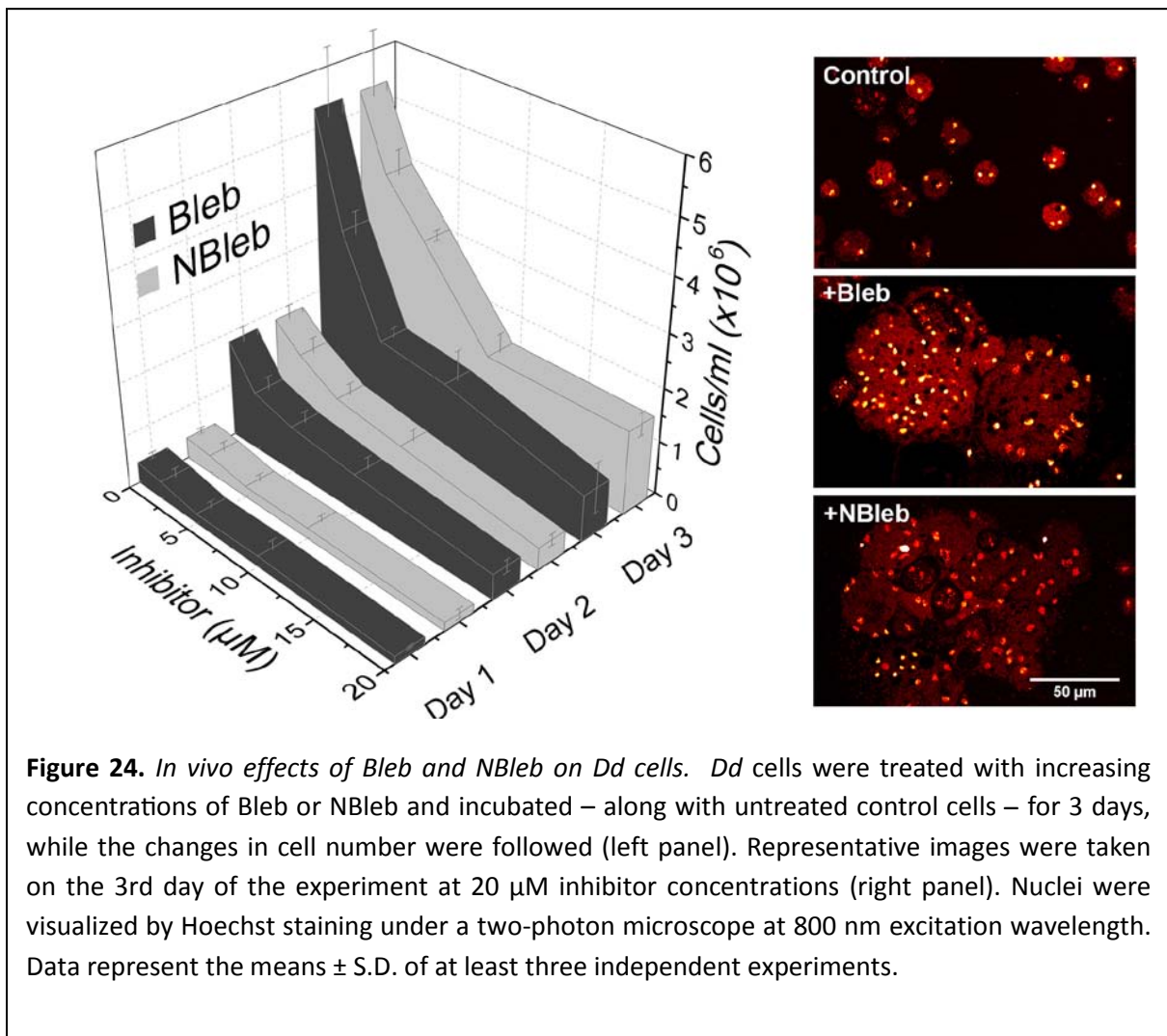


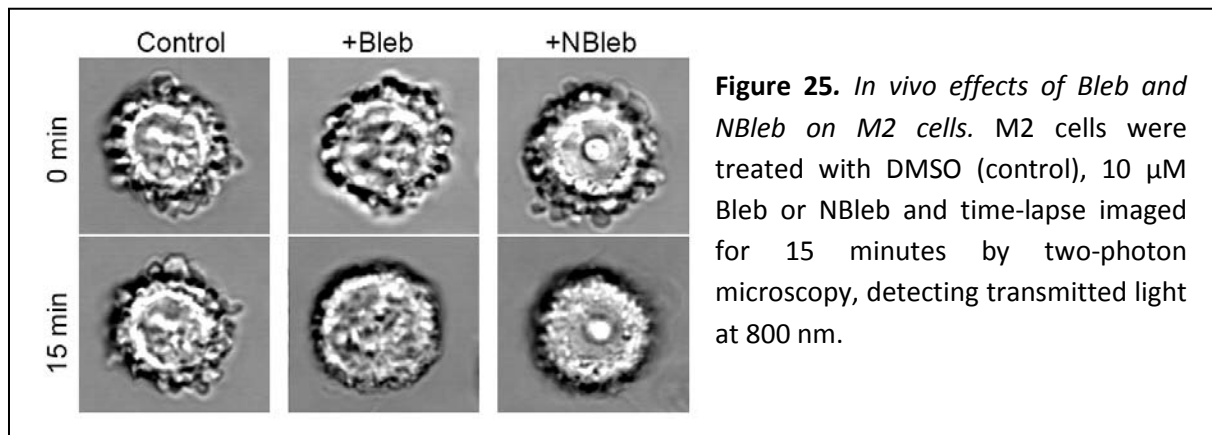
**Figure 23.** *In vivo* effects of Bleb and NBleb on HeLa cells. (a) HeLa cells were treated with  $20 \mu\text{M}$  Bleb or NBleb and incubated for 3 days along with DMSO-treated control cells, while the changes in cell number and the rates of mortality were followed. (b) HeLa cells were treated with  $20 \mu\text{M}$  Bleb, NBleb or DMSO and incubated for 3 days, while the ratio of their multinuclearity was followed. (c) Representative images of Hoechst-stained HeLa cells were taken on the 3rd day of the experiment by confocal microscopy, excited by 405 nm wavelength. Data represent the means  $\pm$  S.D. of at least three independent experiments.

Both drugs efficiently inhibited cytokinesis, therefore the initial cell number did not rise during the experiment. Consistently, the ratio of multinuclear cells among live cells continuously increased and by the 3<sup>rd</sup> day, practically all cells were multinuclear. Blebbistatin treatment resulted in significant cell mortality, leading to 90% death ratio of HeLa cells in three days. Since the entire experiment was performed in the dark, this result reflects the cytotoxicity of blebbistatin even without irradiation. In contrast, para-nitroblebbistatin did not affect the death rate of the cells. Additionally, the live blebbistatin-treated cells displayed severely defected cellular morphologies, while para-nitroblebbistatin treatment did not damage the cells.

Furthermore, we compared the *in vivo* effects of para-nitroblebbistatin and blebbistatin on *Dd* cells, a popular model system to study cellular, genetic and biochemical processes.



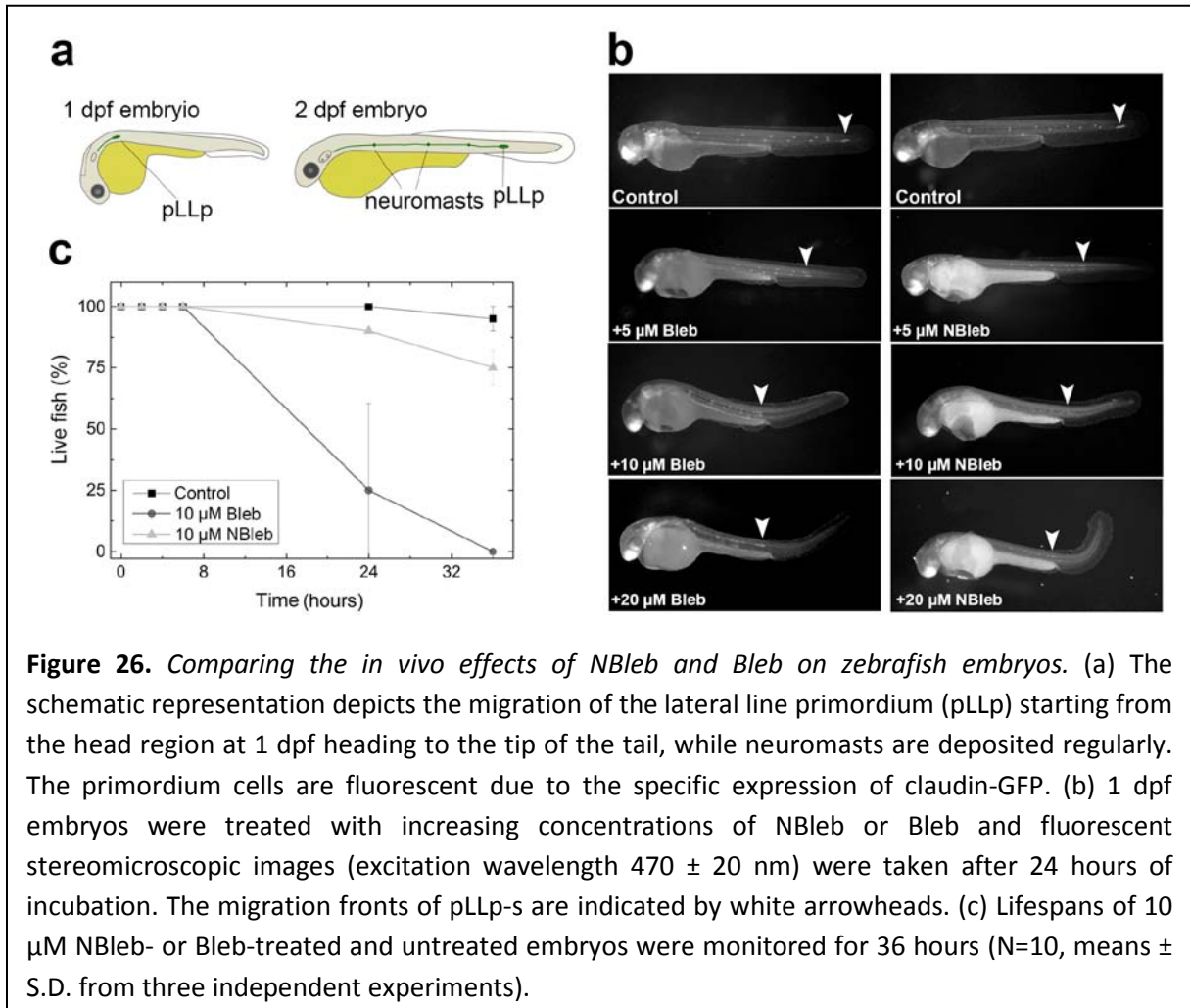
Cells were treated with increasing concentrations of the inhibitors while cell number, viability and multinuclearity were followed for 3 days (Figure 24, left panel). Blebbistatin and para-nitroblebbistatin inhibited cytokinesis to similar extents and induced multinuclearity in almost all cells (Figure 24, right panels). No cytotoxic effect was observed on *Dd* cells in case of the inhibitors.



Blebbistatin was named after its characteristic effect of suppressing the blebbing of cells. Using the continuously and rapidly blebbing M2 human melanoma cell line, we compared the effect of para-nitroblebbistatin and blebbistatin on this process. Both drugs completely inhibited blebbing within 10 minutes and no morphological difference was detected between cells treated by the two inhibitors (Figure 25).

In order to explore functional effects of para-nitroblebbistatin on vertebrates, we studied the development of the lateral line organ in zebrafish embryos. The lateral line is a sensory organ of fish and amphibian species, located on both sides of the animals, close to the surface (Figure 26a). It consists of a series of innervated mechanosensory receptors and their supporting neighbor cells, the so-called neuromasts. Neuromast precursors in the bodywall are deposited at regular intervals by the migrating posterior lateral line primordia (pLLp), which are formed behind the ear and migrate along the two sides of the body to the tip of the tail [106]. Its relative simplicity, well defined migratory behavior and good accessibility make the zebrafish pLLp a prime model to study intra-organ patterning and collective cell migration [106, 107]. Recent results indicate that non-muscle myosin II function, activated through the Fgf-Ras-MAPK pathway, is necessary for the correct development of the protoneuromasts [108, 109]. Inhibition of myosin-II-dependent processes with blebbistatin causes aberrant organ formation in the developing fish embryos [108].

Transgenic *cldnb:gfp* zebrafish embryos [110] with GFP-labeled pLLp and neuromasts were treated with increasing concentrations of blebbistatin and para-nitroblebbistatin starting at 1 dpf. After 24 hours of incubation (at 2 dpf), the positions of the pLLp were observed. The treatment resulted in similar effects for both inhibitors, including the halt of the pLLp and a curved body shape (Figure 26b).



However, we also recognized an important difference between the para-nitroblebbistatin and blebbistatin treated embryos: blebbistatin administration resulted in elevated animal mortality compared to the para-nitroblebbistatin treatment. In 36 hours, all fish died in the presence of 10 μM of blebbistatin, while the mortality rate for para-nitroblebbistatin was comparable to the control (Figure 26c). Since none of the embryos were irradiated, the observed toxic effect of blebbistatin clearly differs from its blue light induced phototoxicity.

## New insight into cytokinesis

The non-phototoxicity of para-nitroblebbistatin enables fluorescent time-lapse imaging of living organisms providing an improved tool to investigate the role of myosin IIs *in vivo*. We were interested in the dynamics of cytokinesis in the presence of para-nitroblebbistatin, so we treated HeLa Kyoto cells with increasing amounts of the inhibitor and time-lapse imaged them for 12 hours (Figure 27). At high inhibitor concentrations (>30  $\mu\text{M}$ ), we observed the well-known phenotype, that after anaphase the cleavage furrow does not ingress and the cell becomes binuclear [57]. However, at lower concentrations (<30  $\mu\text{M}$ ) of para-nitroblebbistatin, a new phenotype emerged. Here, after anaphase, the furrow does ingress, the midbody forms but scission does not occur. Instead of scission, the cell collapses and becomes binuclear. The outcome in both cases (mechanism 1, 2) is a binuclear cell, but the mechanism behind the phenomena is different.

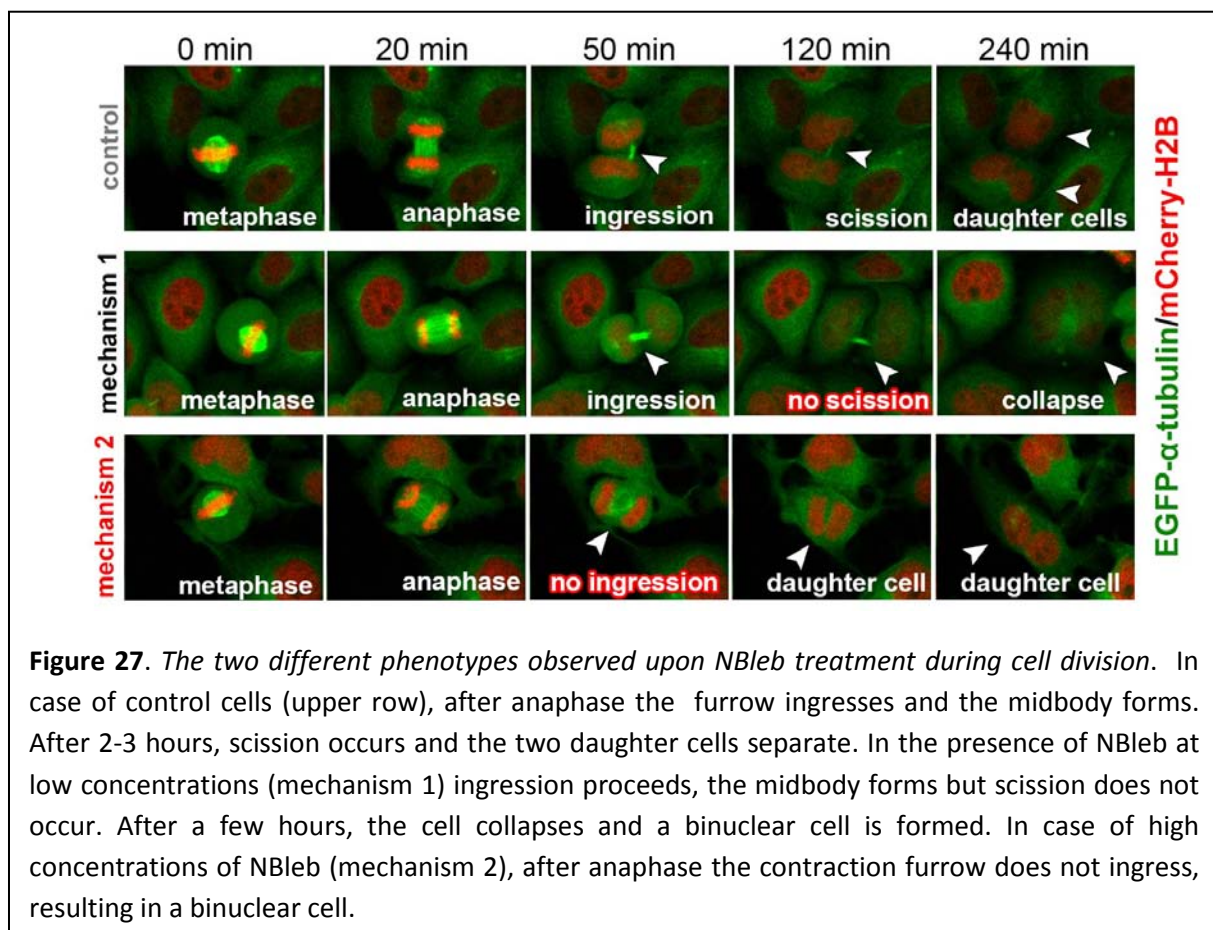


**Figure 27.** The two different phenotypes observed upon NBleb treatment during cell division. In case of control cells (upper row), after anaphase the furrow ingresses and the midbody forms. After 2-3 hours, scission occurs and the two daughter cells separate. In the presence of NBleb at low concentrations (mechanism 1) ingression proceeds, the midbody forms but scission does not occur. After a few hours, the cell collapses and a binuclear cell is formed. In case of high concentrations of NBleb (mechanism 2), after anaphase the contraction furrow does not ingress, resulting in a binuclear cell.

One possible explanation of the two observed phenotypes is that they are the consequence of the different extent of myosin II inhibition. However, it is also possible that at high

inhibitor concentrations para-nitroblebbistatin (similarly to blebbistatin) becomes aspecific and mechanism II is not solely represents myosin II inhibition.

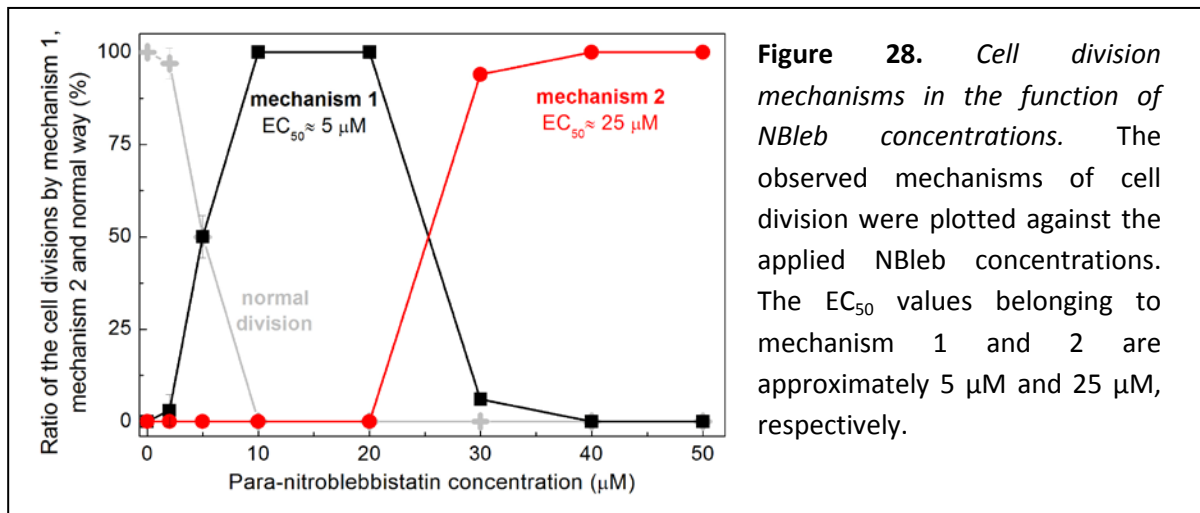


**Figure 28.** Cell division mechanisms in the function of NBleb concentrations. The observed mechanisms of cell division were plotted against the applied NBleb concentrations. The  $EC_{50}$  values belonging to mechanism 1 and 2 are approximately  $5 \mu\text{M}$  and  $25 \mu\text{M}$ , respectively.

To distinguish between these possibilities, we plotted the observed cell division mechanisms in the function of the concentration of para-nitroblebbistatin (Figure 28). Surprisingly, the two observed phenotypes (or mechanisms) separated from each other and they had two distinct  $EC_{50}$  values: mechanism 1  $\approx 5 \mu\text{M}$ , mechanism 2  $\approx 25 \mu\text{M}$ .

To further characterize the revealed mechanism 1 distinct from mechanism 2, we plan to carry out more live-cell experiments at low concentrations of para-nitroblebbistatin, aiming to unveil the dynamic details and structural aspects of mechanism 1 cytokinesis.

## Part 3: Molecular tattooing

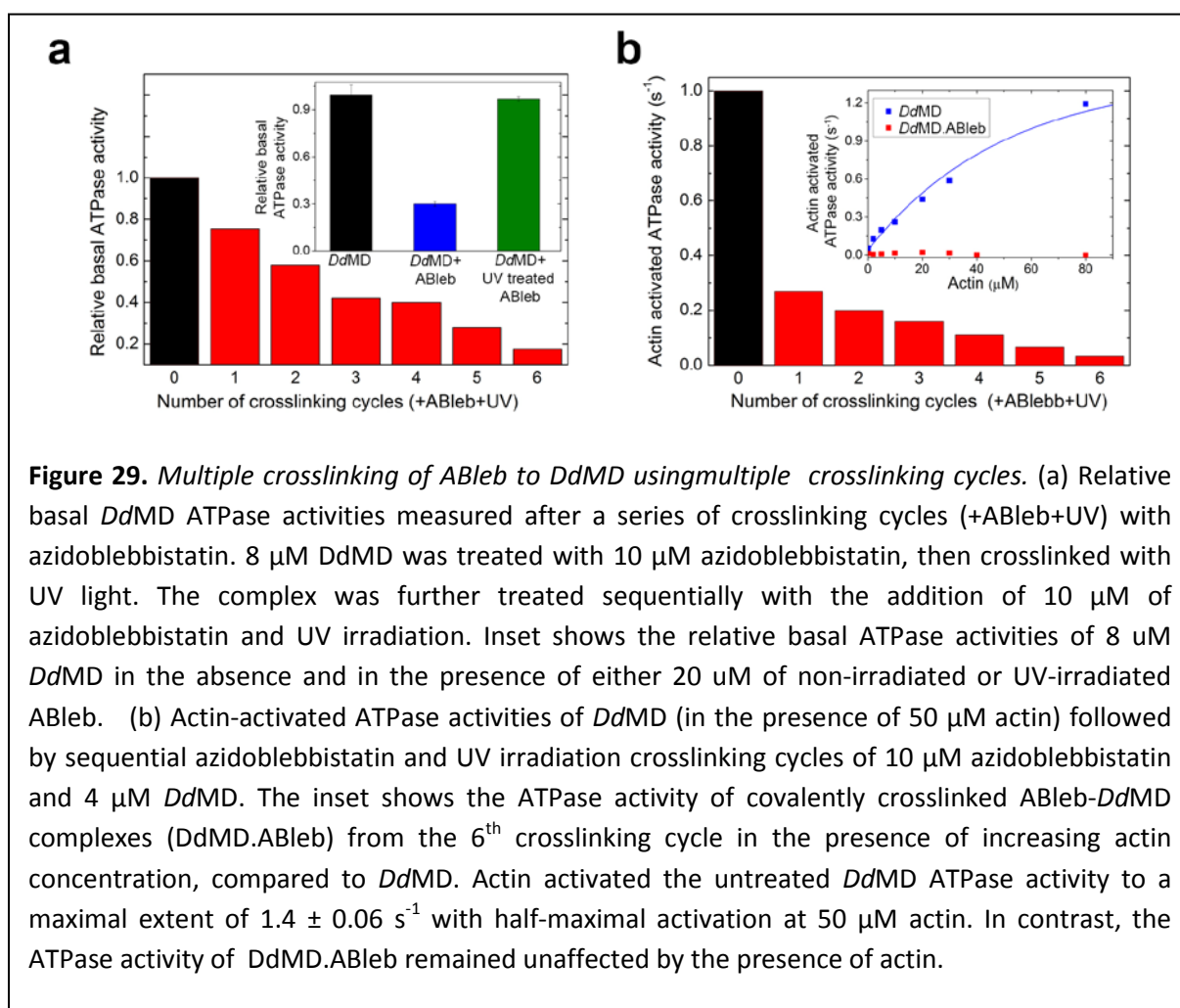
### Sequential photo-crosslinking

The ability of modulating target enzymes in a defined area may unveil molecular mechanisms in detail, thereby helping to answer fundamental biological questions. Optopharmacological tools e.g. caged compounds and chemical photoswitches are extensively used in life sciences for drug targeting. However, optopharmacological techniques available today suffer from great limitations most of which are the consequence of diffusion. As a result of diffusion, the light-triggered jump in the concentration of the bioactive compound in the targeted area is transient, therefore only short time perturbations can be achieved. Moreover, even if the targeted area is spatially well-defined by focused two-photon irradiation, due to diffusion, the bioactive compound can affect off-target areas as well. Additionally, both caged compounds and photoswitches require very high concentrations of the photoreactive ligands, which can be a major concern in experimental design.

An obvious solution for eliminating diffusion is the covalent attachment of the photoreactive ligand to its target by photo-crosslinking. Covalent attachment of a photoreactive ligand to its target enzyme can overcome all of the limitations associated with diffusion. However, if the goal is drug targeting, we have to manage that only the covalently attached ligand affects the target. Washing out the photoreactive ligand after photo-crosslinking can be an option, although it may be difficult to achieve in certain *in vivo* conditions. On the other hand, if we use a photoreactive ligand at low concentrations (below its  $EC_{50}$  value) and we apply multiple photo-crosslinking cycles of a targeted area, we will see mainly the effect of the covalently attached ligand, since the concentration of the non-covalent binders will always stay below the  $EC_{50}$  value.

To test whether sequential crosslinking can covalently saturate an enzyme *in vitro*, we sequentially crosslinked azidoblebbistatin to myosin. 8  $\mu$ M DdMD was treated with 10  $\mu$ M azidoblebbistatin followed by UV irradiation of the whole solution by a Xenon lamp at 310 nm. The azidoblebbistatin addition–irradiation cycles were repeated several times. The results of Figure 29 indicates that using this procedure, almost all myosin molecules were crosslinked to the inhibitor, as measured by the ATPase activity of DdMD in the absence

(Figure 29a) as well as in the presence of actin (Figure 29b). Importantly, the activity of myosin was only affected by the covalently crosslinked azidoblebbistatin, as myosin-unbound azidoblebbistatin in the solution degraded completely upon irradiation and had no effect on myosin ATPase activity (DdMD+UV-treated ABleb, Figure 29a inset). We verified the existence of the covalent enzyme-inhibitor complex and separated it from the unbound, photo-degraded azidoblebbistatin by using His-tag affinity chromatography. The covalently crosslinked azidoblebbistatin co-eluted with the His-tagged DdMD, detected as a yellow colored fraction, providing evidence of a covalent crosslink between the molecules. The azidoblebbistatin-DdMD complex was also verified by mass spectrometry.

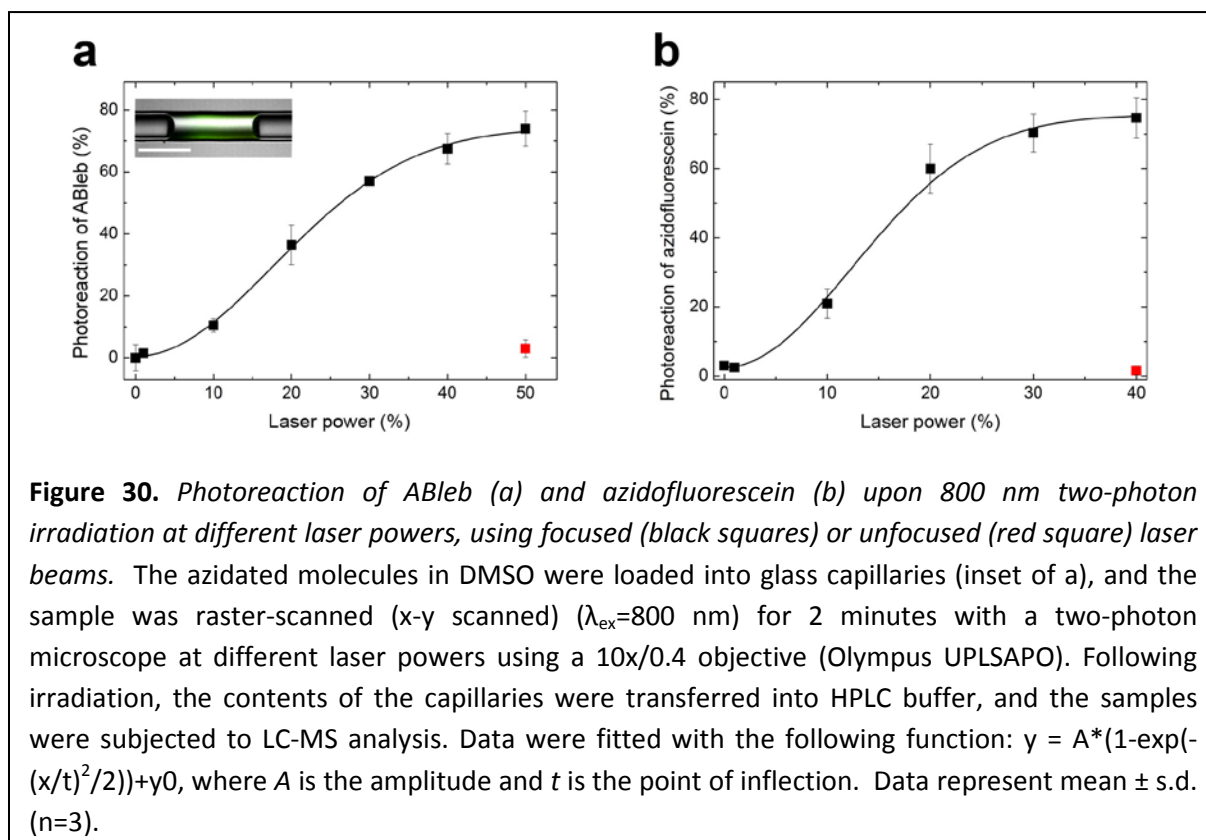


Sequential photo-crosslinking of azidated bioactive compounds has the potential to control their biological effects in space and in time. Systemic treatment of a multicellular organism with an azidated ligand at low concentrations (below its EC<sub>50</sub> value) followed by UV irradiation could covalently saturate the target enzyme on the site of irradiation. However,

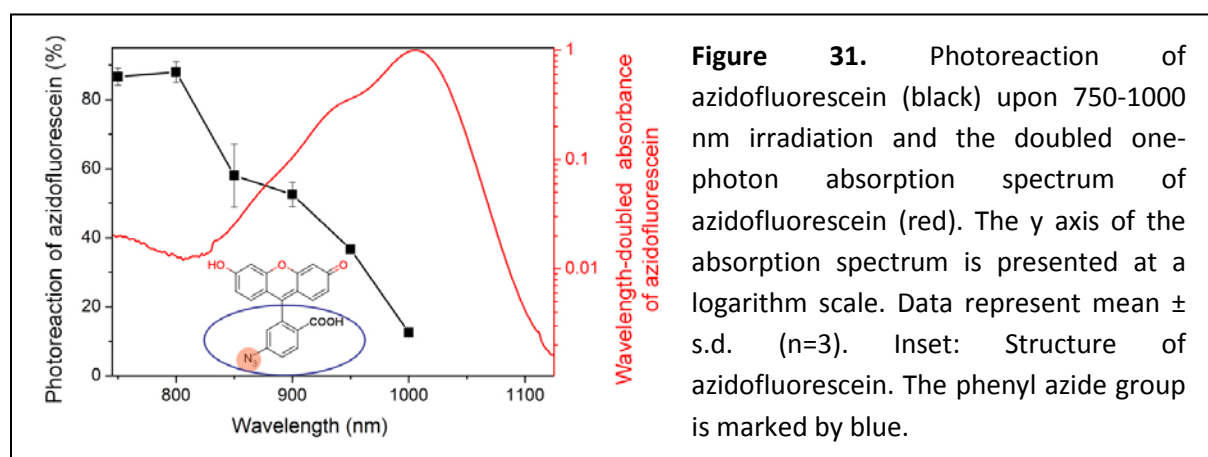
using UV light (one-photon irradiation), the resolution of the method is limited. In order to achieve cellular or even subcellular resolution, two-photon irradiation can be a good solution

### Two-photon activation of aryl azides

To test whether two-photon irradiation could induce photoreaction in azidated ligands, we two-photon irradiated azidoblebbistatin and azidofluorescein [111] solutions and quantified the photoreactions. The inhibitors were loaded into glass capillaries and raster-scanned in a two-photon microscope at 800 nm, applying increasing laser powers. After irradiation of the samples, they were subjected to LC-MS analysis, and the percentage of photoactivation was determined at each laser power (Figure 30). Since the ratio of the photoreaction in the function of the laser power proved to be highly non-linear [90], and unfocused irradiation of the sample (focused above the capillary) resulted in no photoreaction - even at high laser power- we confirmed that azidoblebbistatin and azidofluorescein can be activated by two-photon irradiation at 800 nm.



In case of azidofluorescein, its two-photon activation spectra, i.e. the wavelength dependence of its two-photon activation was also determined. Figure 31 shows that excitation around 1000 nm - which represents the main absorption peak of the molecule - cannot be used for triggering optimal two-photon activation. On the other hand efficient photoreaction occurred in the 750-800 nm range although here the absorption of azidofluorescein is two-order of magnitude lower compared with the 1000 nm region. These results indicate, that for efficient photoreaction, the phenyl-azide ring of azidofluorescein needs to be excited directly, even though it not represents the main absorption peak of the molecule. In addition, these experiments also indicate that by exciting the two orders of magnitude higher absorption peak of the molecule, intramolecular energy transfer is not efficient for azido group activation.



## 2P induced photoaffinity labeling

To confirm and prove directly that PAL crosslinking reaction can be induced by 2PM, *Dictyostelium discoideum* myosin motor domain (*DdMD*) was illuminated with UV light and 2P in the presence of azidoblebbistatin (Figure 32). By LC-MS measurements, we detected covalent bond formation between myosin and azidoblebbistatin both in the case of UV and 2P irradiation. As a control experiment, off-focus irradiation of the azidoblebbistatin-treated myosin sample has not induced PAL, further confirming the 2P effect.

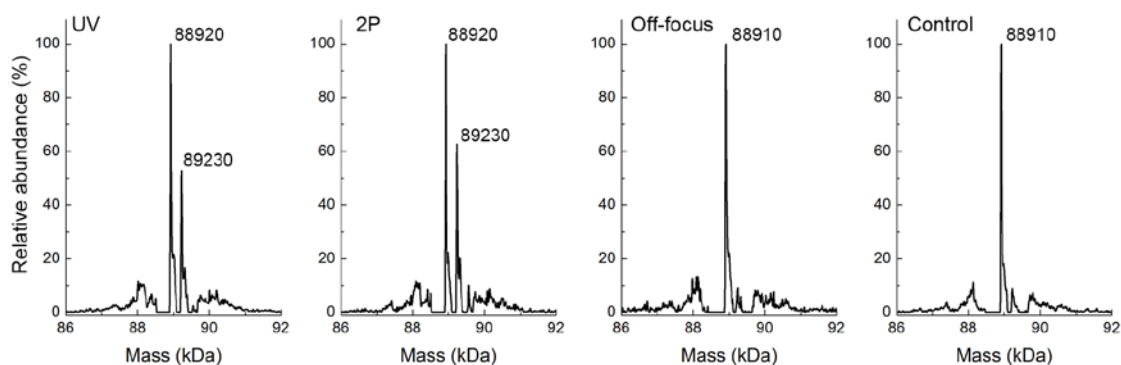


**Figure 32.** MS spectra of DdMD treated with ABleb then irradiated at 300 nm (UV), 2PM-irradiated at 800 nm (2P) and 2PM off-focus irradiated (Off-focus). MS spectrum of DdMD is also presented as a control (Control). The molecular mass of the non-illuminated DdMD is 88910 Da, after irradiation it is 88920 Da, whereas the molecular mass of the DdMD-ABleb covalent complex is 89230 Da (88920 + 310 Da).

### Azidoblebbistatin is a push-and-pull fluorophore

Azidoblebbistatin is a push-and-pull fluorophore, meaning that upon covalent attachment to myosin, its quenched fluorescence due the preliminary attachment of the electron withdrawing azido group to the fluorescent blebbistatin molecule – is restored, resulting in an 8-times increase in its fluorescence (Figure 33).

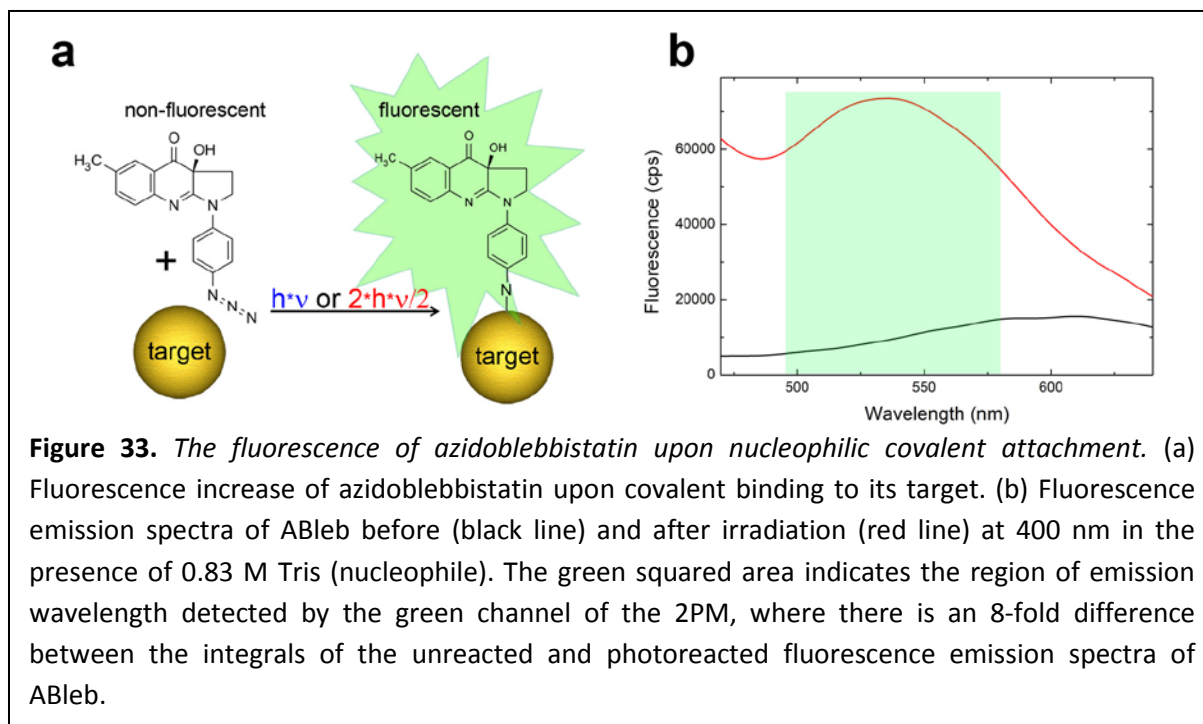
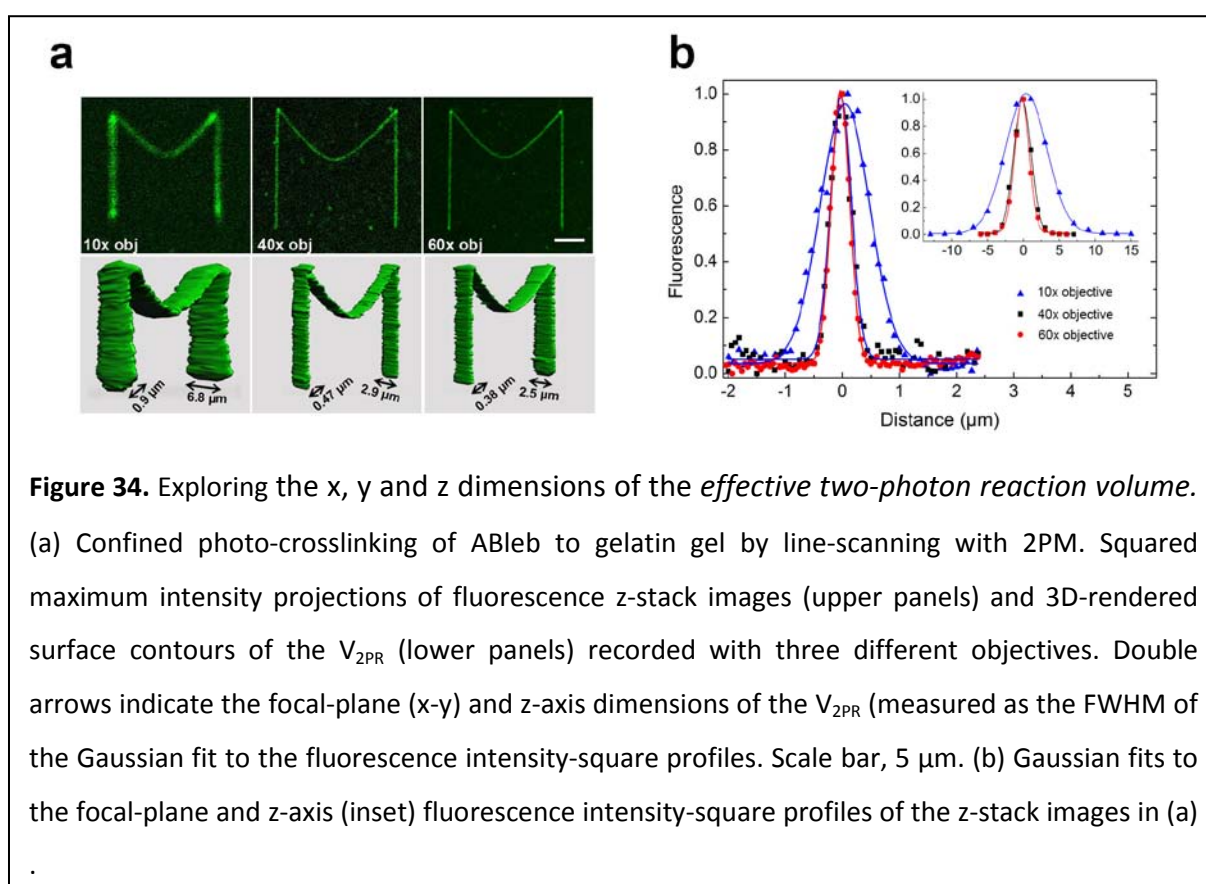


**Figure 33.** The fluorescence of azidoblebbistatin upon nucleophilic covalent attachment. (a) Fluorescence increase of azidoblebbistatin upon covalent binding to its target. (b) Fluorescence emission spectra of ABleb before (black line) and after irradiation (red line) at 400 nm in the presence of 0.83 M Tris (nucleophile). The green squared area indicates the region of emission wavelength detected by the green channel of the 2PM, where there is an 8-fold difference between the integrals of the unreacted and photoreacted fluorescence emission spectra of ABleb.

Since azidoblebbistatin's fluorescence increases upon its covalent attachment to proteins, it provides a unique tool to explore the  $x$ ,  $y$  and  $z$  dimensions of the *effective two-photon reaction volume* ( $V_{2PR}$ ) of two-photon microscopes. Azidoblebbistatin was dissolved in melted gelatin, transferred to an imaging dish and cooled. Using the line-scan function of the two-photon microscope, M letter shaped areas were irradiated at 800 nm applying 10x/0.4, 40/0.8x or 60x/1.35 objectives (Figure 34a, upper panel). After irradiation of the M-letter shapes by a two-photon microscope, the areas were imaged by z-sectioning at a much lower intensity compared to the tattooing process, at which no significant photochemical reaction was detected.



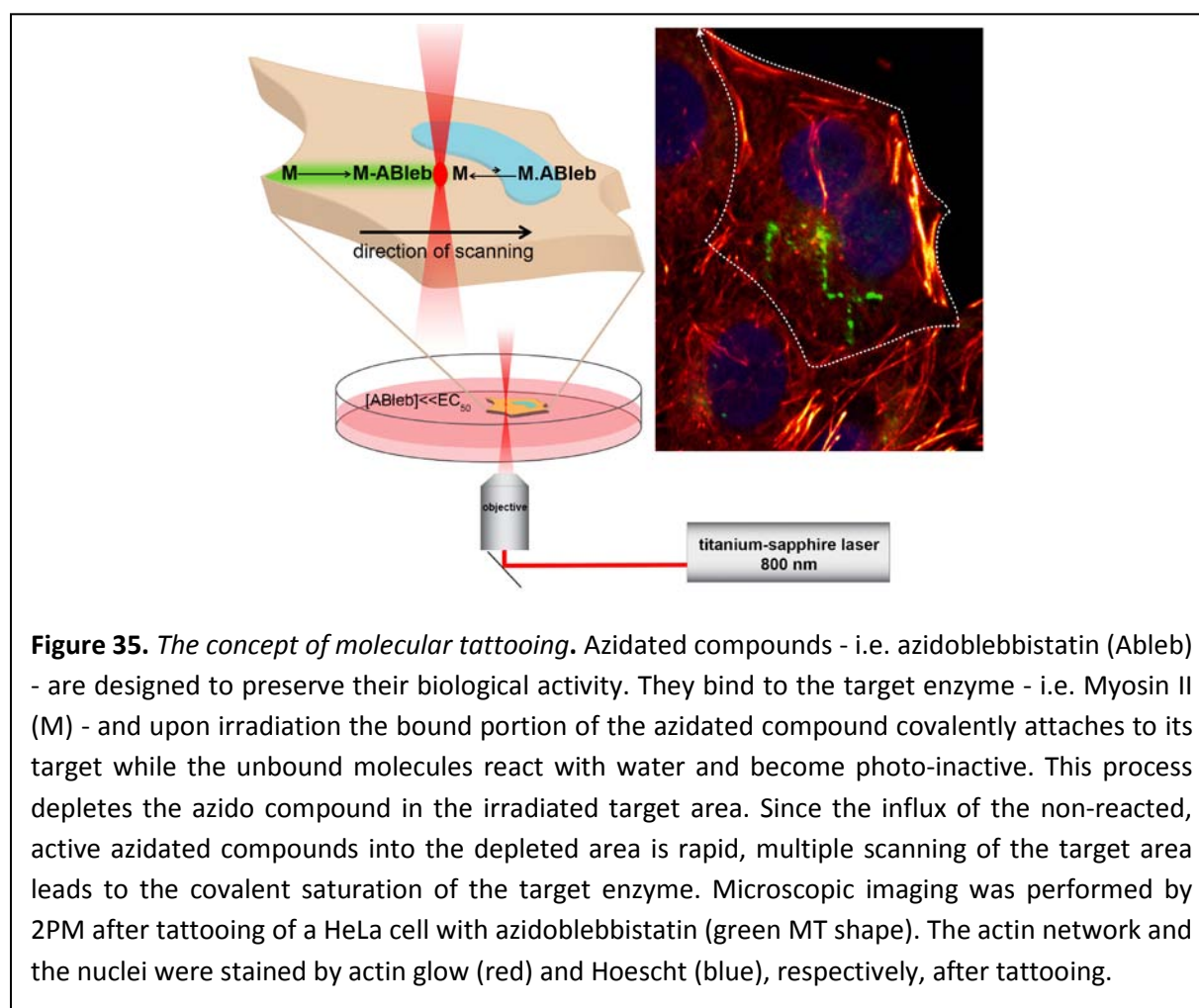
In order to define the 3D true  $V_{2PR}$  for all three objectives, the square of the illumination point-spread function was determined [90]. Using the 60x/1.35NA objective, the lateral ( $x$ , $y$ ) and axial ( $z$ ) resolution (FWHM) of the tattooed line in gelatin gel was found to be 0.38  $\mu\text{m}$  and 2.37  $\mu\text{m}$ , respectively. The determined physical parameters of the two-photon reaction in case of the different objectives can be found in Table 2.

	$\omega_{xy}$ ( $\mu\text{m}$ )	$\omega_z$ ( $\mu\text{m}$ )	FWHM <sub>xy-axis</sub> ( $\mu\text{m}$ )	FWHM <sub>z-axis</sub> ( $\mu\text{m}$ )	$V_{2PR}$ ( $\mu\text{m}^3$ )
10x objective	0.67	4.56	1.02	6.81	11.4
40x objective	0.25	1.51	0.43	2.87	0.52
60x objective	0.18	1.14	0.38	2.37	0.21

**Table 2.** Physical parameters of the 2P reaction volumes. Gaussian fits to the focal-plane (xy) and z-axis fluorescence intensity-square profiles of z-stacked images (Figure 34b) yielded the lateral ( $\omega_{xy}$ ) and axial ( $\omega_z$ ) 1/e radii and FWHM values.  $V_{2PR}$  was calculated as  $V_{2PR} = \pi^{3/2} \omega_{xy}^2 \omega_z$  (equation 2 of [90]).

### The idea of molecular tattooing

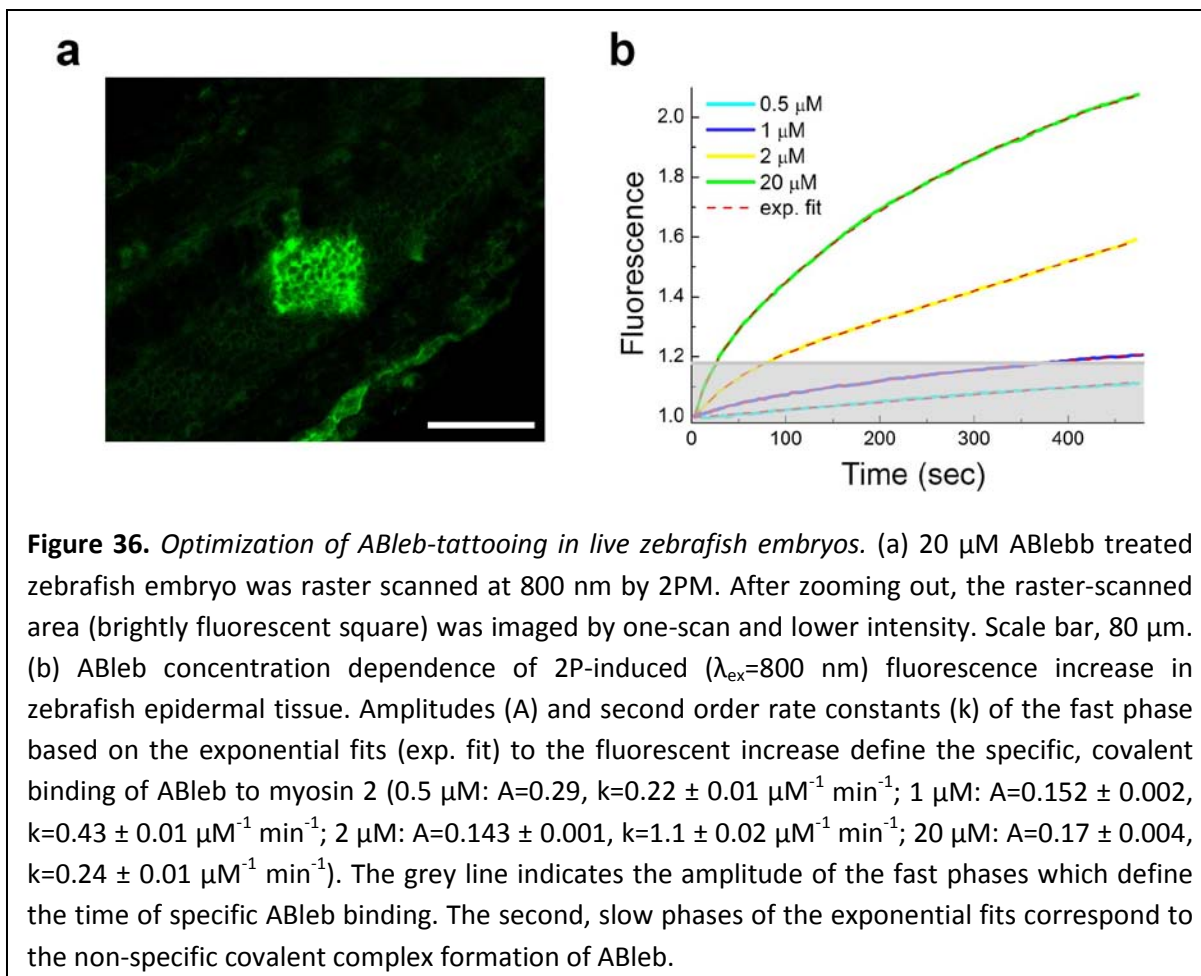
We demonstrated that using photo-crosslinking cycles, azidoblebbistatin can covalently saturate its target enzyme, myosin II, even at non-saturating concentrations of azidoblebbistatin. Furthermore, we revealed that photoactivation can be initiated by two-photon excitation, enabling the localization of the effect into femtoliter volumes.



The basic idea behind molecular tattooing is based on the above mentioned two observations. If a whole organism is treated with low concentrations of an azidated bioactive compound (i.e. [enzyme inhibitor]  $\ll$   $EC_{50}$ ), its specific effect cannot be observed. However, if a defined area (i.e. a cell or subcellular region) is illuminated continuously by two-photon irradiation, it results in the local saturation of the target enzyme as a consequence of two phenomena: covalent attachment of the azidated ligand to its target and the continuous diffusion of the unreacted azidated ligand molecules from the environment into the site of irradiation (Figure 35).

### **Molecular tattooing of live zebrafish embryos**

For live animal tattooing experiments, we tested the technique by the selective inhibition of the posterior lateral line primordium (pLLp) of zebrafish embryos using azidoblebbistatin. First, we checked that azidoblebbistatin in dark inhibits pLLp migration to a similar extent as that of blebbistatin (Figure A2). In order to find the optimal conditions for tattooing *in vivo* by two-photon microscope, we raster-scanned the embryos in the presence of different concentrations of azidoblebbistatin (Figure 36). To circumvent the intrinsic fluorescence of the pLLp of the *cldnb:GFP* zebrafish line [110], the experiment was performed on the non-fluorescent epidermal tissue of the embryo. During two-photon irradiation, two phases of fluorescence increase was detected (Table A1). The fast and the slow phases reflect the specific myosin II-ABLEb and non-specific target-ABLEb complex formations, respectively (Figure 36b). For further studies, we chose the 1  $\mu$ M azidoblebbistatin concentration because of the high specificity of tattooing which occurs on a convenient time-scale without significant non-specific target-binding. Importantly, without irradiation (in dark) this concentration has no effect on the lateral line development (Figure A2). On the basis of these results, we applied the optimized parameters of raster-scanning (Methods) on the GFP-labeled pLLp.



After tattooing of azidoblebsitatin into one of the pLLp in the 36 hpf embryo, its effect on the development of the lateral line was followed for 12 hours by time-lapse confocal microscopy (Figure 37). We found, that the tattooed pLLp moved slower and stopped earlier than the non-tattooed pLLp located on the other side of the fish embryo. This phenotype was very similar to that of whole-animal treatment with para-nitroblebbistatin at high concentrations. The number of the deposited neuromasts was not affected, resulting in shorter inter-neuromast distances. Interestingly, the neuromast pairs on the tattooed and non-tattooed sides were deposited at approximately the same time. Irradiation of the pLLp of the embryos in the presence of 1  $\mu\text{M}$  para-nitroblebbistatin had no effect either on the migration of the pLLp or on the deposition of the neuromasts.

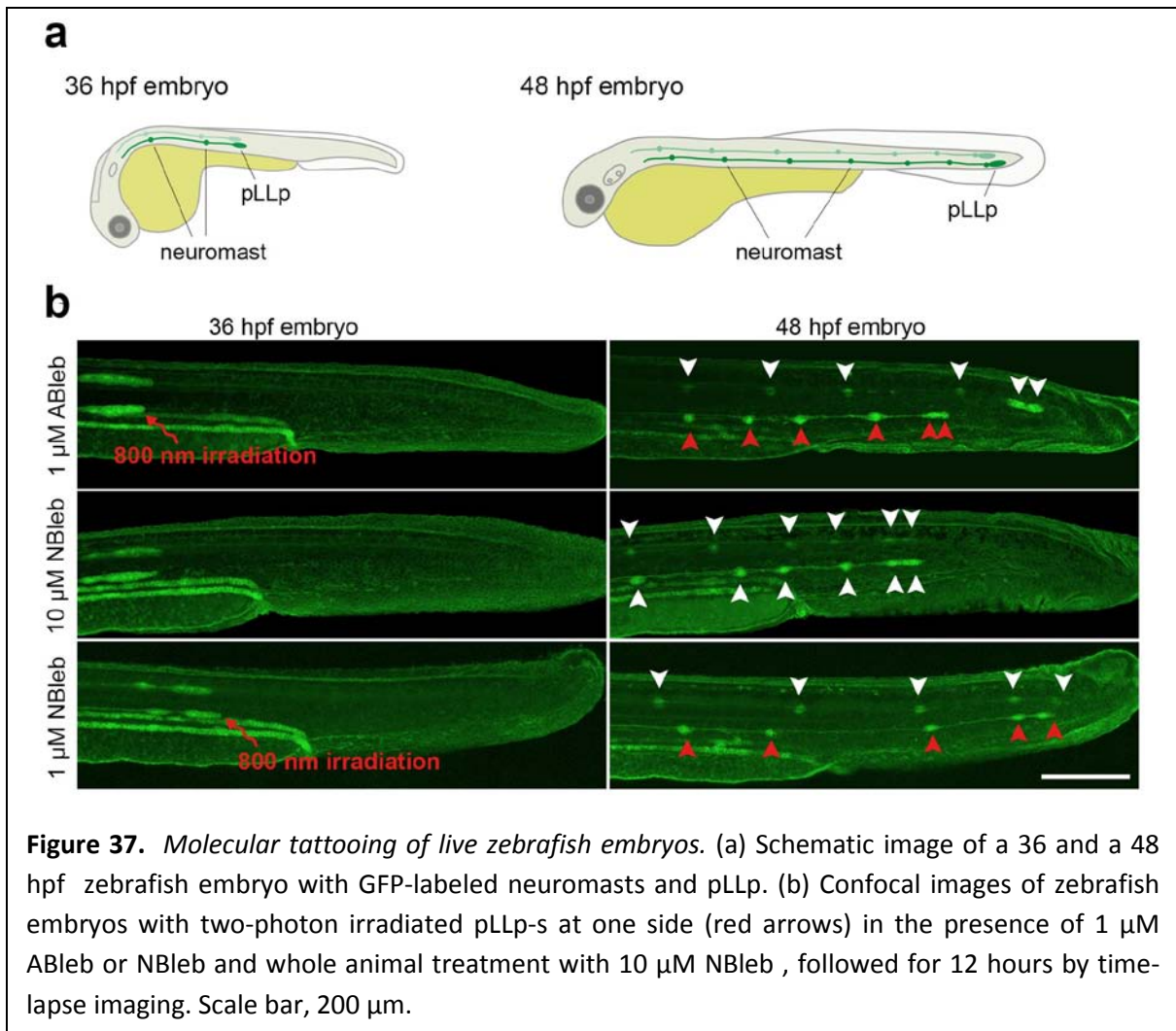
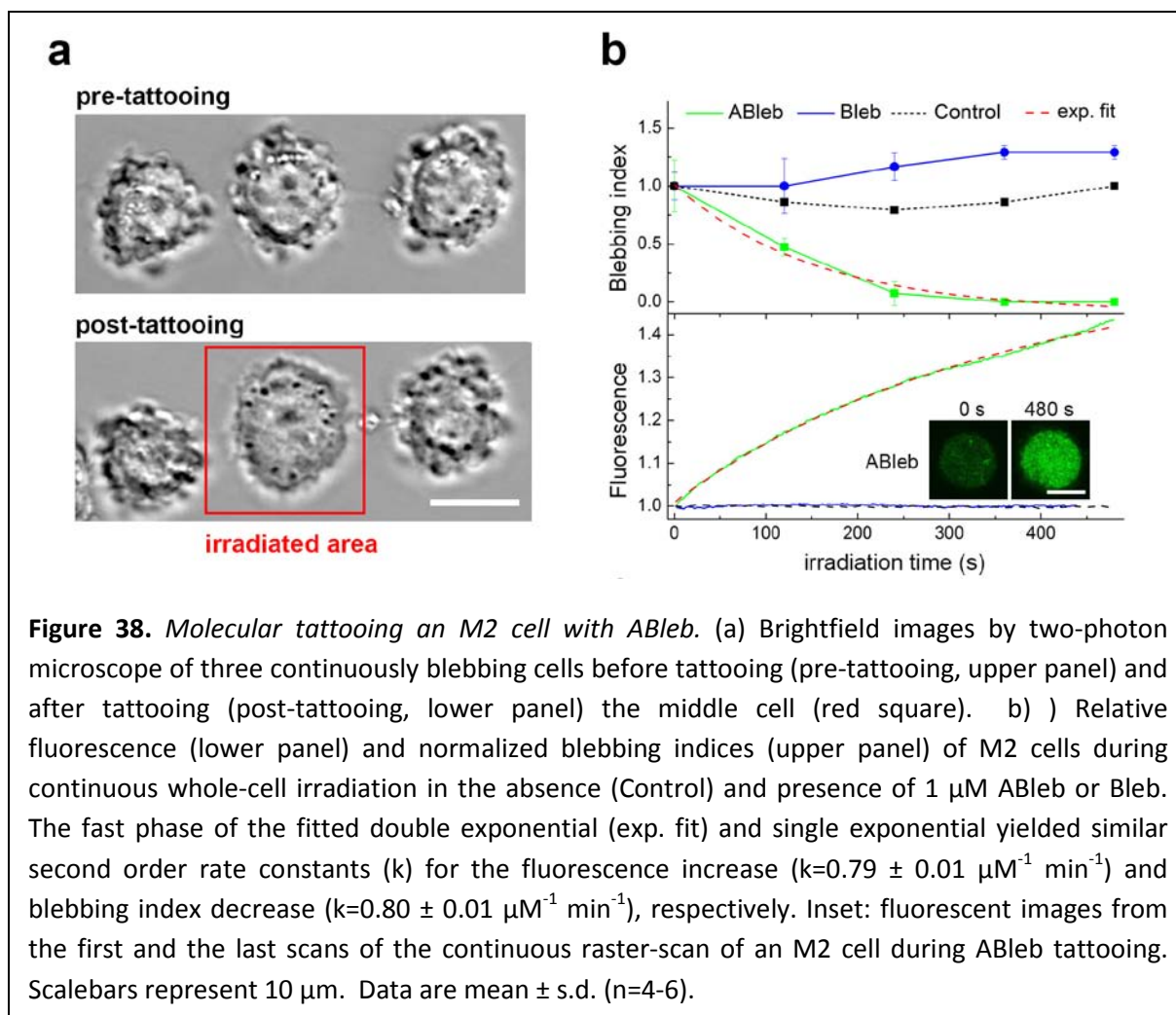


**Figure 37.** *Molecular tattooing of live zebrafish embryos.* (a) Schematic image of a 36 and a 48 hpf zebrafish embryo with GFP-labeled neuromasts and pLLp. (b) Confocal images of zebrafish embryos with two-photon irradiated pLLp-s at one side (red arrows) in the presence of 1 μM ABleb or NBleb and whole animal treatment with 10 μM NBleb, followed for 12 hours by time-lapse imaging. Scale bar, 200 μm.

Molecular tattooing the pLLp of zebrafish embryos with azidoblebbistatin indicates, that the role of myosin II in the migration of the pLLp is autonomous and it is not affected by the surrounding tissue, as local myosin inhibition resulted in the same migration pattern as the systemic para-nitroblebbistatin treatment.

### Molecular tattooing of human melanoma cells

The potentials of molecular tattooing were explored on the continuously blebbing human melanoma cell line, M2 [112]. Since the activity of non-muscle myosin II for the formation of blebs is essential [57], it can be inhibited by blebbistatin or azidoblebbistatin [113].



M2 cells were equilibrated with 1  $\mu\text{M}$  azidoblebbistatin, which concentration is below the  $\text{IC}_{50}$  value of azidoblebbistatin to myosin II. Due to the low concentration of the inhibitor, it has no observable effect on blebbing (Figure 38a, upper panel). However, two-photon irradiation of an M2 cell (raster-scanning, see Methods for parameters) in the presence of 1  $\mu\text{M}$  azidoblebbistatin abolished blebbing of the targeted cell completely, while the surrounding cells kept blebbing continuously. (Figure 38a, lower panel). Quantitative analysis of the irradiated and the non-irradiated cells in the presence of azidoblebbistatin or blebbistatin (control) demonstrates that neither the applied laser power nor the non-photoreactive inhibitor together with irradiation do not decrease the blebbing activity of cells defined by blebbing indices (number of blebs/area/time) [51] (Figure 38b, upper panel). Since azidoblebbistatin become fluorescent upon protein attachment, besides phenotypic observations, the covalent saturation of myosin can also be followed directly by tracking the fluorescence increase of the tattooed area during two-photon irradiation (Figure 38b, lower

panel). We observed two phases in the kinetics of fluorescence increase corresponding to a fast myosin-specific and a slow non-specific covalent binding of ABleb (Table A2), just as it was found in the tattooing of zebrafish embryos. Importantly, the rate constants of the exponential blebbing-index decrease and the fast exponential of the fluorescence increase were essentially identical. In control experiments, irradiation had no effect on the fluorescence intensities of untreated or blebbistatin-treated cells.

### **Subcellular tattooing of M2 cells**

According to recent mechanistic models, the force that produces the pressure for the expansion of a bleb can be the consequence of either globally uniform hydrostatic pressure generated by the contracting actomyosin cortex, or by local contraction of the actomyosin cortex generating local pressure increase [114]. The size of blebs is determined by the cortical tension of the blebbing cell [115]. Following bleb expansion, the retraction of blebs is performed by the direct activity of myosin II molecules, which are recruited to the re-assembled actin cortex along the rim of the bleb, causing the shrinking of the bleb. We examined the effect of local myosin inhibition on blebbing (blebbing indices, size, velocity of expansion and retraction) as well as the diffusion of inhibited myosin molecules within the cell.

For subcellular tattooing, half of a blebbing M2 cell was two-photon irradiated in the presence of 1  $\mu$ M azidoblebbistatin. After tattooing, an increase of fluorescence in the irradiated area was detected, the distribution of which was followed for 20 minutes (Figure 39a, lower panel). No significant change of the highly fluorescent tattooed area could be detected, indicating that myosin II stabilized by azidoblebbistatin in its weak actin-binding state does not perform active migration or diffusion. This result is supported by similar observations of inhibition of non-muscle myosin IIA movement by blebbistatin in bovine aortic endothelial cells [65]. Parallel to fluorescence, blebbing of the half-tattooed cell was also followed (Figure 39a, upper panel). Even after 20 minutes, the cell was blebbing continuously, although the blebbing index of the irradiated side decreased twice as much as of the non-irradiated side of the cell (Figure 37b, left panel).

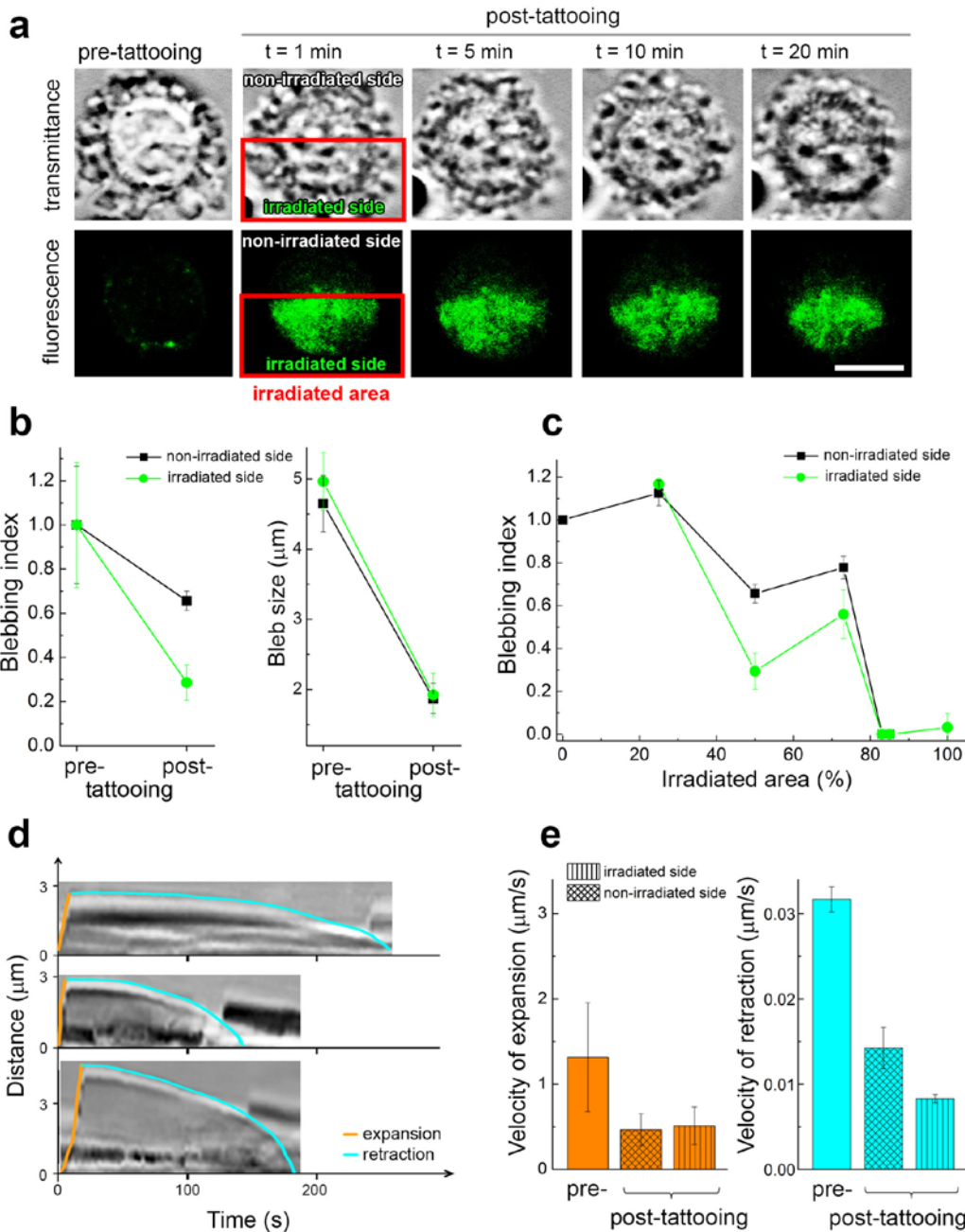


**Figure 39.** *Subcellular tattooing of a single M2 cell.* (a) 2PM-fluorescence (lower panels) and bright-field images (upper panels) of an M2 cell prior to (pre-tattooing) and following irradiation (post-tattooing) in the presence of  $1 \mu\text{M}$  ABleb . Scalebar represents  $10 \mu\text{m}$ . (b) Blebbing index (left panel) and bleb size (right panel) of half-tattooed M2 cells pre- and 20 minutes post-tattooing. (c) Blebbing indices of M2 cells at increasing tattooed areas, 20 minutes post-tattooing. (d) Representative kymographs of blebs from the irradiated (upper panel) and non-irradiated sides (middle panel) of an M2 cell 20 minutes after half-tattooing and also pre-tattooing (lower panel). (e) Kymographic data of the velocity of expansion and retraction of half-tattooed M2 cells. Data represent mean  $\pm$  s.d. ( $n=3-6$ ).

Importantly, the size of blebs on both the irradiated and non-irradiated sides of the cell became uniformly smaller by 2.5-fold (Figure 39b, right panel). As blebs are pressure sensors [115], the decreased size and number of blebs point at a global pressure decrease within the cells. As molecular tattooing of half of the cell did not inhibit blebbing, we were interested in the critical area that is needed to stop blebbing of the cell completely (Figure 39c). Over 80% tattooing of the cell, blebbing on both sides of the cell stopped, indicating that we have exceeded the critical amount of myosin needed to maintain the hydrostatic pressure required for the blebbing of M2 cells.

Kimograph analysis of blebbing of the half-tattooed cell revealed (Figure 39d), that bleb retraction on the irradiated side is significantly slower compared to the non-irradiated side (Figure 39e). The velocity of bleb expansion on either sides of the cell as well as the velocity of bleb retraction on the non-irradiated side were not affected by tattooing half of the cell. Thus, subcellular azidoblebbistatin-tattooing experiments indicate that while bleb expansion is driven by global cellular pressure, its retraction requires local myosin 2 activity.

## VI. Discussion and Conclusions

### Target deconvolution of blebbistatin

Target deconvolution of bioactive compounds is a demanding issue in the pharmaceutical field. Despite the various published techniques there is no general methodology applicable for whole interactom profiling. Affinity purification is the most widely used approach to isolate specific target proteins of bioactive compounds from a complex mixture. Since most of the drug-protein complexes form weak (i.e. non-covalent) interactions, photoaffinity tags are introduced in order to secure and covalently bind the complexes. Azido-substitution is the smallest possible modification to obtain a photoreactive compound, so we have synthesized a series of azidated bioactive ligands and addressed the question whether photoaffinity labeling followed by gel electrophoresis and subsequent mass spectrometry could be used for target deconvolution, eliminating affinity chromatography.

Azidated compounds are usually synthesized applying the corresponding nitro precursors, although, both the nitration and the subsequent reduction of the nitro precursor to amine could be very problematic. We used an improved strategy for azidation, which is based on aromatic iodination followed by a halogen azide exchange step.

Applying iodo precursors, we have synthesized ten azidated bioactive compounds including azidoblebbistatin, the first photoreactive myosin II inhibitor [116]. According to our results, in the absence of UV irradiation, blebbistatin and azidoblebbistatin possess identical myosin inhibition both *in vitro* and *in vivo*. Irradiation of the myosin-azidoblebbistatin complex at 310 nm efficiently induces a covalent crosslink between the enzyme and the inhibitor.

Using azidoblebbistatin, we determined the interaction partners of blebbistatin along with the EC<sub>50</sub> values of the azidoblebbistatin-protein complexes in *Dd* cells. For detection we have not used radiolabeling or any fluorescent tag, instead, we utilized azidoblebbistatin's own fluorescence to detect the crosslinked complexes. Since the crosslinking was performed applying increasing concentrations of azidoblebbistatin, we could determined the EC<sub>50</sub> values of the complexes by densitometry of the fluorescent bands on the SDS gel. Strikingly, the determined EC<sub>50</sub> values of the azidoblebbistatin-myosin II heavy chain ( $5.1 \pm 1.4 \mu\text{M}$ ) or the azidoblebbistatin-DdMD ( $5.2 \pm 0.8 \mu\text{M}$ ) complexes were identical to the azidoblebbistatin-

DdMD IC<sub>50</sub> value measured *in vitro* (basal ATPase measurement, Figure 15). As we demonstrated, photocrosslinking of azidated compounds can be used as an efficient technological solution for interactome profiling, adequate for the experimental determination of the apparent binding constants of the strong as well as weak-binding protein-ligand complexes.

Recent data have been shown that myosin II independent processes in myosin II-null *Dd* cells, such as cell streaming and plaque expansion, are inhibited by blebbistatin [103]. These effects are presumably the results of molecular interactions of blebbistatin with partners other than myosin II. Our results confirm, that while blebbistatin is specific to myosin II (EC<sub>50</sub>≈5 μM) at low concentrations, it has indeed several weak interaction partners with EC<sub>50</sub> value > 30 μM.

Our target deconvolution method can be theoretically extended to whole interactome profiling as well. In this case, however, two-dimensional gel electrophoresis is needed to separate the proteom. The crosslinked protein mixtures - by the different concentrations of the azido derivative - have to be separated on different gels. Importantly, several drug molecules have fluorescent properties which can be applied for in-gel detection and densitometry, which eliminates the need of fluorescent- or radiolabeling. Six out of ten azidated drug molecules what we have synthesized are fluorescent. Although it has to be mentioned, that these molecules are not optimized fluorophores and require UV excitation (300-400 nm). However, commercially available 2D-gel scanners are not equipped with lasers emitting in this range. As a solution, scanners can be readily equipped with UV emitting lasers: an N<sub>2</sub> laser (emitting 337 nm) can be sufficient for the excitation of a variety of such molecules.

### **Azidoblebbistatin in structural biology**

In many cases, the relatively low affinity of the ligand for the enzyme and the low lifetime of the ligand enzyme complex cause serious technical hurdles in the way of detailed structural characterization. Moreover, water-solubility of ligands is usually limited, therefore increasing their concentration is not possible in a water-based environment. This problem can be circumvented by applying cycles of azidated ligands application at low concentration and sequential photoaffinity labeling.

According to a recent study, myosin populates in a previously inaccessible conformational state when bound to ADP and blebbistatin, resembling the start-point of the powerstroke, the force generating step of the actomyosin enzymatic cycle [117]. However, the attempt for crystallizing the complex has failed mainly due to the low affinity of myosin to blebbistatin in the presence of ADP. Additional problem that the water solubility of blebbistatin at room temperature is very poor, around 10-20  $\mu\text{M}$ . On the other hand, covalent saturation by sequential crosslinking of myosin with azidoblebbistatin is possible even in the presence of ADP [118]. Thus, crosslinking myosin and azidoblebbistatin in different nucleotide- and actin-bound states may stabilize important intermediates of the force generating actomyosin enzyme cycle, opening new avenues in the investigation of the structural mechanism of myosin motor activity.

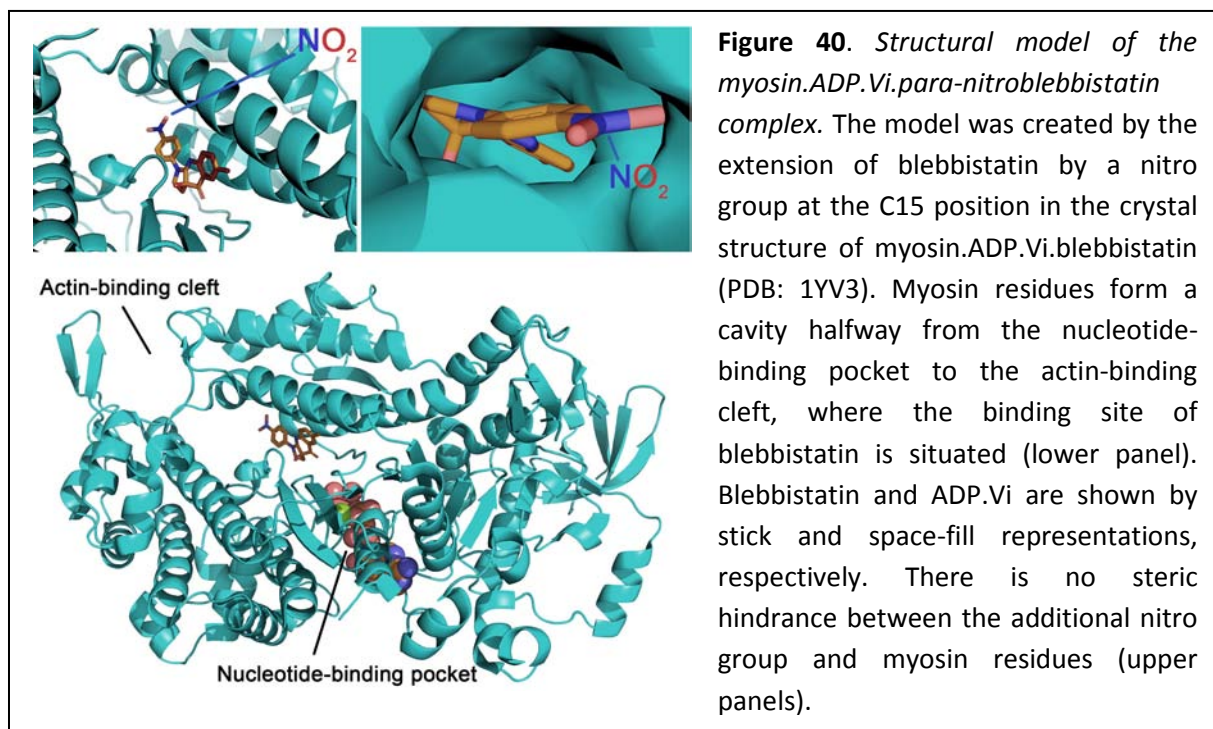
### **Para-nitroblebbistatin**

Blebbistatin is the most commonly used myosin II inhibitor, although its applicability is greatly hampered by its phototoxicity upon blue light irradiation and its cytotoxicity even in dark. Furthermore, the high fluorescence of blebbistatin intervenes with fluorescence microscopic imaging and other fluorescence measurements. Based on our experiments with azidoblebbistatin and a previously published study about a C7 nitro-substituted blebbistatin derivative [104], we presumed that the substitution at the C15 position of blebbistatin with an electron withdrawing nitro group would reduce the blue light sensitivity of the compound while retaining its myosin II inhibitory properties.

Thus, we have synthesized para-nitroblebbistatin and investigated the photochemical behavior as well as the *in vitro* and *in vivo* myosin inhibition. We demonstrated that nitro substitution at this position decreases the fluorescence of the compound by a hundred times, increases the chemical stability upon blue light irradiation and greatly reduces the phototoxicity and cytotoxicity of the molecule without affecting its specific myosin II inhibitory properties. Importantly, the wavelength, time and energies of the illumination applied in the experiments represent everyday microscopic setups e.g. observation by confocal, epifluorescent or fluorescent stereomicroscopes.

The analysis of the molecular structure of myosin.ADP.Vi.blebbistatin complex (PDB: 1YV3) [65] indicates that C15 nitro substitution does not affect significantly the interaction of the

inhibitor with myosin since the substituted nitro group causes no steric hindrance with any of the sidechains in the blebbistatin binding site of myosin (Figure 40).



Using HeLa, M2 and *Dd* cells as well as zebrafish embryos we proved that blebbistatin and para-nitroblebbistatin have identical myosin II inhibitory properties, but distinct cytotoxicity. As we demonstrated, blebbistatin has many interacting partner proteins in cells other than myosin IIs, with different binding affinities [70, 116]. Despite the fact that the observed *in vivo* myosin-II-dependent processes are inhibited by the two molecules similarly, the extreme difference between their cytotoxic effects indicates that their cellular interacting network is different. The cytotoxicity of blebbistatin is a very serious problem – especially in long-term experiments – and according to our results it is much more pronounced than the literature suggests. Furthermore, in many studies blebbistatin is usually applied at 50-100  $\mu\text{M}$  concentrations which may induce non-specific enzymatic interactions and more pronounced cytotoxicity in *in vivo* experiments. Cytotoxicity and other non-specific effects may easily lead to the misinterpretation of the experimental results if the observed defective phenotype is attributed to myosin II dysfunction. Therefore extra care is required in the interpretation of the experiments when blebbistatin is used.

It may be unclear how blebbistatin can be applied at 50-100  $\mu\text{M}$  concentrations when its solubility is limited to around 20  $\mu\text{M}$ . The solubility of blebbistatin depends on the

temperature and DMSO concentration. According to our experience based on zebrafish treatments by blebbistatin (30°C and 0.1% DMSO), precipitation of the molecules start at around 20  $\mu\text{M}$ . At room temperature and 0.1% DMSO concentration the solubility of blebbistatin is around 10  $\mu\text{M}$  at equilibrium [116]. If blebbistatin is applied at higher concentrations than its solubility, supersaturation occurs followed by the slow precipitation of the molecule. We have measured the time dependence of the precipitation reaching equilibrium at room temperature. Applying 100  $\mu\text{M}$  of the inhibitor to buffer containing 0.1 % DMSO, we followed its slow precipitation in time. It took hours to reach equilibrium and until that, the apparent concentration of the inhibitor was higher than its solubility measured in equilibrium (Figure A3). This behavior of blebbistatin may cause further difficulties related to the reproducibility of the experiments because the actual concentration of the dissolved blebbistatin sensitively depends on the time between dissolving of the inhibitor and the measurement.

The non-phototoxicity of para-nitroblebbistatin enables fluorescent microscopic imaging of living organisms providing novel insights into the role of myosin IIs *in vivo*. When we time-lapse imaged HeLa Kyoto cells treated with para-nitroblebbistatin at low concentrations (<30  $\mu\text{M}$ ), we observed a hitherto undescribed phenotype in HeLa cells: after anaphase, the cytokinesis proceeded, the midbody formed but scission did not occur. After a while the cell collapsed and became binuclear (mechanism 1). We also found that treatment with high concentrations (>30  $\mu\text{M}$ ) of para-nitroblebbistatin inhibited the ingression of the cleavage furrow (mechanism 2) in which case cytokinesis did not occur. However, according to our results, para-nitroblebbistatin is not specific at high concentrations which indicates that only mechanism 1 can be attributed to the inhibition of myosin II. This is a quite astonishing discovery, since it suggests that the ATPase activity of myosin IIs are not required for cytokinesis itself, although current concepts of vertebrate cytokinesis favor the notion that contractile ring constriction is driven by non-muscle myosin IIs [42, 119]. Our finding is supported by a recent publication stating that in vertebrate cytokinesis non-muscle myosin IIs do not translocate actin. According to the authors the major roles of non-muscle myosin II in vertebrate cytokinesis are to bind and crosslink actin filaments and to exert tension on actin during contractile ring constriction [44].

On the other hand, we found that scission - the final stage of cell division - depends on the activity of myosin IIs. The significance of the observation is highlighted by the fact that no myosin II involvement has been reported in scission yet. Understanding the molecular mechanism of the different stages of cell division is extremely important, therefore further experiments are needed to clarify the exact roles of myosin II in both cytokinesis and scission.

Consequently, para-nitroblebbistatin, our newly developed blebbistatin derivative, has greatly advanced properties over blebbistatin and therefore it is an ideal replacement of blebbistatin in physiological, developmental and cell biological studies, especially in cases when blue light irradiation is required.

### **Molecular tattooing**

To investigate and understand elemental mechanisms underlying the extreme complexity of living systems, selective intervention into cellular processes is a fundamental experimental demand. Pharmacology has given a great variety of bioactive compounds enabling to influence receptors, ion channels, signaling molecules and many other types of proteins or enzymes at the molecular level. Although bioactive compounds perform certainly well in the sense of systemic intervention, they are generally incapable of targeting individual areas, distinct cells or subcellular regions inside a living organism.

The overall goal of targeted drug delivery would be to achieve 1. prolonged, 2. target-specific and 3. localized effect of bioactive compounds. A series of techniques have been developed for the target-specific delivery of bioactive compounds spatially and temporally, including photoactive caged and switchable molecules, although none of them have fulfilled the above mentioned three criteria at the same time.

Molecular tattooing is a novel approach in drug targeting which enables local and prolonged modulation of target enzymes in the cellular, subcellular level. It applies two-photon microscopy for photo-activation and photo-crosslinking of azidated ligands to their targets in well-defined areas. This finding illustrated that cell or organ autonomous and non-autonomous mechanisms can be efficiently distinguished by molecular tattooing, which was hitherto only possible by transplantation experiments. Furthermore, the activity of myosin II

can also be inhibited in distinct regions of the migrating pLLp, thereby mapping the effect of myosin II inhibition on the lateral line development. Using different azidated pharmacological compounds, even complete signaling pathways may be inhibited or overdriven in preferred locations in zebrafish. Such bioactive ligands could be the azidated form of the Wnt agonist 1-Azakenpaullone or the FGF receptor antagonist SU-5402, which control the development of the lateral line of zebrafish [120]. Toxicity and other adverse effects of bioactive compounds can be alleviated by molecular tattooing. This is well demonstrated by systemic blebbistatin treatment of zebrafish embryos (Figure 26) which resulted in curved body shape, heart oedema and pronounced lethality. On the other hand, by azidoblebbistatin tattooing we did not observe any of these phenotypes, since outside the targeted area the concentration of azidoblebbistatin is below its effective concentration.

Using the technique of molecular tattooing, we were able to unveil details of the blebbing mechanism of M2 cells, which type of cellular protrusion is a commonly used migration mode of tumor and embryonic cells. According to recent models, bleb expansion in M2 cells is driven by local pressure increase [51]. These models are based on the observation that the pressure equilibration over an M2 cell is slower than the timescale of bleb growth. On the other hand our experiments indicate that in case of M2 cells the expansion of blebs are driven by globally uniform hydrostatic pressure since inhibition of myosin molecules in half of the cell lead to uniform decrease in both the velocity of expansion and the size of the blebs. On the other hand we found that the velocity of retraction was significantly slower in the myosin II inhibited half of the cell so our results confirm that bleb retraction is mediated by local myosin II activity [47].

In the sense of propagating molecular tattooing in life sciences, the availability of azidated ligands is a key question. In case of several pharmacological compounds the synthetic route of their halo derivative (iodo, bromo) - the direct precursor of the azido compound - has been explored due to the need of radiolabeling for receptor binding assays, ADME (Absorption, Distribution, Metabolism, and Excretion) studies or SPECT (Single Photon Emission Computed Tomography) imaging. Importantly, in this case structure-activity relationship (SAR) studies must have been performed in order to evaluate the effect of the substitution on the bioactivity of the compound. Thus, these data are available: if the halo-substitution has significantly not affected the binding properties of the compound, it is a

very good indication that the azido group will neither. Moreover, tritiation of a variety of pharmacological compounds have been worked out, which is also important in the sense of azidation since the preferred tritiation method involves aromatic halogenation (mainly iodination or bromination) followed by reduction, using tritium gas. Furthermore, in the drug discovery pipeline, SAR studies generate several halo-substituted derivatives of leading compounds providing valuable synthetic routes and SAR data about the modifiable positions.

Titanium:sapphire lasers are the only commercially available mode-locked lasers applicable for two-photon excitation, consequently, all two-photon microscopes are equipped with Ti:Sa lasers. However, the tuning range of these lasers are usually between 700 and 1000 nm meaning that only molecules which have absorption in this region ( $\approx$ 350-500 nm one-photon absorption) can be photoactivated. Molecules without proper conjugated structure, usually those which consist of only one aromatic ring (e.g. azidolidocaine or azidoQX314), cannot be two-photon activated. Moreover, as we demonstrated by two-photon activation of azidofluorescein, in order to achieve efficient photoreaction, the aromatic ring containing the azido group may need to be excited directly.

The most ideal two-photon excitation wavelength for aryl azide-based molecular tattooing would be around 550-600 nm, since this is the absorption range of the aromatic ring. Although Ti:Sa lasers cannot emit at this wavelengths, their output beam can be altered by optical methods such as frequency doubling and the use of optical parametric oscillators (OPOs) [121]. Frequency doubling (or second harmonic generation) is a nonlinear optical process, in which photons with the same frequency interacting with a nonlinear material are "combined" to generate new photons with twice the frequency and half the wavelength of the initial photons. An OPO, on the other hand, converts an input laser wave to two output waves of lower frequency by means of second-order nonlinear optical interaction. In such ways, OPOs can asymmetrically split a laser beam, although the sum of the output waves' frequencies is equal to the input wave frequency. Using second harmonic generation and OPOs, the output of Ti:Sa lasers can be tuned from 345 nm to 2500 nm, therefore the aromatic ring can be directly two-photon activated. Such optical devices are commercially available.

Molecular tattooing is a powerful tool for the exploration of local, target-specific mechanisms within an organism or within even single cells. Since subfemtoliter resolutions can be achieved, neurophysiology might be an important area of the technique, targeting specific receptors of single synapses. Due to the high resolution, spatial and temporal control of targeting, molecular tattooing may become a powerful technique in a series of further research fields, especially in developmental biology and cell biology.

## VII. Materials and Methods

Reagents and solvents were purchased from Sigma-Aldrich, WVR and Santa Cruz Biotechnology. Chemical reactions were performed using a CEM BenchMate 300W microwave reactor. For LC-MS analysis an Agilent 1100 instrument combined with a Waters sqd was used. Semi preparative purification of compounds was achieved by an Agilent 1100 HPLC while preparative purifications were carried out using an Agilent 971-FP flash chromatography system. The UV-VIS spectra were recorded by a Shimadzu UV-2101 spectrophotometer. Fluorescence measurements, photoactivation and phototoxicity assays were performed in an Edinburgh Instruments F900 Fluorescence Spectrometer equipped with a 450W Xenon Lamp. Dictyostelium discoideum cells were irradiated using BioLogic Science Instrument 200 W Mercury-Xenon lamp. Images of zebrafish were captured by a Zeiss Stereo Lumar.V12 microscope. Confocal microscopy was carried out by a Zeiss LSM 710. For two-photon microscopy a Femto 2D (Femtonics) instrument was used.

NMR analysis were carried out by by ChiroBlock GmbH or in the case of azidoblebbistatin Andrea Bodor.

LC-MS analysis of tryptic proteins was performed in BRC, Szeged.

### Organic syntheses

#### Synthesis of azidoblebbistatin

**Iodoblebbistatin.** 5 mg (-)-blebbistatin was dissolved in 300  $\mu$ l methanol and transferred to a 10-ml microwave reaction vessel. During continuous stirring 700  $\mu$ l boron trifluoride dihydrate and 5,7 mg (1,5-fold excess) N-Iodosuccinimide was added and the reaction mixture was placed into a microwave reactor at 50°C for 30 minutes with magnetic stirring. A Strata XL 500 mg SPA column (Phenomenex) was equilibrated with 50 ml acetonitrile then 50 ml water and the crude reaction mixture was pipetted onto the column. It was sequentially washed with 20 ml water, 3 ml sodium bisulfite, 3 ml saturated sodium bicarbonate, 20 ml water, and then eluted with 20 ml acetonitrile containing 1 % trifluoroacetic acid and dried in vacuum. The brownish powder was dissolved in 0.5 ml

acetonitrile containing 0.15 % triethylamine (TEA) and it was further purified by HPLC using a Luna 250x10 mm C18 column (Phenomenex). HPLC conditions were as follows: isocratic elution, content of buffer: water (0.15 % TEA): acetonitrile (0.15 % TEA) 3:7 (vol/vol), flow rate: 3.5 ml/min, detection wavelength: 254 nm.

**Azidoblebbistatin.** Pure iodoblebbistatin was dissolved in 1 ml of DMSO:H<sub>2</sub>O mixture (5:1 vol/vol) and pipetted into a 10 ml reaction vessel containing 15 mg sodium azide, 2 mg copper(I) iodide and 1 mg sodium ascorbate. 2 µl N,N -dimethylethylenediamine was added and the reaction mixture was stirred for 30 minutes at room temperature. The purification was performed in the same way as in case of iodoblebbistatin.

(-)-para-azido-blebbistatin: <sup>1</sup>H chemical shifts , ppm: 2.26 (2, 2H, multiplet), 2.30 (11, 3H, singlet), 3.95 (3A, 1H, multiplet), 4.05 (3B, 1H, multiplet), 6.84 (12, 1H, singlet), 7.12 (8, 1H, doublet, <sup>3</sup>J<sub>HH</sub>=8.1Hz), 7.19 (3', 2H, doublet, <sup>3</sup>J<sub>HH</sub>=8.9Hz), 7.40 (7, 1H, dd, <sup>3</sup>J<sub>HH</sub>=8.1Hz, <sup>4</sup>J<sub>HH</sub>=1.8Hz ), 7.54 (5, 1H, doublet, <sup>4</sup>J<sub>HH</sub>=1.8Hz), 8.15 (2', 2H, doublet, <sup>3</sup>J<sub>HH</sub>=8.9Hz). <sup>13</sup>C chemical shifts, ppm: 20.0 (11), 28.0 (2), 47.2 (3), 73 (3a), 119.1 (3'), 120.8 (2'), 121.1 (10), 125.5 (8), 126.0 (5), 132.4 (6), 134.4 (1'), 136.0 (7), 138.1 (4'), 148.9 (9), 165.4 (2x), 194.7 (4). MS (ESI): *m/z* = 334 [M+H]<sup>+</sup> Brownish yellow powder. Storage: -20°C. Protect from light. No degradation in 1 year.

### **Synthesis of azidocelecoxib (isomer 1)**

**Iodocelecoxib (isomer 1).** 200 mg iodoacetophenone and 40 mg NaH were dissolved in 5 ml dry THF. The mixture was stirred at 0°C for 60 min and 290 µl trifluoroacetate was added dropwise. After stirring at 0°C for 12 hours and at room temperature for 12 hours, the reaction mixture was acidified with 1N HCl then neutralized with 1N NaOH. Then the reaction mixture was extracted with chloroform. After concentrating it in vacuum, the brownish oil was dissolved in 0.5 ml acetonitrile containing 0.1 % triethylamine (TEA) and it was further purified by HPLC using a Luna 250x10 mm C18 semiprep column (Phenomenex). HPLC conditions W:ACN=A:B (0.1% TEA), 3 ml/min, 254 nm. Elution: 0-7 min: 40% B, 7-8 min 40-90% B.

The isolated product was concentrated under vacuum and the remaining yellow oil (50 mg) was dissolved in 3 ml ethanol. 33 mg 4-methylsulfonyl-phenylhydrazine hydrochloride was

added and the mixture was refluxed for 4 hours. It was concentrated in vacuum and separated by HPLC using C18 semiprep column. HPLC conditions: W:ACN=A:B (0.1% TEA), 3 ml/min, 254 nm. Elution: 0-10 min 40-80% B. White crystals.

**Azidocelecoxib (isomer 1).** 42 mg iodocelecoxib was dissolved in 1 ml of DMSO:H<sub>2</sub>O mixture (5:1 vol/vol) and pipetted into a 10 ml reaction vessel containing 65 mg sodium azide, 10 mg copper(I) iodide and 5 mg sodium ascorbate. 8  $\mu$ l N,N -dimethylethylenediamine was added and the reaction mixture was placed in a microwave reactor for 30 min at 60 °C.

**SPA cleaning procedure:** A Strata XL 2 mg SPA column (Phenomenex) was equilibrated with 50 ml acetonitrile then 50 ml water and the crude reaction mixture was pipetted onto the column. It was sequentially washed with 20 ml water, 3 ml sodium bisulfite, 3 ml saturated sodium bicarbonate, 20 ml water, and then eluted with 20 ml acetonitrile containing 1 % trifluoroacetic acid and dried in vacuum.

The remaining oil was dissolved in 0.5 ml acetonitrile containing 0.1% TFA, and separated by HPLC using C18 semiprep column. HPLC conditions: isocratic elution, W:ACN=4:6 (0.1% TFA), 3 ml/min, 254 nm. MS (ESI):  $m/z = 409$  [M+H]<sup>+</sup>

### **Synthesis of azidocelecoxib (isomer 2)**

**Iodocelecoxib (isomer 2).** 110 mg 3 -Iodo-4'-methoxyacetophenone and 20 mg NaH were dissolved in 5 ml dry THF. The mixture was stirred for 60 min and 290  $\mu$ l trifluoroacetate was added dropwise. After stirring the mixture at 0 °C for 12 hours and at room temperature for 12 hours, it was concentrated under vacuum. The remaining solid was dissolved in 1 ml DMSO and pipetted onto a Strata XL 2 mg SPA column (Phenomenex) equilibrated with 50 ml acetonitrile then 50 ml water, washed with 100 ml water than eluted with acetonitrile containing 1% TFA and dried under vacuum. The remaining oil was dissolved in acetonitrile containing 0.1 % TEA, than separated with HPLC using C18 semiprep column. HPLC conditions: W:ACN=A:B (0.15% TEA), 3.5 ml/min, 254 nm. Elution: 0-9 min: 35% B, 9-10 min 35-90% B. The combined fractions were concentrated under vacuum and dissolved in 1.5 ml ACN (0.15% TEA). The undissolved white precipitate was centrifuged in an eppendorf centrifuge at 14.000 RPM. The product was in the supernatant which was concentrated under vacuum.

The remaining oil (116 mg) was dissolved in 6 ml ethanol while 70 mg 4-methylsulfonyl-phenylhydrazine hydrochloride was added. The mixture was refluxed for 4 hours, cooled, concentrated under vacuum, and washed with water on a 2g Strata column (see above the conditions of the washing). The product was separated by HPLC using C18 semiprep column. HPLC conditions: isocratic elution, W:ACN=35:65 (0.1% TEA), 3.5 ml/min, 254 nm.

**Azidocelecoxib (isomer 2).** 40 mg iodocelecoxib (isomer 2) was dissolved in 1 ml of DMSO:H<sub>2</sub>O mixture (5:1 vol/vol) and pipetted into a 10 ml reaction vessel containing 65 mg sodium azide, 10 mg copper(I) iodide and 5 mg sodium ascorbate. 8 µl N,N-dimethylethylenediamine was added and the reaction mixture was placed in a microwave reactor for 30 min at 70 °C.

Following SPA cleaning procedure, the remaining oil was dissolved in 0.5 ml acetonitrile containing 0.1% TEA, and separated by HPLC. HPLC conditions: W:ACN=A:B (0.1% TEA), 3.5 ml/min, 254 nm. Elution: 0-15 min: 45-55% B. The combined fraction were concentrated under vacuum. MS (ESI):  $m/z = 439$  [M+H]<sup>+</sup>

### **Synthesis of azidoBTS**

**IodoBTS.** 250 mg iodobenzyl amine was dissolved in 60 ml water. The pH of the solution was set to 8 by 1M NaOH. 178 mg toluenesulfonyl chloride was added and the mixture was stirred for 2 hours. The pH was set to 2 while the product precipitated. It was filtered and dried.

**AzidoBTS.** 100 mg iodocelecoxib was dissolved in 1 ml of DMSO:H<sub>2</sub>O mixture (5:1 vol/vol) and pipetted into a 10 ml reaction vessel containing 65 mg sodium azide, 10 mg copper(I) iodide and 5 mg sodium ascorbate. 8 µl N,N-dimethylethylenediamine was added and the reaction mixture was placed in a microwave reactor for 30 min at 80 °C.

Following SPA cleaning procedure, the remaining oil was dissolved in 1.5 ml acetonitrile containing 0.1% TEA, and separated by HPLC on semiprep C18 column. HPLC conditions: isocratic elution, W:ACN=3:7 (0.1% TEA), 3.5 ml/min, 254 nm. MS (ESI):  $m/z = 302$  [M+H]<sup>+</sup>

### **Synthesis of azidolidocaine**

**Iodolidocaine.** 100 lidocaine and 106 mg N-Iodosuccinimide were dissolved in 1 ml boron trifluoride dihydrate. 0.5 ml acetonitrile was added and the reaction mixture was stirred at room temperature for 15 min. Following SPA cleaning procedure, it was dissolved in acetonitrile containing 0.1% TFA and separated by semiprep HPLC. HPLC conditions: isocratic elution, W:ACN=6:4 (0.1% TFA), 3 ml/min, 254 nm.

**Azidolidocaine.** Iodolidocaine was dissolved in 1.5 ml of DMSO:H<sub>2</sub>O mixture (5:1 vol/vol) and pipetted into a 10 ml reaction vessel containing 130 mg sodium azide, 20 mg copper(I) iodide and 10 mg sodium ascorbate. 16 µl 'N,N -dimethylethylenediamine was added and the reaction mixture was placed in a microwave reactor for 30 min at 90°C. Following SPA cleaning procedure, the remaining solid was dissolved in acetonitrile containing 0.1 % TEA and separated by semiprep HPLC. HPLC conditions: isocratic elution, W:ACN=35:65 (0.1% TEA), 4 ml/min, 254 nm. MS (ESI):  $m/z = 276$  [M+H]<sup>+</sup>

#### **Synthesis of azidoQX314**

**IodoQX314.** 50 lidocaine and 39 mg N-Iodosuccinimide were dissolved in 0.8 ml boron trifluoride dihydrate. 0.5 ml acetonitrile was added and the reaction mixture was stirred at room temperature for 15 min. Following SPA cleaning procedure, it was dissolved in acetonitrile containing 0.1% TFA and separated by semiprep HPLC. HPLC conditions: isocratic elution, W:ACN=6:4 (0.1% TFA), 3 ml/min, 254 nm.

**AzidoQX314.** Iodolidocaine was dissolved in 1.5 ml of DMSO:H<sub>2</sub>O mixture (5:1 vol/vol) and pipetted into a 10 ml reaction vessel containing 130 mg sodium azide, 20 mg copper(I) iodide and 10 mg sodium ascorbate. 16 µl 'N,N -dimethylethylenediamine was added and the reaction mixture was placed in a microwave reactor for 30 min at 90°C. Following SPA cleaning procedure, the remaining solid was dissolved in acetonitrile containing 0.1 % TEA and separated by HPLC using semiprep C18 column. HPLC conditions: isocratic elution, W:ACN=35:65 (0.1% TEA), 4 ml/min, 254 nm.

#### **Synthesis of azidosulpride**

50 mg amisulpride was dissolved in 1 ml 1M HCl and stirred at 0°C for 10 minutes. 10 mg NaNO<sub>2</sub> in 0.1 ml water was added slowly to the mixture and it was further stirred for 2 minutes at 0 °C. 390 mg NaN<sub>3</sub> in 1 ml cooled HCl was slowly added and stirred for 5 minutes

at 0 °C and at room temperature for 1 hour. The reaction mixture was applied to a water-equilibrated 2 g Strata column and washed with 50 ml water. It was eluted with methanol containing 1% TFA and concentrated under vacuum. The remaining solid was dissolved in 0.5 ml acetonitrile containing 0.1 % TFA and separated by HPLC using C18 semiprep column. HPLC conditions: isocratic elution, W:ACN=3:7 (0.1% TFA), 3 ml/min, 320 nm. MS (ESI):  $m/z = 396 [M+H]^+$

### **Synthesis of perphenazine azidobenzoate**

80 mg perphenazine, 65 mg azidobenzoic acid and 5 mg 4-Dimethylaminopyridine were dissolved in 1 ml water-free dimethylformamide and stirred for 5 minutes at 0 °C. 83 mg N,N'-Dicyclohexylcarbodiimide was added and the reaction was stirred for 5 minutes at 0 °C and 12 hours at room temperature. The reaction mixture was applied to a water-equilibrated 2 g Strata column and washed with 50 ml water. It was eluted with methanol containing 1% TFA and concentrated under vacuum. The remaining solid was dissolved in 1 ml acetonitrile containing 0.1% TFA. It was incubated at room temperature for 30 minutes while white precipitate was formed. It was centrifuged and the supernatant was further purified by HPLC using semiprep C18 column. HPLC conditions: isocratic elution, W:ACN=4:6 (0.1% TFA), 3 ml/min, 320 nm. MS (ESI):  $m/z = 549 [M+H]^+$

### **Synthesis of azidotelmisartan**

**Iodotelmisartan.** 10 mg telmisartan and 10 mg N-Iodosuccinimide was dissolved in 1.2 ml boron trifluoride dihydrate. 0.8 ml acetonitrile was added and the reaction was placed into a microwave reactor at 110 °C for 40 minutes. Following SPA cleaning procedure, it was dissolved in acetonitrile containing 0.1% TFA and separated by semiprep HPLC. HPLC conditions: isocratic elution, W:ACN=6:4 (0.1% TFA), 5 ml/min, 254 nm.

**Azidotelmisartan.** Iodotelmisartan was dissolved in 1.5 ml of DMSO:H<sub>2</sub>O mixture (5:1 vol/vol) and pipetted into a 10 ml reaction vessel containing 15 mg sodium azide, 2 mg copper(I) iodide and 1 mg sodium ascorbate. 2 µl N,N -dimethylethylenediamine was added and the reaction mixture was placed in a microwave reactor for 30 min at 60°C. Following SPA cleaning procedure, the remaining solid was dissolved in acetonitrile containing 0.1 %

TEA and separated by HPLC using semiprep C18 column. HPLC conditions: isocratic elution, W:ACN=6:4 (0.1% TEA), 5 ml/min, 254 nm. MS (ESI):  $m/z = 556 [M+H]^+$

### Synthesis of azidoclozapine

**Iodoclozapine.** 50mg clozapine and 52 mg N-Iodosuccinimide was dissolved in 1.2 ml boron trifluoride dihydrate. 0.5 ml methanol was added and the reaction was placed into a microwave reactor at 40°C for 45 minutes. Following SPA cleaning procedure, it was dissolved in acetonitrile containing 0.1% TFA and separated by semiprep HPLC. HPLC conditions: isocratic elution, W:ACN=6:4 (0.1% TFA), 4 ml/min, 254 nm.

**Azidoclozapine.** Iodoclozapine was dissolved in 1 ml of DMSO:H<sub>2</sub>O mixture (5:1 vol/vol) and pipetted into a 10 ml reaction vessel containing 30 mg sodium azide, 5 mg copper(I) iodide and 2.5 mg sodium ascorbate. 4  $\mu$ l N,N-dimethylethylenediamine was added and the reaction mixture was placed in a microwave reactor for 30 min at 80°C. Following SPA cleaning procedure, the remaining solid was dissolved in acetonitrile containing 0.1 % TFA and separated by HPLC using semiprep C18 column. HPLC conditions: isocratic elution, W:ACN=6:4 (0.1% TFA), 4 ml/min, 254 nm. MS (ESI):  $m/z = 369 [M+H]^+$

### Synthesis of para-nitroblebbistatin

**1-(4-nitrophenyl)pyrrolidin-2-one (compound 8).** 10 g 1-Phenyl-2-pyrrolidinone (compound 1) was dissolved in 15 ml cc.H<sub>2</sub>SO<sub>4</sub> and the solution was cooled to 0°C in ice bath. A mixture of 4.4 ml 70% HNO<sub>3</sub> and 4.4 ml cc. H<sub>2</sub>SO<sub>4</sub> was added dropwise. After 15 min of magnetic stirring the solution was poured onto 120 g of ice where the yellowish product precipitated. It was washed with water and crystallized from hot ethyl acetate and a drop of hexane. The yield was 90%.

<sup>1</sup>H NMR (400 MHz, Chloroform-*d*)  $\delta$  8.26 – 8.17 (m, 2H), 7.87 – 7.78 (m, 2H), 3.92 (t,  $J = 7.1$  Hz, 2H), 2.67 (d,  $J = 16.2$  Hz, 1H), 2.22 (p,  $J = 7.6$  Hz, 2H); MS (ESI):  $m/z = 206 [M+H]^+$

**Methyl amino-5-methylbenzoate (compound 3).** 5g 2-methyl-2-amonobenzoate is dissolved in 75mL methanol. 7.5 ml cc. H<sub>2</sub>SO<sub>4</sub> was added and the solution was refluxed for 48 hours at 60°C. The mixture was cooled and vacuum dried. The remaining solid was washed with saturated Na<sub>2</sub>HCO<sub>3</sub>, extracted 3 times with ethyl acetate, dried by Na<sub>2</sub>SO<sub>4</sub> and lyophilized. The yield was 90%.

$^1\text{H}$  NMR (400 MHz, Chloroform-*d*)  $\delta$  7.68 (d,  $J$  = 1.5 Hz, 2H), 7.12 (dd,  $J$  = 8.3, 2.2 Hz, 1H), 6.61 (d,  $J$  = 8.3 Hz, 1H), 5.56 (s, 2H), 3.89 (s, 4H); MS (ESI):  $m/z$  = 166  $[\text{M}+\text{H}]^+$

**Methyl 2-[(2E)-1-(4-nitrophenyl)pyrrolidin-2-ylidene]amino-5-methylbenzoate (compound 9).** We note that step 3, 4 and 5 required strictly water free conditions. In order to obtain water free conditions, all containers were heated for a day on 120°C and dried subsequently on  $\text{P}_2\text{O}_5$ . 5.8 g (28 mmol) compound 3 was dissolved in 30 ml water free DCM. During magnetic stirring, 2.8 ml (30 mmol)  $\text{POCl}_3$  was added and the mixture was stirred for 3 hours. 30 ml dry DCM containing 4.3 g (26 mmol) compound 8 was added and the mixture was refluxed under argon (dried by drierite) for 18 hours at 50°C. After cooling to room temperature the precipitate was removed by centrifugation and the supernatant was dried under vacuum. The remaining sticky material was extracted by 0.3 M HCl with the help of a sonicator, for half an hour in each extraction. The pH of the extracted solution was set to 8 by NaOH. At this pH the pale yellow colored solution changed to a dark yellow suspension. The desired material was extracted 3 times with ethyl acetate and dried under vacuum. The yellow solid was dissolved in 15 ml acetonitrile and compound 9 was isolated by reverse phase flash chromatography using a 25 g C18 column and isocratic elution: 65% water: 35% acetonitrile. The yield was 10 %.

$^1\text{H}$  NMR (400 MHz, Chloroform-*d*)  $\delta$  8.27 – 8.17 (m, 2H), 8.12 – 8.02 (m, 3H), 7.73 (d,  $J$  = 2.0 Hz, 2H), 7.32 – 7.21 (m, 2H), 3.94 (t,  $J$  = 7.0 Hz, 2H), 3.82 (s, 4H), 2.53 (t,  $J$  = 7.9 Hz, 2H), 2.12 (t,  $J$  = 7.5 Hz, 2H); MS (ESI):  $m/z$  = 354  $[\text{M}+\text{H}]^+$

**1-(4-nitrophenyl)-6-methyl-1H,2H,3H,4H,9H-pyrrolo[2,3-b]quinolin-4-one (compound 10).** 950 mg (2.7 mmol) compound 9 was dried overnight over  $\text{P}_2\text{O}_5$ . 25 ml THF was added and the mixture was stirred for 20 min under dry argon. The reaction was chilled to -78°C in an acetone-dry ice bath and stirred for 10 min. 10.8 ml (10.8 mmol) lithium bis(trimethylsilyl)amide (1 M in THF) was added dropwise and the reaction mixture was warmed slowly to 0°C in 3 hours. 150 ml saturated  $\text{NH}_4\text{Cl}$  was added while the color of the mixture changed from yellow to red. It was extracted 3 times by 80 ml of DCM and dried under vacuum. The solid was dissolved in 20 ml DCM and purified by flash chromatography applying silica column (25 g) and gradient elution from hexane:DCM=40:60 to hexane:DCM=25:75. The yield was 20%.

$^1\text{H}$  NMR (400 MHz,  $\text{DMSO-}d_6$ )  $\delta$  8.31 (d,  $J$  = 9.4 Hz, 2H), 8.22 (d,  $J$  = 9.5 Hz, 2H), 7.80 (s, 1H), 7.61 (d,  $J$  = 8.4 Hz, 1H), 7.38 (dd,  $J$  = 8.5, 1.9 Hz, 1H), 4.13 (t,  $J$  = 8.1 Hz, 2H), 3.19 (t,  $J$  = 8.0 Hz, 2H), 2.42 (s, 3H); MS (ESI):  $m/z$  = 322  $[\text{M}+\text{H}]^+$

**(3aS)-3a-hydroxy-1-(4-nitrophenyl)-6-methyl-1H,2H,3H,3aH,4H-pyrrolo[2,3-b]quinolin-4-one (compound 11).** 160 mg compound 10 was dissolved in 15 ml water free THF. It was chilled to  $-78^\circ\text{C}$  and under dry argon 650  $\mu\text{l}$  (0.65 mmol) lithium bis(trimethylsilyl)amide was added (1M in THF). The mixture was stirred for 30 min and in 10 ml THF 375 mg (1.25 mmol) (8,8-dichlorocamphorylsulfonyl)oxaziridine was added. The reaction was warmed to  $-10^\circ\text{C}$  and stirred for 16 hours under argon. The reaction was quenched with 10 ml saturated ammonium iodide. 15 ml ether and 15 ml saturated  $\text{Na}_2\text{S}_2\text{O}_3$  were added and the product was extracted 3 times by 10 ml ether. The ether fraction was dried in vacuum. The solid was dissolved in 10 ml DCM and extracted 3 times by 100 ml 0.3 M HCl. The pH of the HCl fraction was set to 8 by NaOH and extracted 3 times by 80 ml ethyl acetate and dried in vacuum. The remaining brown oil was dissolved in acetonitrile containing 0.1 % TFA and purified by HPLC (Luna 250  $\times$  10 mm C18 column, isocratic elution, water:acetonitrile=6:4, 0.1% TFA). The yield was 54%. The ratio of the (-) enantiomer was 80% determined by chiral HPLC. The applied stationary phase and the eluents: Lux Cellulose-1 column (Phenomenex), isocratic elution, heptane:ethanol=9:1.

$^1\text{H}$  NMR (500 MHz,  $\text{DMSO-}d_6$ )  $\delta$  8.37 – 8.30 (m, 2H), 8.29 – 8.22 (m, 2H), 7.54 (d,  $J$  = 1.6 Hz, 1H), 7.43 – 7.37 (m, 1H), 7.19 (d,  $J$  = 8.0 Hz, 1H), 6.93 (s, 1H), 4.03 (d,  $J$  = 14.8 Hz, 1H), 2.45 (d,  $J$  = 7.1 Hz, 3H), 2.27 (d,  $J$  = 15.5 Hz, 4H); MS (ESI):  $m/z$  = 338  $[\text{M}+\text{H}]^+$ . Chemical purity: consistent with > 95% purity (LC, 210nm). Appearance: orange solid.

### **Synthesis of para-chloroblebbistatin**

2.5 mg (-)-blebbistatin was dissolved in 350  $\mu\text{l}$  boron trifluoride dihydrate and 100  $\mu\text{l}$  methanol. The mixture was transferred to a 10-ml microwave reaction vessel and 2.8 mg *N*-Chlorosuccimide was added in 350  $\mu\text{l}$  boron trifluoride dihydrate during continuous stirring. The reaction mixture was placed into a microwave reactor at  $100^\circ\text{C}$  for 30 minutes with magnetic stirring. A Strata XL 500 mg SPA column was equilibrated with 50 ml acetonitrile then 50 ml water and the crude reaction mixture was transferred onto the column. It was

sequentially washed with 20 ml water, 3 ml sodium bisulfite, 3 ml saturated sodium bicarbonate, 20 ml water, and then eluted with 20 ml acetonitrile containing 1 % trifluoroacetic acid and dried in vacuum. The yellowish powder was dissolved in 0.5 ml acetonitrile containing 0.15 % triethylamine (TEA) and it was further purified by HPLC using a Luna 250x10 mm C18 column. HPLC conditions were as follows: isocratic elution, content of buffer: water (0.15 % TEA): acetonitrile (0.15 % TEA) 3:7 (vol/vol), flow rate: 3.5 ml/min, detection wavelength: 254 nm. Yield: 40%. MS (ESI):  $m/z = 330 [M+H]^+$ . Analytical data match the literature [122].

### **Stock solutions**

Stock solutions of the synthesized molecules were prepared in DMSO and were used for further experiments.

### **Degradation kinetics of azidoblebbistatin**

0.5 ml 5  $\mu$ M azidoblebbistatin solution in assay buffer (40 mM NaCl, 4 mM MgCl<sub>2</sub>, 20 mM HEPES pH 7.3) was irradiated at 247, 278 and 310 nm (with 10 nm slit width) for 0 (control), 1, 2 and 5 minutes in a fluorimeter (450W Xenon lamp). At each time point 10  $\mu$ l solution was taken and analyzed by HPLC using conditions described at the synthesis of azidoblebbistatin section.

### **Fluorescence spectroscopic measurements**

5  $\mu$ M azidoblebbistatin solution was prepared in 0.8 M Tris-HCl (pH=9). The high concentration of Tris-HCl ensured that photoactivated ABleb attached mainly to the primary amine (nucleophile), which is required for fluorescence increase. Fluorescence emission spectra ( $\lambda_{ex}=400$ ) were recorded prior to and following irradiation of azidoblebbistatin at  $\lambda_{irrad}=400\pm 18$  nm for 10 min with a 450W Xenon lamp. The intensity of excitation during the emission spectral scan was as low as that no photoreaction of azidoblebbistatin occurred. The applied  $\lambda_{ex}$  and  $\lambda_{irrad}$  correspond to the half of the wavelength used in 2PM.

### **Basal and actin activated ATPase measurements**

Relative basal or actin activated ATPase activities of 3  $\mu$ M or 0.5  $\mu$ M DdMD W501+ [123] and 3  $\mu$ M or 0.2  $\mu$ M SkS1 constructs [124] were measured at increasing concentrations of

blebbistatin/para-nitroblebbistatin or actin using a pyruvate kinase/lactate dehydrogenase coupled assay (NADH-coupled assay) [125] at 20°C. In the actin activated ATPase measurements, 20 µM inhibitor was preincubated with myosin for 15 minutes on ice. G-actin was prepared accordingly from rabbit skeletal muscle [126] and polymerized by 2mM MgCl<sub>2</sub> for 1 hour at room temperature. Basal ATPase activity measurements were carried out in assay buffer (40 mM NaCl, 4 mM MgCl<sub>2</sub>, 20 mM HEPES, 2 mM 2-mercaptoethanol, pH 7.3) and actin activated ATPase activity measurements were performed in low salt buffer (2 mM MgCl<sub>2</sub>, 1 mM HEPES, 2 mM 2-mercaptoethanol, pH 7.3).

### **Sequential crosslinking and actin-activated ATPase measurements**

4 µM *DdMd* was crosslinked *via* sequential rounds of 10 µM azidoblebbistatin addition and UV irradiation. Following each crosslinking cycle, the ATPase activity of myosin was measured before and after the addition of 50 µM actin. The ATPase activity of completely crosslinked *DdMd* was also measured at increasing actin concentrations (0-80 µM) by the NADH-coupled assay described above. Actin was purified and prepared as described previously [127]. A 1.5-fold molar excess of phalloidin (Sigma) was used to stabilize actin filaments.

### **Preparation of *Dd* myosin-enriched protein fraction**

*Dd* ORF+ cells were cultured, collected and lysed as described in [123]. Whole cell lysates were centrifuged at 13,000 rpm for 30 minutes at 4°C in a tabletop centrifuge, and supernatants were used for analysis. Myosin-enriched fractions were prepared by ultracentrifugation of the lysates for 60 min at 55,000 rpm in a Beckman 55.1Ti rotor in the absence of ATP, washing the pellet in a similar ultracentrifugation step, and subsequent release of ATP-sensitive proteins by ultracentrifugation in the presence of 20 mM MgATP. Supernatants of the last step were analysed as “myosin-enriched fraction”. This fraction is dominantly a crude sample of actin and microtubule binding proteins which can be dissociated by ATP.

### **Azidoblebbistatin crosslinking and analysis of *Dd* myosin-enriched fractions**

Myosin-enriched fraction were crosslinked with azidoblebbistatin at concentrations of 2.5 µM, 5 µM, 10 µM, 15 µM, 25 µM, 50 µM and 100 µM. Samples were irradiated in one round

for 10 minutes after azidoblebbistatin addition. The optical arrangement was as described in the *Degradation kinetics* section. The protein content of the samples was analyzed by SDS-PAGE using UV transillumination to detect azidoblebbistatin fluorescence, and also by subsequent Coomassie staining using a Syngene Gene Genius Bio Imaging System.

### **Mass spectrometry of protein bands**

Fluorescent SDS-PAGE bands gel were excised, alkylated with iodoacetamide and digested with trypsin for 4 hours at 37 °C. After extraction, samples were dried and resolved in 10 µl of 1 % formic acid. Mass spectrometry was carried out using a Waters Q-TOF instrument. Data were analyzed using the Mascot Distiller program.

### **Cell cultures**

HeLa cells were kindly provided by Tibor Vellai (Eötvös University, Department of Genetics) and were maintained in Dulbecco's Modified Eagle Medium (DMEM, *Lonza*) supplemented with 3.7 g/l sodium-bicarbonate (pH 8.25), 40µg/mL gentamicin, and 10% FBS (*Lonza*). HeLa Kyoto cells were purchased from CLS Cell Lines Service GmbH and maintained in DMEM supplemented with 10% FBS, 2mM glutamine, 100 U/ml streptomycin, 100µg/ml penicillin, 0.5mg/ml G418 and 0.5µg/ml puromycin. M2 cells – a kind gift of Tom Stossel and Fumihiko Nakamura (Brigham & Women's Hospital, Harvard Medical School, Translational Medicine Division) – were grown in MEM (*Lonza*) supplemented with 8% newborn calf serum (*Sigma*) and 2% FCS. All human cell cultures were maintained in a humidified atmosphere of 5% CO<sub>2</sub> at 37°C. Cells were grown as monolayers in T-75 cm<sup>2</sup> culture flasks and subcultured by 0.02% EDTA (200 mg/l) 2–3 times each week when reached 90% confluency.

*Dd* (*Dictyostelium discoideum*) ORF+ cells were grown by shaking (150 rpm, <sup>90</sup>) in HL-5 medium (*Formedium*) complemented with penicillin-streptomycin (*Sigma*, in 100-fold dilution), glucose (12,4 g/l) and geneticin (0,03 mg/ml, *Gibco*) until 4\*10<sup>6</sup> cell/ml.

### **Cellular phototoxicity assay and microscopic imaging**

HeLa cells were grown into 96-well plates achieving monolayer cultures. Cells were treated with 10 µM blebbistatin or para-nitroblebbistatin and irradiated with 480±10 nm light for 15 minutes. The applied energy was 3.3 µJ/µm<sup>2</sup>. After 18 hours of incubation, the mortality rate

was determined by direct trypan blue staining and subsequent counting of the cells in the illuminated area.

### **Microscopic imaging**

Widefield images of HeLa cells were acquired on a modified light microscope (Motic AE31) equipped with a Sony cyber-shot camera using an LWD PH 20x/0.40 objective (Figure 20b). Confocal imaging of HeLa cells was performed using Plan Apo 63x/1.40 Oil DIC objective (Figure 23C). For acquisition and image analysis Zeiss LSM 710 Zen 2011 software was used. For live cell confocal time-lapse imaging of HeLa Kyoto cells, DMEM medium was supplemented with 25 mM HEPES in order to achieve CO<sub>2</sub> independent media. Confocal time-lapse imaging was performed on a Zeiss LSM 710 using a Plan Apo 20x/0.8 objective (Figure 21). Two-photon microscopy of the samples was carried out in a Femtonics Femto 2D two-photon microscope equipped with a mode-locked MaiTai Deep See Laser source (Spectra-Physics) with 100 fs pulse width and 80 MHz repetition rate. Image acquisition was performed by using MES software (Femtonics). Two photon imaging of *Dd* and M2 cells was performed using an Olympus UPLSAPO 60x/1.35 O objective (Figures 24, 25, 36, 37).

### **Phototoxicity assay using zebrafish embryos**

Zebrafish embryos were incubated with 5  $\mu$ M blebbistatin and nitroblebbistatin and irradiated with  $470 \pm 20$  nm light for 10 minutes. The applied energy was  $0.4 \mu\text{J}/\mu\text{m}^2$ . The embryos were monitored for 36 hours and were considered to be dead when became necrotic. Images of zebrafishes were captured by a Zeiss Stereo Lumar.V12 microscope using a NeoLumar S 0.8x FWD 80mm objective. For acquisition AxioVision 4.8 software was used (Figure 26).

### **Photoactivation of azidoblebbistatin and azidofluorescein in the function of two-photon laser power**

10 mM azidoblebbistatin or azidofluorescein in DMSO was loaded into glass capillaries (0.2  $\mu$ m inner diameter), and the sample was raster-scanned (x-y scanned) ( $\lambda_{\text{ex}}=800$  nm) for 2 minutes with the 2PM at different laser powers using a Olympus UPLSAPO 10x/0.4 objective. During the scan, the step size and the dwell time were 3  $\mu$ m and 2.72  $\mu$ s, respectively.

Following irradiation, the contents of the capillary was transferred into HPLC buffer (water:acetonitrile=1:1, supplemented with 0.1 % TFA), and the sample was subjected to LC-MS analysis using a C18 column and isocratic elution (water:acetonitril=1:1, 0.1% TFA). The resulted datapoints presented in Figures 30 a and b were fitted by  $y=y_0+Ae^{-kl^2/2}$  where  $y$  is the conversion of the photoreaction,  $A$  is the amplitude,  $k$  is the rate constant and  $l$  is the power of the laser.

### **Measuring the lateral (xy)- and z-dimensions of $V_{2PR}$**

Assay buffer (40 mM NaCl, 4 mM  $MgCl_2$ , 20 mM HEPES pH 7.3) was supplemented with 0.16 g/ml type B gelatin (Sigma-Aldrich) and the mixture was heated for 20 minutes at 40°C. Azidoblebbistatin in DMSO was added to the warm gelatin at 50  $\mu$ M final concentration and the mixture was pipetted into an imaging dish (MoBiTec, Imaging dish 1.5). After cooling, 300  $\mu$ l 50  $\mu$ M azidoblebbistatin in assay buffer was pipetted onto the gel surface to circumvent drying. Three letters 'M' were engraved (by line-scanning i.e. one-dimensional scanning) in the gel with 2PM irradiation ( $\lambda_{ex}=800$  nm), each by using different objective lenses: 10x/0.4 UPLSAPO (Olympus), 40x/0.8 LUMPLFLN W (Olympus), and 60x/1.35 UPLSAPO O (Olympus). The irradiation settings were: dwell time= 21.76  $\mu$ s, step size=0.005  $\mu$ m, scanning time=50 sec. Laser power was 20, 25 and 40% for the 10, 40 and 60x objectives, respectively (100% laser power=904 mW). The line-scanned areas were imaged by z-sectioning (2, 1 and 1  $\mu$ m z-steps with the 10, 40 and 60x objectives, respectively). Image analysis was performed by using ImageJ software (public domain).

### **2P induced photoaffinity labeling of myosin with azidoblebbistatin**

34  $\mu$ M *Dd* myosin motor domain was treated with 50  $\mu$ M azidoblebbistatin. 1  $\mu$ l of the sample was UV irradiated by a transilluminator table for 30 sec at 0°C. 1-1  $\mu$ l of the samples were two-photon irradiated at 800 nm with focused or unfocused laser beam using a 10x/0.4 objective, 80% laser power with 3  $\mu$ m step size and 2.72  $\mu$ s dwell time for 15 minutes at 0 °C. The crosslinked samples were analyzed by LC-MS (Waters sqd). For deconvolution the MaxEnt software was used (Waters).

## **Fish husbandry and treatment of embryos**

Transgenic *Tg(-8.0cldnb:lynEGFP)<sup>zf106</sup> (cldn:gfp)* fish stocks [110] were maintained in the animal facility of Eötvös Loránd University according to standard protocols [128]. 1-dpf-old embryos were dechorionated and incubated for 10 minutes in standard E3 embryo medium containing azidoblebbistatin, blebbistatin, para-nitroblebbistatin or DMSO as a control. Subsequently, they were transferred to preheated (40) 1% low melting-point agarose (Sigma-Aldrich) and placed in imaging dishes (MoBiTec, Imaging dish 1.5). After cooling, the embedded embryos were incubated in E3 medium containing DMSO or the inhibitors for 10 minutes. DMSO concentration of the E3 buffer was 0.1% throughout the experiments. In case of systemic treatment (with 10  $\mu$ M para-nitroblebbistatin), the embryos were imaged with confocal microscopy (z-stack every 10 minutes for 12 hours,  $\lambda_{ex}$ =488 nm, Plan-Apochromat 10x/0.45 M27, Zeiss Zen driver and image analysis software).

## **Two-photon irradiation of zebrafish embryos**

In case of molecular tattooing experiments, two-photon irradiation was performed by raster-scanning of the pLLp at  $\lambda_{ex}$ =800 nm for 8 minutes using an Olympus 10x/0.4 UPLSAPO objective. The parameters of the raster-scan were the following: dwell time=21.76  $\mu$ s, step size=0.1  $\mu$ m, laser power=3%. The duration of 1 scan was 3 s. Following irradiation, the embryos were imaged with confocal microscopy as described above. All protocols used in this study were approved by the Hungarian National Food Chain Safety Office (Permit Number: XIV-I-001/515-4/2012).

## **Two-photon irradiation of M2 cells**

Experiments were performed 18 hours after plating onto imaging dishes (MoBiTec, Imaging dish 1.0), when nearly 90% of the cells displayed extensive blebbing [129]. Prior to two-photon irradiation, cells were incubated for 5 minutes in PBS (140 mM NaCl, 2.7 mM KCl, 10.1 mM Na<sub>2</sub>HPO<sub>4</sub>, 1.8 mM KH<sub>2</sub>PO<sub>4</sub>, pH 7.9) containing DMSO, azidoblebbistatin or blebbistatin. DMSO concentration in PBS was 0.1% throughout all the experiments. Continuous raster-scanning and z-sectioning of the cells were performed at  $\lambda_{ex}$ =800 nm for the indicated times. The continuous laser scanning parameters using a 40x/0.8 LUMPLFLN W objective (Olympus) were the following: dwell time=21.76, step size=0.1  $\mu$ m, laser

power=4%. The duration of 1 scan was 6 s. For better resolution, subcellular experiments were performed using a 60x 1.35 NA UPLSAPO O objective (Olympus). Since its z-dimensions, z-sectioning was applied and parameters were optimized accordingly, to keep specificity: dwell time=43.52  $\mu$ s, step size=0.1  $\mu$ m, laser power=2%, z-step=3  $\mu$ m, number of slices=4, number of z-stacks: 13. Images were analyzed with ImageJ software. The parameters of continuous raster-scanning for movies of single cells were the following: dwell time=21.76, step size=0.2  $\mu$ m, laser power=0.3%. Blebbing indices are defined as the number of blebs observed during a given period of time over a given perimeter of the cell [51].

## IX. Acknowledgements

I am thankful for my supervisor, András Málnási-Csizmadia, who introduced me to the world of science. I feel very lucky that I had the opportunity to work in his lab during my PhD years. András is not only an inexhaustible source of ideas but he is also the one who actually knows how to accomplish ideas. I am thankful for Mihály Kovács, whose critics and bright opinions helped me a lot to overcome publication related difficulties. I would like to thank to György Hegyi his help and advices in the daily arising problems in the mooreland of chemical reactions. A special thank you goes to Máté Varga, László Végner, Gergely Vörös, István Ádám Horváth, Wanda Imrich, Anna Rauscher and Ilona Ozoróczyiné Szász for their contribution to our common projects. I am thankful to all of the recent and previous members of Malnalab especially Zoltán Simon, István Lőrincz, Gábor Szegvári, Szilvia Ráti, Chrystyna Mayor, Vitalii Stadnyk and Erzsébet Gerené Pászti. I would like to thank to Balázs Jelinek who has a quite large contribution to our lab being such an exceptional working environment. I would like to thank László Gráf and László Nyitray for operating such a successful Biochemistry Department, giving the opportunity for many students to perform high quality research. I would like to thank the work and help of our collaborators as well, Miklós Z. Kellermayer, Katalin Kis Petik, Péter Hári, László Drahos and Andrea Bodor. I am grateful to all my teachers who taught me both in primary or secondary school as well as in Eötvös Loránd University. I cannot be grateful enough for my family, Sára Németh, Zoltán Percsy, László Képiró and Gáspár Képiró for their everlasting support. I would especially thank to my mother for providing such ideal circumstances for my growth and education, even in the hard times. Finally, I would like to express my deepest gratitude to the most special person in my life, Boglárka Várkuti who is my wife, my best friend and my particularly bright and always very critic collage. She has been adding at least a factor of two to everything what I have accomplished - including this PhD Thesis - since we are such a strongly bound complex.



## VIII. Appendix

ABleb concentration	$A_1$	$k_1$ ( $\mu\text{M}^{-1} \text{min}^{-1}$ )	$A_2$	$k_2$ ( $\text{min}^{-1}$ )	functions
0.5 $\mu\text{M}$	0.29	$0.22 \pm 0.01$	-	-	$y=A_1e^{(-xk_1)}+y_0$
1 $\mu\text{M}$	$0.152 \pm 0.002$	$0.43 \pm 0.01$	-	-	$y=A_1e^{(-xk_1)}+cx+y_0$
2 $\mu\text{M}$	$0.143 \pm 0.001$	$1.1 \pm 0.02$	-	-	$y=A_1e^{(-xk_1)}+cx+y_0$
20 $\mu\text{M}$	$0.17 \pm 0.004$	$0.24 \pm 0.01$	1.26	$0.285 \pm 0.003$	$y=A_1e^{(-xk_1)}+A_2e^{(-xk_2)}+y_0$

**Table A1.** Parameters of fluorescence increase in 2P-irradiated areas of live zebrafish embryos equilibrated with different concentrations of ABleb. The similar amplitudes ( $A_1$ ) and second order rate constants ( $k_1$ ) indicate the specific, covalent binding of ABleb to myosin 2. The linear and the slow exponential fits refer to the non-specific covalent binding of ABleb<sup>4</sup>.

	A	$k$ ( $\mu\text{M}^{-1} \text{min}^{-1}$ )	
Fluorescence	$0.18 \pm 0.01$	$0.79 \pm 0.01$	$y=Ae^{(-xk)}+cx+y_0$
blebbing index	$-1.02 \pm 0.07$	$0.80 \pm 0.01$	$y=Ae^{(-xk)}$

**Table A2.** Parameters of fluorescence increase and blebbing index during ABleb-tattooing of M2 cells equilibrated with 1  $\mu\text{M}$  concentration of ABleb. The decrease of blebbing index was fitted satisfactory by a single exponential equation while the fluorescence increase could be fitted by single exponential and a linear equation as in Table II.

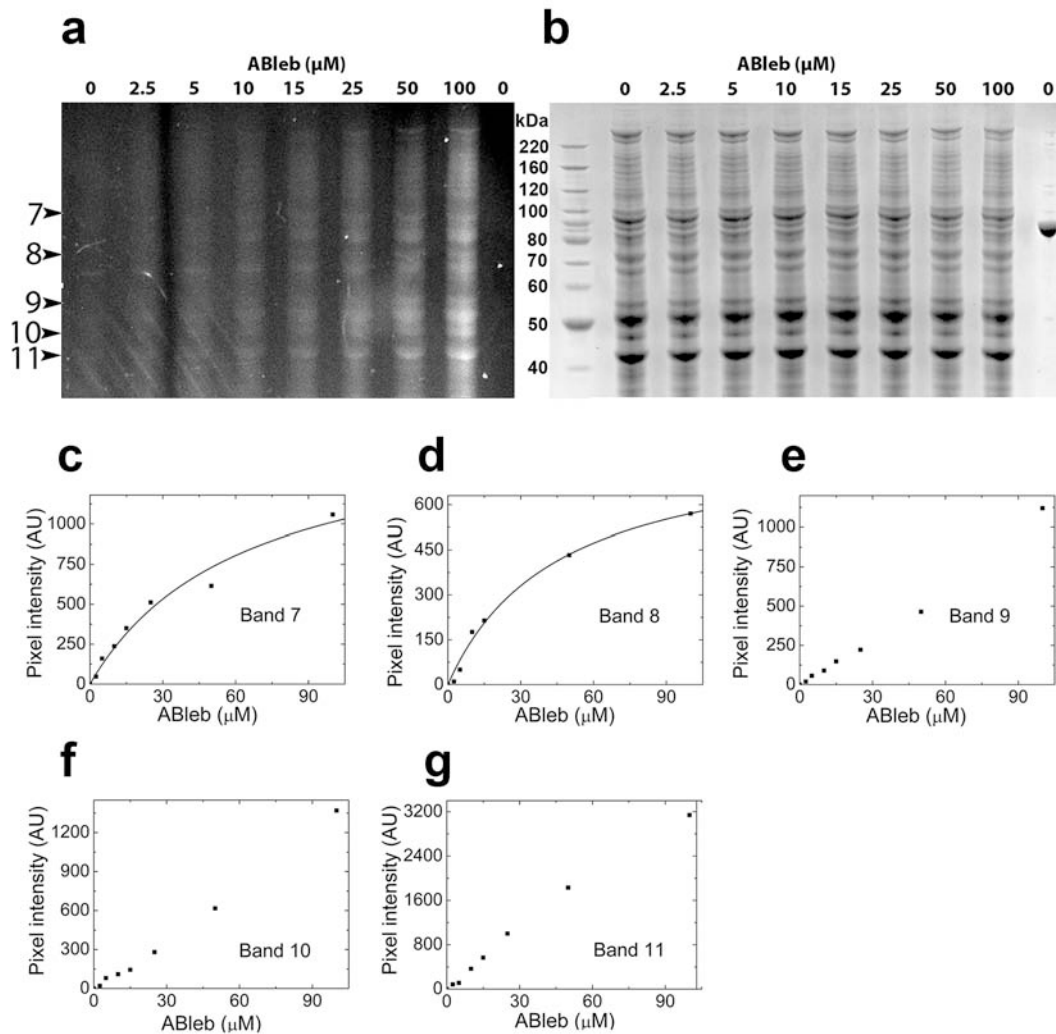


**Figure A1.** SDS-PAGE analysis of azidoblebbistatin crosslinking of proteins in *Dd* whole-cell lysates. Azidoblebbistatin-attached proteins in *Dd*Md-expressing *Dd* whole-cell lysates were detected by fluorescence of the covalently bound inhibitor (a) and, on the same gel, the protein contents were analyzed by subsequent Coomassie staining (b). Purified *Dd*Md was loaded in the right-most lane of the gel as a control. Fluorescent bands are indicated at the left side of panel A in the order of increasing mobility. Panels c-g show the azidoblebbistatin concentration dependence of the fluorescence intensity of azidoblebbistatin-crosslinked protein bands. Determined  $\text{EC}_{50}$  values were  $63 \mu\text{M}$  and  $45 \mu\text{M}$  for bands 7 and 8, respectively. In the case of bands 9, 10 and 11, the  $\text{EC}_{50}$  values were higher than  $100 \mu\text{M}$ .

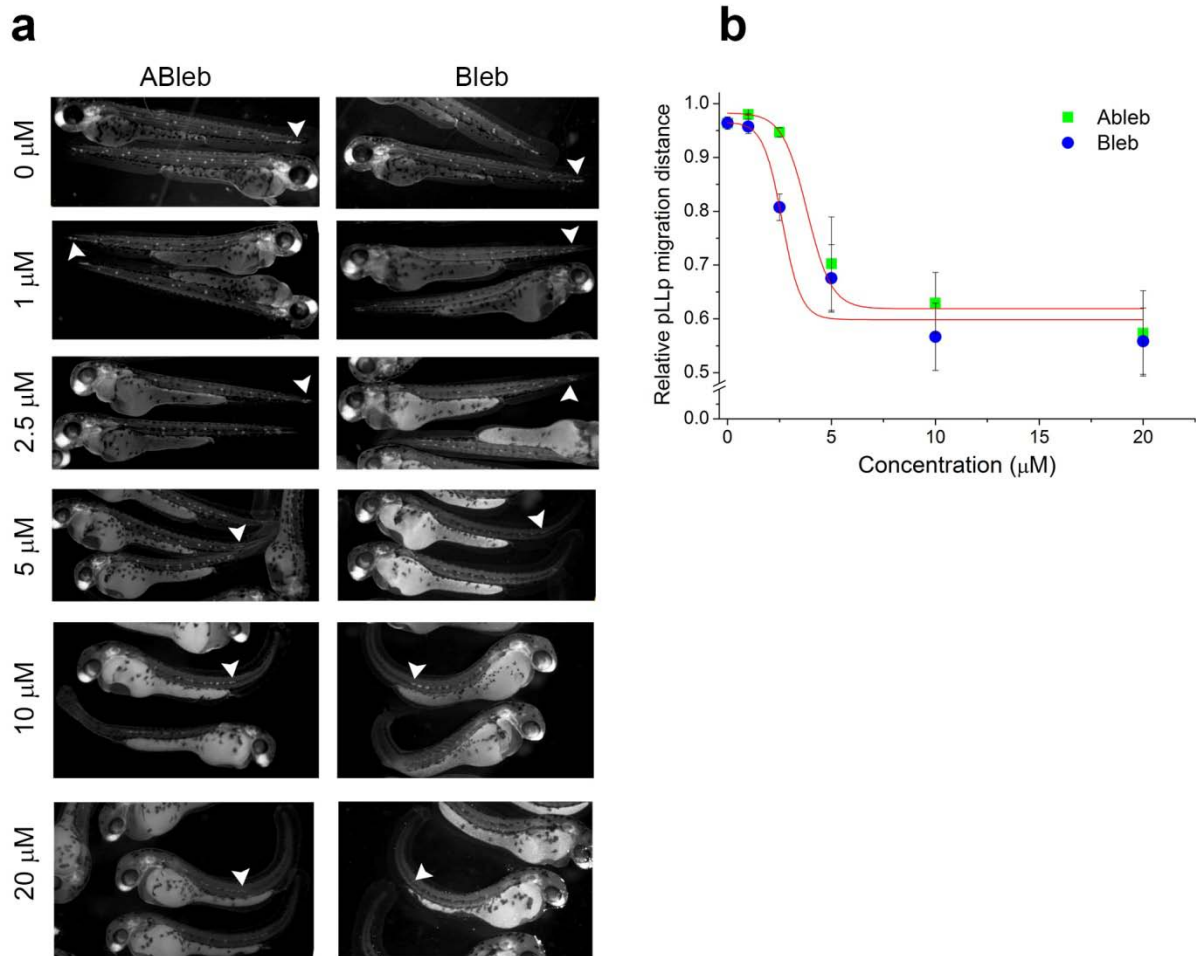


**Figure A2.** Inhibition of pLLp migration in zebrafish embryos. (a) Fluorescence images of 48 hpf zebrafish embryos incubated in the presence of the indicated inhibitor concentrations for 24 hours. Incubation started prior to the emergence of pLLp-s from the otic vesicle. White arrowheads mark the position of the halted pLLp. (b) Relative distance of pLLp migration (1 = distance from the otic vesicle to the tip of the tail). Dose-response curves (red) were fitted to mean  $\pm$  s.d. ( $n=4$ ), yielding  $EC_{50}$  values of  $3.8 \pm 0.9 \mu\text{M}$  and  $2.6 \pm 0.2 \mu\text{M}$  for Ableb and Bleb, respectively.  $EC_{50}$  is defined as the inhibitor concentration at 50% inhibition of pLLp migration. At 100% myosin 2 inhibition, the distance migrated by the pLLp is  $62 \pm 6 \%$  and  $60 \pm 4 \%$  of the distance between the otic vesicle and the tip of the tail in the case of Ableb and Bleb, respectively.

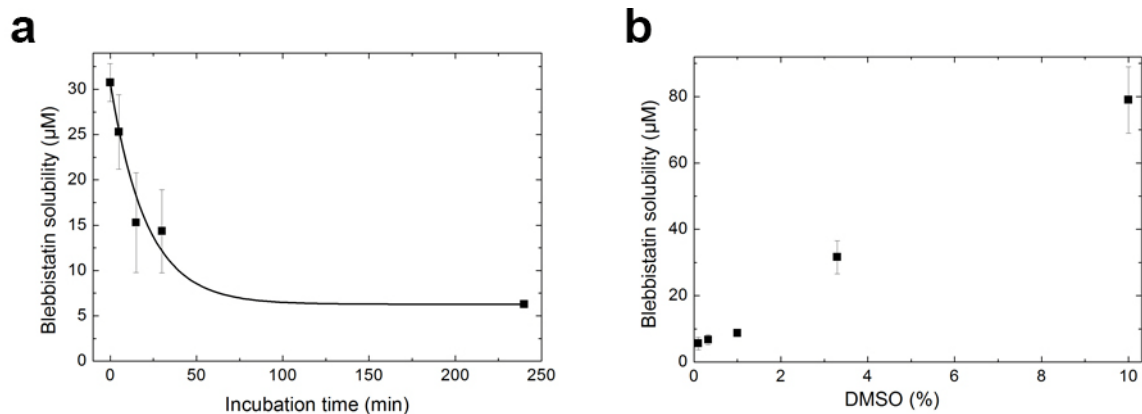


**Figure A3. Solubility of blebbistatin.** (a) 50 µM blebbistatin solutions were prepared in assay buffer in the presence of 0.1% DMSO. After the incubation for the indicated times at 25°C, the samples were centrifuged at 14,000 RPM for 1 minute. Absorption spectra of the supernatants were recorded and the concentrations of the dissolved blebbistatin ( $\epsilon_{427}^{\circ} = 6100 \text{ M}^{-1}\text{cm}^{-1}$ ) were determined. (b) 100 µM blebbistatin solutions were prepared in assay buffer containing 0.1 %, 0.3 %, 1 %, 3.3 % and 10 % DMSO. After vortexing, the solutions were centrifuged at 14,000 RPM for 5 minutes. Absorption spectra of the supernatants were recorded and the concentrations of dissolved blebbistatin were determined ( $\epsilon_{427}^{\circ} = 6100 \text{ M}^{-1}\text{cm}^{-1}$ ). The solubility of blebbistatin increased quasi-linearly with DMSO concentration to 80 µM at 10 % DMSO.

## IX. Abbreviations

2PM	two-photon microscope
ABleb	azidoblebbistatin
ACN	acetonitrile
ADME	absorption, distribution, metabolism, and excretion
ATP	adenosine triphosphate
ATPase	adenosine triphosphatase
Bleb	blebbistatin
CBleb	para-chloroblebbistatin
DARTS	drug affinity responsive target stability
Dd	Dictyostelium discoideum
Dd	Dictyostelium discoideum
DdMD	Dictyostelium discoideum myosin II motor domain
DMSO	dimethyl sulfoxide
dpf	days post fertilization
EC <sub>50</sub>	half maximal effective concentration
FWHM	full width at half maximum
HEPES	4-(2-hydroxyethyl)-1-piperazineethanesulfonic acid
HPLC	high pressure liquid chromatography
IC <sub>50</sub>	half-maximal inhibition values
IPSF	illumination point spread function
MHC	myosin II heavy chains
MS	mass spectrometry
NBleb	para-nitroblebbistatin
NMHC	nonmuscle myosin II heavy chains

NMR	nuclear magnetic resonance spectroscopy
OPO	optical parametric oscillator
PAL	photoaffinity labeling
PBS	phosphate buffered saline
pLLp	posterior lateral line promurdium
S	singlet
SAR	structure–activity relationship
SkS1	rabbit skeletal muscle subfracgment 1
SPECT	single photon emission computed tomography
SPROX	stability of proteins from rates of oxidation
TEA	triethylamine
TFA	trifluoroacetic acid
Ti:Sa	titanium-sapphire
V2PR	effective two-photon reaction volume
W	water

## X. List of Figures and Tables

**Figure 1.** *Traditional vs. target based drug discovery.*

**Figure 3.** *Synthesis of arylazides.*

**Figure 4.** *Photoactivation of aryl azides.*

**Figure 5.** *Carbene generating photophores.*

**Figure 6.** *Schematic representation of a conventional hexamer myosin II.*

**Figure 7.** *Cytokinesis in animal cells.*

**Figure 8.** *The life cycle of a bleb.*

**Figure 9.** *Myosin II inhibitors.*

**Figure 10.** *One vs. two-photon excitation.*

**Figure 11.** *Confocal vs. two-photon microscopy.*

**Figure 12.** *Optopharmacological tools.*

**Figure 13.** *Azidated bioactive compounds synthesized in this study.*

**Figure 14.** *Photoreaction of azidoblebbistatin.*

**Figure 15.** *Myosin II inhibition of azidoblebbistatin.*

**Figure 16.** *Target deconvolution of blebbistatin.*

**Figure 17.** *Fluorescence emission spectra of blebbistatin and its derivatives.*

**Figure 18.** *In vitro myosin II inhibition of blebbistatin and its derivatives.*

**Figure 19.** *Photoconversion of blebbistatin and its derivatives.*

**Figure 20.** *Phototoxicity of blebbistatin and its derivatives.*

**Figure 21.** *Confocal time-lapse imaging of Kyoto cells in the presence of blebbistatin (Bleb) or para-nitroblebbistatin (NBleb).*

**Figure 22.** *Phototoxicity of Bleb and NBleb on zebrafish embryos.*

**Figure 23.** *In vivo effects of Bleb and NBleb on HeLa cells.*

**Figure 24.** *In vivo effects of Bleb and NBleb on Dd cells.*

**Figure 25.** *In vivo effects of Bleb and NBleb on M2 cells.*

**Figure 26.** *Comparing the in vivo effects of NBleb and Bleb on zebrafish embryos.*

**Figure 27.** *The two different phenotypes observed upon NBleb treatment during cell division.*

**Figure 28.** *Cell division mechanisms in the function of NBleb concentrations.*

**Figure 29.** *Multiple crosslinking of ABleb to DdMD using multiple crosslinking cycles.*

**Figure 30.** *Photoreaction of ABleb (a) and azidofluorescein (b) upon 800 nm two-photon irradiation at different laser powers, using focused (black squares) or unfocused (red square) laser beams.*

**Figure 31.** *Photoreaction of azidofluorescein (black) upon 750-1000 nm irradiation and the doubled one-photon absorption spectrum of azidofluorescein (red).*

**Figure 32.** *MS spectra of DdMD treated with ABleb then irradiated at 300 nm (UV), 2PM-irradiated at 800 nm (2P) and 2PM off-focus irradiated (Off-focus).*

**Figure 33.** *The fluorescence of azidoblebbistatin upon nucleophilic covalent attachment.*

**Figure 34.** *Exploring the x, y and z dimensions of the effective two-photon reaction volume.*

**Figure 35.** *The concept of molecular tattooing.*

**Figure 36.** *Optimization of ABleb-tattooing in live zebrafish embryos.*

**Figure 37.** *Molecular tattooing of live zebrafish embryos.*

**Figure 38.** *Molecular tattooing an M2 cell with ABleb.*

**Figure 39.** *Subcellular tattooing of a single M2 cell.*

**Figure 40.** *Structural model of the myosin.ADP.Vi.para-nitroblebbistatin complex.*

**Table 1.** *Half maximal inhibitory concentrations (IC<sub>50</sub>) of blebbistatin for various myosins*

**Table 2.** *Physical parameters of the 2P reaction volumes.*

## XI. Publications Concerning this Thesis

Képiró, M., Várkuti, B. H., Bodor, A., Hegyi, G., Drahos, L., Kovács, M., & Málnási-Csizmadia, A. (2012). **Azidoblebbistatin, a photoreactive myosin inhibitor**. Proceedings of the National Academy of Sciences of the United States of America, 109(24), 9402-9407.

Képiró, M., Várkuti, B. H., Végner, L., Vörös, G., Hegyi, G., Varga, M., & Málnási-Csizmadia, A. (2014). **para-Nitroblebbistatin, the Non-Cytotoxic and Photostable Myosin II Inhibitor**. Angewandte Chemie, 126(31), 8350-8354.

Képiró, M., Várkuti, B. H., Rauscher, A. A., Kellermayer, S. Z. M., Varga, M., Málnási-Csizmadia, A. **Molecular tattoo: subcellular confinement of drug effects**. Under review.

### Conference proceedings

#### **Molecular tattooing in live zebrafish: inhibition of myosin II dependent processes in space and time**

Miklós Képiró, Boglárka Várkuti, Máté Varga, András Málnási-Csizmadia 8th European Zebrafish Meeting, 2013 Barcelona, Spain, oral presentation

#### **Molecular tattooing in live zebrafish**

Miklós Képiró, Boglárka Várkuti, Máté Varga, András Málnási-Csizmadia Budapest Science Meetup, 2013 Budapest, Hungary, oral presentation

#### **Interactomics of blebbistatin**

Miklós Képiró, Boglárka Várkuti and András Málnási-Csizmadia Biophysical Society 57th Annual Meeting, 2013 Philadelphia, US, poster presentation

#### **Partner mapping of azidoblebbistatin, the novel photo-inducible myosin inhibitor**

Miklós Képiró, Boglárka H. Várkuti, György Hegyi, Mihály Kovács, András Málnási-Csizmadia European Muscle Conference, 2012 Rhodes, Greece, poster presentation

**Synthesis and functional characterization of azido-blebbistatin, a photoreactive myosin inhibitor**

Miklós Képiró, Boglárka H. Várkuti, György Hegyi, Mihály Kovács, András Málnási-Csizmadia  
Biophysical Society 56th Annual Meeting, 2012 San Diego, US, poster presentation

**Synthesis and functional characterization of azido-blebbistatin, a photoreactive myosin inhibitor**

Miklós Képiró, Boglárka H. Várkuti, György Hegyi, Mihály Kovács, András Málnási- Csizmadia  
European Muscle Conference, 2011 Berlin, Germany, oral presentation

**Synthesis and functional characterization of azido-blebbistatin, a photoreactive myosin inhibitor**

Miklós Képiró, Boglárka Várkuti and András Málnási-Csizmadia  
4th European Conference on Chemistry for Life Sciences, 2011 Budapest, Hungary, poster presentation

## XII. References

1. Ji, H.F., X.J. Li, and H.Y. Zhang, *Natural products and drug discovery*. Embo Reports, 2009. **10**(3): p. 194-200.
2. Drews, J., *Drug discovery: A historical perspective*. Science, 2000. **287**(5460): p. 1960-1964.
3. Moore, F.J., *A history of chemistry*. 1st ed. 1918, New York/London: McGraw-Hill Book Company ; Hill Publishing Co. xiv, 292 p., 48 p. of plates.
4. Langley, J.N., *On the reaction of cells and of nerve-endings to certain poisons, chiefly as regards the reaction of striated muscle to nicotine and to curari*. J Physiol, 1905. **33**(4-5): p. 374-413.
5. Sams-Dodd, F., *Target-based drug discovery: is something wrong?* Drug Discovery Today, 2005. **10**(2): p. 139-147.
6. Bennani, Y.L., *Drug discovery in the next decade: innovation needed ASAP*. Drug Discov Today, 2012. **17** Suppl: p. S31-44.
7. Scannell, J.W., et al., *Diagnosing the decline in pharmaceutical R&D efficiency*. Nat Rev Drug Discov, 2012. **11**(3): p. 191-200.
8. Rix, U. and G. Superti-Furga, *Target profiling of small molecules by chemical proteomics*. Nature Chemical Biology, 2009. **5**(9): p. 616-624.
9. Mestres, J., et al., *The topology of drug-target interaction networks: implicit dependence on drug properties and target families*. Molecular Biosystems, 2009. **5**(9): p. 1051-1057.
10. Frantz, S., *Drug discovery: playing dirty*. Nature, 2005. **437**(7061): p. 942-3.
11. Overington, J.P., B. Al-Lazikani, and A.L. Hopkins, *Opinion - How many drug targets are there?* Nature Reviews Drug Discovery, 2006. **5**(12): p. 993-996.
12. Sato, S., et al., *Biochemical target isolation for novices: affinity-based strategies*. Chem Biol, 2010. **17**(6): p. 616-23.
13. Mamidyala, S.K. and M.G. Finn, *In situ click chemistry: probing the binding landscapes of biological molecules*. Chem Soc Rev, 2010. **39**(4): p. 1252-61.
14. Lee, J. and M. Bogoy, *Target deconvolution techniques in modern phenotypic profiling*. Current Opinion in Chemical Biology, 2013. **17**(1): p. 118-126.
15. Fontana, A., et al., *Probing protein structure by limited proteolysis*. Acta Biochim Pol, 2004. **51**(2): p. 299-321.
16. West, G.M., et al., *Quantitative proteomics approach for identifying protein-drug interactions in complex mixtures using protein stability measurements*. Proc Natl Acad Sci U S A, 2010. **107**(20): p. 9078-82.
17. Singh, A., E.R. Thornton, and F.H. Westheimer, *The photolysis of diazoacetylchymotrypsin*. J Biol Chem, 1962. **237**: p. 3006-8.
18. Vodovozova, E.L., *Photoaffinity labeling and its application in structural biology*. Biochemistry (Mosc), 2007. **72**(1): p. 1-20.
19. Shacham, S., et al., *PREDICT modeling and in-silico screening for G-protein coupled receptors*. Proteins, 2004. **57**(1): p. 51-86.
20. Kanety, H. and S. Fuchs, *Immuno-photoaffinity labeling of the D2-dopamine receptor*. Biochem Biophys Res Commun, 1988. **155**(2): p. 930-6.
21. Hodek, P. and H.W. Strobel, *Preparation of [<sup>3</sup>H] Labeled Benzphetamine Photoaffinity Probes for Cytochrome-P-450*. Journal of Labelled Compounds & Radiopharmaceuticals, 1995. **36**(4): p. 321-329.
22. Andersen, J., et al., *Rapid synthesis of aryl azides from aryl halides under mild conditions*. Synlett, 2005(14): p. 2209-2213.
23. Prakash, G.K.S., et al., *N-Halosuccinimide/BF<sub>3</sub>-H<sub>2</sub>O, efficient electrophilic halogenating systems for aromatics*. Journal of the American Chemical Society, 2004. **126**(48): p. 15770-15776.

24. Brunner, J., *New photolabeling and crosslinking methods*. Annu Rev Biochem, 1993. **62**: p. 483-514.
25. Keana, J.F.W. and S.X. Cai, *New Reagents for Photoaffinity-Labeling - Synthesis and Photolysis of Functionalized Perfluorophenyl Azides*. Journal of Organic Chemistry, 1990. **55**(11): p. 3640-3647.
26. Borden, W.T., et al., *The interplay of theory and experiment in the study of phenylnitrene*. Accounts of Chemical Research, 2000. **33**(11): p. 765-771.
27. Dubinsky, L., B.P. Krom, and M.M. Meijler, *Diazirine based photoaffinity labeling*. Bioorganic & Medicinal Chemistry, 2012. **20**(2): p. 554-570.
28. Mccray, J.A., et al., *A New Approach to Time-Resolved Studies of Atp-Requiring Biological-Systems - Laser Flash-Photolysis of Caged Atp*. Proceedings of the National Academy of Sciences of the United States of America-Biological Sciences, 1980. **77**(12): p. 7237-7241.
29. Haustein, E. and P. Schwille, *Single-molecule spectroscopic methods*. Current Opinion in Structural Biology, 2004. **14**(5): p. 531-540.
30. Kishino, A. and T. Yanagida, *Force measurements by micromanipulation of a single actin filament by glass needles*. Nature, 1988. **334**(6177): p. 74-6.
31. Spudich, J.A., *Optical trapping: Motor molecules in motion*. Nature, 1990. **348**(6299): p. 284-5.
32. van den Heuvel, M.G.L. and C. Dekker, *Motor proteins at work for nanotechnology*. Science, 2007. **317**(5836): p. 333-336.
33. Odrionitz, F. and M. Kollmar, *Drawing the tree of eukaryotic life based on the analysis of 2,269 manually annotated myosins from 328 species*. Genome Biology, 2007. **8**(9).
34. Foth, B.J., M.C. Goedecke, and D. Soldati, *New insights into myosin evolution and classification*. Proceedings of the National Academy of Sciences of the United States of America, 2006. **103**(10): p. 3681-3686.
35. Berg, J.S., B.C. Powell, and R.E. Cheney, *A millennial myosin census*. Mol Biol Cell, 2001. **12**(4): p. 780-94.
36. Conti, M.A. and R.S. Adelstein, *Nonmuscle myosin II moves in new directions*. J Cell Sci, 2008. **121**(Pt 1): p. 11-8.
37. Coluccio, L.M., *Myosins a superfamily of molecular motors*. Proteins and cell regulation. 2008, Dordrecht: Springer. computer files (xii, 475 p., [17] p. of plates.
38. Vicente-Manzanares, M., et al., *Non-muscle myosin II takes centre stage in cell adhesion and migration*. Nat Rev Mol Cell Biol, 2009. **10**(11): p. 778-90.
39. de la Roche, M.A. and G.P. Cote, *Regulation of Dictyostelium myosin I and II*. Biochim Biophys Acta, 2001. **1525**(3): p. 245-61.
40. Green, R.A., E. Paluch, and K. Oegema, *Cytokinesis in animal cells*. Annu Rev Cell Dev Biol, 2012. **28**: p. 29-58.
41. Agromayor, M. and J. Martin-Serrano, *Knowing when to cut and run: mechanisms that control cytokinetic abscission*. Trends Cell Biol, 2013. **23**(9): p. 433-41.
42. Pollard, T.D., *Mechanics of cytokinesis in eukaryotes*. Curr Opin Cell Biol, 2010. **22**(1): p. 50-6.
43. Bohnert, K.A. and K.L. Gould, *On the cutting edge: post-translational modifications in cytokinesis*. Trends Cell Biol, 2011. **21**(5): p. 283-92.
44. Ma, X., et al., *Nonmuscle myosin II exerts tension but does not translocate actin in vertebrate cytokinesis*. Proc Natl Acad Sci U S A, 2012. **109**(12): p. 4509-14.
45. Guha, M., M. Zhou, and Y.L. Wang, *Cortical actin turnover during cytokinesis requires myosin II*. Curr Biol, 2005. **15**(8): p. 732-6.
46. Murthy, K. and P. Wadsworth, *Myosin-II-dependent localization and dynamics of F-actin during cytokinesis*. Curr Biol, 2005. **15**(8): p. 724-31.
47. Charras, G. and E. Paluch, *Blebs lead the way: how to migrate without lamellipodia*. Nat Rev Mol Cell Biol, 2008. **9**(9): p. 730-6.
48. Fackler, O.T. and R. Grosse, *Cell motility through plasma membrane blebbing*. J Cell Biol, 2008. **181**(6): p. 879-84.

49. Friedl, P. and K. Wolf, *Tumour-cell invasion and migration: diversity and escape mechanisms*. Nat Rev Cancer, 2003. **3**(5): p. 362-74.
50. Blaser, H., et al., *Migration of zebrafish primordial germ cells: a role for myosin contraction and cytoplasmic flow*. Dev Cell, 2006. **11**(5): p. 613-27.
51. Charras, G.T., et al., *Non-equilibration of hydrostatic pressure in blebbing cells*. Nature, 2005. **435**(7040): p. 365-9.
52. Mitchison, T.J., G.T. Charras, and L. Mahadevan, *Implications of a poroelastic cytoplasm for the dynamics of animal cell shape*. Semin Cell Dev Biol, 2008. **19**(3): p. 215-23.
53. Bond, L.M., et al., *Small-molecule inhibitors of myosin proteins*. Future Med Chem, 2013. **5**(1): p. 41-52.
54. Herrmann, C., et al., *Effect of 2,3-butanedione monoxime on myosin and myofibrillar ATPases. An example of an uncompetitive inhibitor*. Biochemistry, 1992. **31**(48): p. 12227-32.
55. Higuchi, H. and S. Takemori, *Butanedione monoxime suppresses contraction and ATPase activity of rabbit skeletal muscle*. J Biochem, 1989. **105**(4): p. 638-43.
56. Cheung, A., et al., *A small-molecule inhibitor of skeletal muscle myosin II*. Nat Cell Biol, 2002. **4**(1): p. 83-8.
57. Straight, A.F., et al., *Dissecting temporal and spatial control of cytokinesis with a myosin II inhibitor*. Science, 2003. **299**(5613): p. 1743-7.
58. Kovacs, M., et al., *Mechanism of blebbistatin inhibition of myosin II*. Journal of Biological Chemistry, 2004. **279**(34): p. 35557-35563.
59. Ramamurthy, B., et al., *Kinetic mechanism of blebbistatin inhibition of nonmuscle myosin IIb*. Biochemistry, 2004. **43**(46): p. 14832-9.
60. Ostap, E.M., *2,3-Butanedione monoxime (BDM) as a myosin inhibitor*. Journal of Muscle Research and Cell Motility, 2002. **23**(4): p. 305-308.
61. Chinthalapudi, K., et al., *Mechanism and specificity of pentachloropseudilin-mediated inhibition of myosin motor activity*. J Biol Chem, 2011. **286**(34): p. 29700-8.
62. Burkholder, P.R., R.M. Pfister, and F.H. Leitz, *Production of a pyrrole antibiotic by a marine bacterium*. Appl Microbiol, 1966. **14**(4): p. 649-53.
63. Islam, K., et al., *A myosin V inhibitor based on privileged chemical scaffolds*. Angew Chem Int Ed Engl, 2010. **49**(45): p. 8484-8.
64. Heissler, S.M., et al., *Kinetic properties and small-molecule inhibition of human myosin-6*. FEBS Lett, 2012. **586**(19): p. 3208-14.
65. Allingham, J.S., R. Smith, and I. Rayment, *The structural basis of blebbistatin inhibition and specificity for myosin II*. Nat Struct Mol Biol, 2005. **12**(4): p. 378-9.
66. Eddinger, T.J., et al., *Potent inhibition of arterial smooth muscle tonic contractions by the selective myosin II inhibitor, blebbistatin*. J Pharmacol Exp Ther, 2007. **320**(2): p. 865-70.
67. Loudon, R.P., et al., *RhoA-kinase and myosin II are required for the maintenance of growth cone polarity and guidance by nerve growth factor*. J Neurobiol, 2006. **66**(8): p. 847-67.
68. Swaminathan, V., et al., *Mechanical stiffness grades metastatic potential in patient tumor cells and in cancer cell lines*. Cancer Res, 2011. **71**(15): p. 5075-80.
69. Limouze, J., et al., *Specificity of blebbistatin, an inhibitor of myosin II*. J Muscle Res Cell Motil, 2004. **25**(4-5): p. 337-41.
70. Shu, S., X. Liu, and E.D. Korn, *Blebbistatin and blebbistatin-inactivated myosin II inhibit myosin II-independent processes in Dictyostelium*. Proceedings of the National Academy of Sciences of the United States of America, 2005. **102**(5): p. 1472-1477.
71. Sakamoto, T., et al., *Blebbistatin, a myosin II inhibitor, is photoinactivated by blue light*. Biochemistry, 2005. **44**(2): p. 584-8.
72. Kolega, J., *Phototoxicity and photoinactivation of blebbistatin in UV and visible light*. Biochem Biophys Res Commun, 2004. **320**(3): p. 1020-5.
73. Mikulich, A., S. Kavaliauskiene, and P. Juzenas, *Blebbistatin, a myosin inhibitor, is phototoxic to human cancer cells under exposure to blue light*. Biochim Biophys Acta, 2012. **1820**(7): p. 870-7.

74. Kondo, T., et al., *Enhancement of myosin II/actin turnover at the contractile ring induces slower furrowing in dividing HeLa cells*. *Biochem J*, 2011. **435**(3): p. 569-76.
75. Schaub, S., et al., *Comparative maps of motion and assembly of filamentous actin and myosin II in migrating cells*. *Mol Biol Cell*, 2007. **18**(10): p. 3723-32.
76. Kanada, M., A. Nagasaki, and T.Q. Uyeda, *Adhesion-dependent and contractile ring-independent equatorial furrowing during cytokinesis in mammalian cells*. *Mol Biol Cell*, 2005. **16**(8): p. 3865-72.
77. Rex, C.S., et al., *Myosin IIb regulates actin dynamics during synaptic plasticity and memory formation*. *Neuron*, 2010. **67**(4): p. 603-17.
78. Myers, K.A., et al., *Antagonistic forces generated by cytoplasmic dynein and myosin-II during growth cone turning and axonal retraction*. *Traffic*, 2006. **7**(10): p. 1333-51.
79. Murthy, K. and P. Wadsworth, *Dual role for microtubules in regulating cortical contractility during cytokinesis*. *J Cell Sci*, 2008. **121**(Pt 14): p. 2350-9.
80. Sanborn, K.B., et al., *Myosin IIA associates with NK cell lytic granules to enable their interaction with F-actin and function at the immunological synapse*. *J Immunol*, 2009. **182**(11): p. 6969-84.
81. Sandquist, J.C. and A.R. Means, *The C-terminal tail region of nonmuscle myosin II directs isoform-specific distribution in migrating cells*. *Mol Biol Cell*, 2008. **19**(12): p. 5156-67.
82. Yu, H.Y. and W.M. Bement, *Multiple myosins are required to coordinate actin assembly with coat compression during compensatory endocytosis*. *Mol Biol Cell*, 2007. **18**(10): p. 4096-105.
83. Shiba, Y., et al., *Human ES-cell-derived cardiomyocytes electrically couple and suppress arrhythmias in injured hearts*. *Nature*, 2012. **489**(7415): p. 322-5.
84. Ketschek, A.R., S.L. Jones, and G. Gallo, *Axon extension in the fast and slow lanes: substratum-dependent engagement of myosin II functions*. *Dev Neurobiol*, 2007. **67**(10): p. 1305-20.
85. Seabrooke, S., X. Qiu, and B.A. Stewart, *Nonmuscle Myosin II helps regulate synaptic vesicle mobility at the Drosophila neuromuscular junction*. *BMC Neurosci*, 2010. **11**: p. 37.
86. Verma, P., A.G. Ostermeyer-Fay, and D.A. Brown, *Caveolin-1 induces formation of membrane tubules that sense actomyosin tension and are inhibited by polymerase I and transcript release factor/cavin-1*. *Mol Biol Cell*, 2010. **21**(13): p. 2226-40.
87. Affentranger, S., et al., *Dynamic reorganization of flotillins in chemokine-stimulated human T-lymphocytes*. *BMC Cell Biol*, 2011. **12**: p. 28.
88. Wong, K., A. Van Keymeulen, and H.R. Bourne, *PDZRhoGEF and myosin II localize RhoA activity to the back of polarizing neutrophil-like cells*. *J Cell Biol*, 2007. **179**(6): p. 1141-8.
89. Oheim, M., et al., *Principles of two-photon excitation fluorescence microscopy and other nonlinear imaging approaches*. *Adv Drug Deliv Rev*, 2006. **58**(7): p. 788-808.
90. Zipfel, W.R., R.M. Williams, and W.W. Webb, *Nonlinear magic: multiphoton microscopy in the biosciences*. *Nat Biotechnol*, 2003. **21**(11): p. 1369-77.
91. White, N.S. and R.J. Errington, *Fluorescence techniques for drug delivery research: theory and practice*. *Adv Drug Deliv Rev*, 2005. **57**(1): p. 17-42.
92. Frangioni, J.V., *In vivo near-infrared fluorescence imaging*. *Curr Opin Chem Biol*, 2003. **7**(5): p. 626-34.
93. Jacques, S.L., *Optical properties of biological tissues: a review*. *Phys Med Biol*, 2013. **58**(11): p. R37-61.
94. Kramer, R.H., A. Mouro, and H. Adesnik, *Optogenetic pharmacology for control of native neuronal signaling proteins*. *Nat Neurosci*, 2013. **16**(7): p. 816-23.
95. Ellis-Davies, G.C., *Caged compounds: photorelease technology for control of cellular chemistry and physiology*. *Nat Methods*, 2007. **4**(8): p. 619-28.
96. Fehrentz, T., M. Schonberger, and D. Trauner, *Optochemical genetics*. *Angew Chem Int Ed Engl*, 2011. **50**(51): p. 12156-82.

97. Dai, H.X., et al., *Divergent C-H functionalizations directed by sulfonamide pharmacophores: late-stage diversification as a tool for drug discovery*. J Am Chem Soc, 2011. **133**(18): p. 7222-8.
98. Kuge, Y., et al., *Synthesis and evaluation of radioiodinated cyclooxygenase-2 inhibitors as potential SPECT tracers for cyclooxygenase-2 expression*. Nucl Med Biol, 2006. **33**(1): p. 21-7.
99. Castanet, A.S., F. Colobert, and P.E. Broutin, *Mild and regioselective iodination of electron-rich aromatics with N-iodosuccinimide and catalytic trifluoroacetic acid*. Tetrahedron Letters, 2002. **43**(29): p. 5047-5048.
100. Hegyi, G., L. Szilagyi, and M. Elzinga, *Photoaffinity-Labeling of the Nucleotide Binding-Site of Actin*. Biochemistry, 1986. **25**(19): p. 5793-5798.
101. Scheurich, P., H.J. Schafer, and K. Dose, *8-Azido-Adenosine 5'-Triphosphate as a Photoaffinity Label for Bacterial-F1 AtPase*. European Journal of Biochemistry, 1978. **88**(1): p. 253-257.
102. Mo, F., et al., *Gold-catalyzed halogenation of aromatics by N-halosuccinimides*. Angew Chem Int Ed Engl, 2010. **49**(11): p. 2028-32.
103. Shu, S., X. Liu, and E.D. Korn, *Blebbistatin and blebbistatin-inactivated myosin II inhibit myosin II-independent processes in Dictyostelium*. Proc Natl Acad Sci U S A, 2005. **102**(5): p. 1472-7.
104. Lucas-Lopez, C., et al., *The small molecule tool (S)-(-)-blebbistatin: novel insights of relevance to myosin inhibitor design*. Org Biomol Chem, 2008. **6**(12): p. 2076-84.
105. Lucas-Lopez, C., et al., *Absolute stereochemical assignment and fluorescence tuning of the small molecule tool, (-)-blebbistatin*. European Journal of Organic Chemistry, 2005(9): p. 1736-1740.
106. Ma, E.Y. and D.W. Raible, *Signaling pathways regulating zebrafish lateral line development*. Curr Biol, 2009. **19**(9): p. R381-6.
107. Friedl, P. and D. Gilmour, *Collective cell migration in morphogenesis, regeneration and cancer*. Nat Rev Mol Cell Biol, 2009. **10**(7): p. 445-57.
108. Ernst, S., et al., *Shroom3 is required downstream of FGF signalling to mediate proneuromast assembly in zebrafish*. Development, 2012. **139**(24): p. 4571-81.
109. Harding, M.J. and A.V. Nechiporuk, *Fgfr-Ras-MAPK signaling is required for apical constriction via apical positioning of Rho-associated kinase during mechanosensory organ formation*. Development, 2012. **139**(17): p. 3130-5.
110. Haas, P. and D. Gilmour, *Chemokine signaling mediates self-organizing tissue migration in the zebrafish lateral line*. Dev Cell, 2006. **10**(5): p. 673-80.
111. Salic, A. and T.J. Mitchison, *A chemical method for fast and sensitive detection of DNA synthesis in vivo*. Proc Natl Acad Sci U S A, 2008. **105**(7): p. 2415-20.
112. Byers, H.R., et al., *Cell migration and actin organization in cultured human primary, recurrent cutaneous and metastatic melanoma. Time-lapse and image analysis*. Am J Pathol, 1991. **139**(2): p. 423-35.
113. Kepiro, M., et al., *para-Nitroblebbistatin, the Non-Cytotoxic and Photostable Myosin II Inhibitor*. Angew Chem Int Ed Engl, 2014.
114. Charras, G. and E. Paluch, *Blebs lead the way: how to migrate without lamellipodia*. Nature Reviews Molecular Cell Biology, 2008. **9**(9): p. 730-736.
115. Tinevez, J.Y., et al., *Role of cortical tension in bleb growth*. Proc Natl Acad Sci U S A, 2009. **106**(44): p. 18581-6.
116. Kepiro, M., et al., *Azidoblebbistatin, a photoreactive myosin inhibitor*. Proc Natl Acad Sci U S A, 2012. **109**(24): p. 9402-7.
117. Takacs, B., et al., *Myosin complexed with ADP and blebbistatin reversibly adopts a conformation resembling the start point of the working stroke*. Proc Natl Acad Sci U S A, 2010. **107**(15): p. 6799-804.
118. Várkuti, B.H., *Structural Background of Force Generation in Myosins*. 2013.
119. Glotzer, M., *The molecular requirements for cytokinesis*. Science, 2005. **307**(5716): p. 1735-9.

120. Head, J.R., et al., *Activation of canonical Wnt/beta-catenin signaling stimulates proliferation in neuromasts in the zebrafish posterior lateral line*. Dev Dyn, 2013. **242**(7): p. 832-46.
121. Pelouch, W.S., P.E. Powers, and C.L. Tang, *Ti:sapphire-pumped, high-repetition-rate femtosecond optical parametric oscillator*. Opt Lett, 1992. **17**(15): p. 1070-2.
122. Lawson, C.P.A.T., A.M.Z. Slawin, and N.J. Westwood, *Application of the copper catalysed N-arylation of amidines in the synthesis of analogues of the chemical tool, blebbistatin*. Chemical Communications, 2011. **47**(3): p. 1057-1059.
123. Malnasi-Csizmadia, A., R.J. Woolley, and C.R. Bagshaw, *Resolution of conformational states of Dictyostelium myosin II motor domain using tryptophan (W501) mutants: implications for the open-closed transition identified by crystallography*. Biochemistry, 2000. **39**(51): p. 16135-46.
124. Okamoto, Y. and T. Sekine, *A streamlined method of subfragment one preparation from myosin*. J Biochem, 1985. **98**(4): p. 1143-5.
125. Gyimesi, M., et al., *The mechanism of the reverse recovery step, phosphate release, and actin activation of Dictyostelium myosin II*. Journal of Biological Chemistry, 2008. **283**(13): p. 8153-63.
126. Spudich, J.A. and S. Watt, *The regulation of rabbit skeletal muscle contraction. I. Biochemical studies of the interaction of the tropomyosin-troponin complex with actin and the proteolytic fragments of myosin*. J Biol Chem, 1971. **246**(15): p. 4866-71.
127. Pardee, J.D. and J.A. Spudich, *Purification of muscle actin*. Methods Cell Biol, 1982. **24**: p. 271-89.
128. Westerfield, M., *The zebrafish book. A guide for the laboratory use of zebrafish (Danio rerio)*. 4th edition ed. 2000, Eugene: University of Oregon Press.
129. Cunningham, C.C., *Actin polymerization and intracellular solvent flow in cell surface blebbing*. J Cell Biol, 1995. **129**(6): p. 1589-99.